2011

A Time-efficient Method for Accurate T1 Mapping of The Human Brain

Yung-Yeh Chang
Virginia Commonwealth University

A Time-efficient Method for Accurate T_1 Mapping of The Human Brain

A Dissertation submitted in partial fulfillment of the requirements for the degree of Doctor of Philosophy at Virginia Commonwealth University.

by

Yung-Yeh Chang

Master of Science, Virginia Commonwealth University

August 2004

Director: Alen Docef Ph.D.

Associate Professor, Department of Electrical & Computer Engineering

Virginia Commonwealth University

Richmond, Virginia

December, 2011

Acknowledgment

To dear Mom, Dad, my beloved wife Min-Fen, and my son Ethan

This research project would not have been possible without the support of many people. I wish to express my gratitude to my advisors, Dr. Alen Docef who was abundantly helpful and offered invaluable assistance, support and guidance, and Dr. Kenneth Kraft, who has supported me throughout my thesis with his knowledge whilst allowing me access to the hospital facility to perform the experiments.

Deepest gratitude is also due to the members of the supervisory committee, Dr. Ashok Iyer, Dr. Afroditi V. Filippas, and Dr. Ding-Yu Fei. Without their knowledge and assistance, this study would not have been successful.

I would like to convey thanks to Prof. Dr. Panos Fatouros for inspiring and encouraging me to undertake this study. Special thanks also to the Siemens IDEA technical support team for the timely response and invaluable assistance.

Lastly, I wish to express my love and gratitude to my beloved families; for their understanding and endless love, through the duration of my studies.

Table of Contents

List of Tables

List of Figures

List of Abbreviations

Abbreviation	Full text
2D	Two dimensional
3D	Three dimensional
CSF	Cerebro spinal fluid
EPI	Echo-planar imaging, a MRI imaging technique
ETL	Echo train length, a turbo factor setting in a MRI sequence
GE	Gradient echo, a MRI pulse sequence
ICE	Image Calculation Environment in IDEA
IDEA	Integrated Development Environment Applications
IR-EPI	Inver recovery echo-planar imaging, a MRI pulse sequence
IR-FSE	Inversion recovery fast spin echo, a MRI pulse sequence
IRSE	Inversion Recovery Spin Echo, a MRI pulse sequence
LL	Look-Locker, a MRI pulse sequence
LM	Levenberg-Marquardt, a curve fitting algorithm
MR	Magnetic resonance
MRI	Magnetic resonance imaging
NMR	Nuclear magnetic resonance
POET	Sequence protocol editor in IDEA

RARE	Rapid Acquisition with Refocused Echoes, a MRI pulse sequence
RF	Radio frequency
RMSE	Root mean square error
ROI	Region of interest
SE	Spin echo, a MRI pulse sequence
SNR	Signal-to-noise ratio
T_1	Spin-lattice relaxation time
T_2	Spin-spin relaxation time
TE	Echo Time
TESO-IRFSE	Time efficient smart ordering inversion recovery fast spin echo, a MRI pulse sequence
TI	Inversion Time
TR	Repetition time

Abstract

A TIME-EFFICIENT METHOD FOR ACCURATE T_1 MAPPING OF THE HUMAN BRAIN

By Yung-Yeh Chang, MS

A dissertation submitted in partial fulfillment of the requirements for the degree of Doctor of Philosophy at Virginia Commonwealth University.

Virginia Commonwealth University, 2011.

Major Director: Alen Docef, Ph.D., Associate Professor,
Department of Electrical and Computer Engineering

The signal resulting from the IR-FSE sequence has been thoroughly analyzed in order to improve the accuracy of quantitative T_1 mapping of the human brain. Several optimized post-processing algorithms have been studied and compared in terms of their T_1 mapping accuracy. The modified multipoint two-parameter fitting method was found to produce less underestimation compared to the traditional multipoint three-parameter fitting method, and therefore, to result in a smaller T_1 estimation error. Two correction methods were proposed to reduce the underestimation problem which is commonly seen in IR-FSE sequences used for measuring T_1, especially when a large turbo factor is used. The intra-scan linear regression method corrects the systematic error effectively but the RMSE may still increase due to the increase of uncertainty in sequences with large turbo factors. The weighted fitting model corrects not only the systematic error but also the random error and therefore the aggregate RMSE for T_1 mapping can be effectively reduced. A

new fitting model that uses only three different TI measurements for T_1 estimation was proposed. The performance for the three-point fitting method is as good as that of the multipoint fitting method with correction in the phantom simulation. In addition, a new ordering scheme that implements the three-point fitting method is proposed; it is theoretically able to reduce the total scan time by 1/3 compared to the TESO-IRFSE sequence. The performance of the three-point fitting method on the real human brain is also evaluated, and the T_1 mapping results are consistent to with the conventional IR-FSE sequence. More samples of true anatomy are needed to thoroughly evaluate the performance of the proposed techniques when applied to T_1 mapping of the human brain.

Chapter 1 Introduction

Among clinical examination modalities, Magnetic Resonance Imaging (MRI) is one of the most widely used. It has been used not only to distinguish pathologic tissues (such as tumors) from normal tissues, but also in various quantitative analyses of pathologic conditions.[1-4] Contrast images like T_1- or T_2- weighted images have been routinely used in various scenarios, and they reasonably preserve anatomic detail. These types of images, however, are qualitative images that cannot accurately measure quantitative tissue parameters such as T_1 or T_2. The diagnosis of abnormal conditions would be much more practical if quantitative information could be conveniently obtained.

Recent research efforts have shown interest in quantifying the spin-lattice relaxation time (T_1), especially in brain tissue.[1-4] Many studies have reported that pathologic conditions such as brain edema, hydrocephalus, or stroke can be accurately detected by T_1 assessment.[1,2,5] The spin-lattice relaxation time, T_1, indicates the time required for a substance to regain longitudinal magnetization following an RF pulse.[6] T_1 values are directly affected by both the magnetic field strength and the water content of the tissues. The occurrence of brain edema, which implies a high water concentration with longer T_1 than normal brain tissues, can be then accurately evaluated by using T_1 images. This approach has been successfully used to detect brain edema

resulting from head trauma[1,2] as well as low-grade edema in patients with hepatic encephalopathy.[7]

The advantages of using quantitative imaging and especially T_1 mapping methods in MRI studies are evident. They provide an unambiguous evidence for the change of various pathologic conditions. Moreover, the inherent marked sensitivity of relaxation times to changes in water content, and the non-invasive nature of MR imaging make it more amenable to imaging critical organs. Since the T_1 parameter is an intrinsic property of tissue, it can be used to derive other quantitative parameters such as blood perfusion.[8] Knowing T_1 also allows radiologists to optimize some MR protocols; for example by choosing the optimum flip angle in T_1-weighted fat-suppressed images. Finally, a complete database of T_1 values for various tissues could provide a very valuable standard for miscellaneous analyses.

The main difficulty in T_1 mapping is the impractically long scan time, which is uncomfortable for the patient and can lead to inaccurate measurements due to patient motion. The gold standard method [9,10] for T_1 measurement, also known as inversion recovery spin echo (IR-SE) T_1 mapping, requires an extremely long repetition time (TR). For a reasonably accurate measurement of T_1, at least five different inversion times (TI) should be used. The whole process can take hours to complete for a large region of interest and high resolution image. Many efforts have been made to shorten the T_1 measurement time.[11-18] Most of them, however, propose methods to speed up the scanning time and fitting procedure at the expense of accuracy and precision. While these methods achieve good reproducibility, their accuracy still needs improvement. Moreover, a thorough analysis of the T_1 estimation errors has never been performed. Using these methods for diagnostic or quantitative assessment of disease may lead to incorrect conclusions.

Among these fast methods for T_1 mapping, the MR sequence developed by Zhu and Penn[15] is the closest to the gold standard method. Their time-efficient slice ordering inversion recovery fast spin echo (TESO-IRFSE) sequence utilizes a fast spin echo (FSE) and efficient ordering schemes to effectively shorten the total scan time. A whole brain scan with 12 slices can be completed within 12 minutes with the TESO-IRFSE sequence, and results in T_1 values with 5% relative error. The TESO-FSE sequence provides not only a reasonable scan time, but also accurate T_1 estimation. Although the TESO-IRFSE sequence is considered a relatively accurate and fast T_1 mapping method, the effects of T_1 mapping accuracy due to change in sequence protocol settings have not been properly studied. Besides, the T_1 mapping post-processing algorithm for IRFSE sequence has never been optimized. We are also aware that the hardware incompatibility by reason of different makes of scanners restricts the usability of clinical T_1 mapping application. We hardly see TESE-IRFSE sequence in use in any known scenario such as research of a particular disease or clinical examination. Therefore, we also try to identify the difficulties of implementing the sequence and improve the efficiency based on the optimized algorithm while it is possible.

T_1 being such an important property of tissues, we believe that quantitative T_1 measurement will be widely put to use. To that end, a robust, fast and accurate T_1 measuring method needs to be developed. Our perspective is to try to further shorten the T_1 measurement by reducing not only the scan time, using a time-efficient pulse sequence, but also the post-processing algorithm. In order to achieve our objective, a full study on MRI imaging for T_1 estimation method is very important. We first examined the signals obtained from IR-FSE sequence under the constraint of using a finite repetition time. The quality of the signal was carefully evaluated. A number of phantom simulations were properly set up for performing an in-depth analysis on different curve

fitting methods for T_1 estimation. From the result of analysis, we justified the need of each TI value and developed a new fitting method, which requires only three measurements with different inversion times, while achieving a level of accuracy better than the original fitting method. The result of phantom simulation shows that the three-point measurement is better in terms of accuracy and efficiency of T_1 estimation than multipoint fitting methods. The precision, however, slightly decreases compared to multipoint fitting methods in our simulation. We also investigated methods that optimally exploit correlations between different T_1 measurements in the IR-FSE MRI sequence. The efficiency is then further improved by choosing proper initial parameters while applying Levenberg-Marquardt (LM) algorithm in the fitting. The correlation between TI measurements also helps to calibrate the measurement data and therefore increases the accuracy. In addition, a real human experiment shows that the three-point subtraction fitting method is more sensitive to the dramatic change in T_1 values and movement artifacts.

Chapter 2 Background

2.1 Relaxation Times and T_1 Mapping

The spin-lattice relaxation time (T_1) and spin-spin relaxation time (T_2) are two basic tissue characteristics widely used in MRI. These relaxation times describe how fast nuclear magnetization brought to non-equilibrium state returns to the equilibrium state. T_1 or T_2 relaxation times vary from tissue to tissue in human body. For example, fluids have longer T_1 (1500-2000 ms) than fat-based tissues (100-150 ms). During the relaxation process, spins start to lose energy they absorbed from the pulse and the released signals can be picked up by the antenna in the coils. The different intensity of signals induced by T_1 and T_2 will then be able to be interpreted by a signal processing algorithm and reproduce the contour of internal tissues. These images which have contrast depending on either T_1 or T_2 are called T_1- or T_2-weighted images. Both T_1- and T_2-weighted images can be produced using either spin echo (SE) or gradient echo (GE) sequences. With proper parameter settings for the pulse sequences, physicians can distinguish pathological changes of tissues.

2.1.1 Spin-Lattice Relaxation Time (T_1)

Spin-lattice or longitudinal relaxation time (T_1) is the time constant, which determines the rate at which excited protons return to equilibrium within the lattice. The spinning protons will re-align with the external magnetic field and the magnetization will grow after a 90˚ flip angle excitation from zero to a value of about 63% of its final value in a time of T_1.

Water in the bulk phase present in cerebro-spinal fluid (CSF) has a long T_1 relaxation time because the frequency of its natural motions is much higher than the range of Larmor frequencies used clinically. In the case of interstitial edema (due to ventricular obstruction), however, the T_1 relaxation time of CSF will become much shorter. The T_1 shortening reflects the fact that water is now in hydration layers around the myelin protein rather than in the bulk phase because CSF is forced out into the periventricular white matter.

2.1.2 Spin-Spin Relaxation Time (T_2)

Spin-spin or transverse relaxation time (T_2) is the time constant for the loss of phase coherence among spins following a 90° RF pulse. The decay is due to magnetic interactions that occur between spinning protons. This results in a loss of the MRI signal. T_2 is always shorter than T_1 for a given tissue (Figure 1). Water-based tissues tend to have longer T_2s than fat-based tissues.

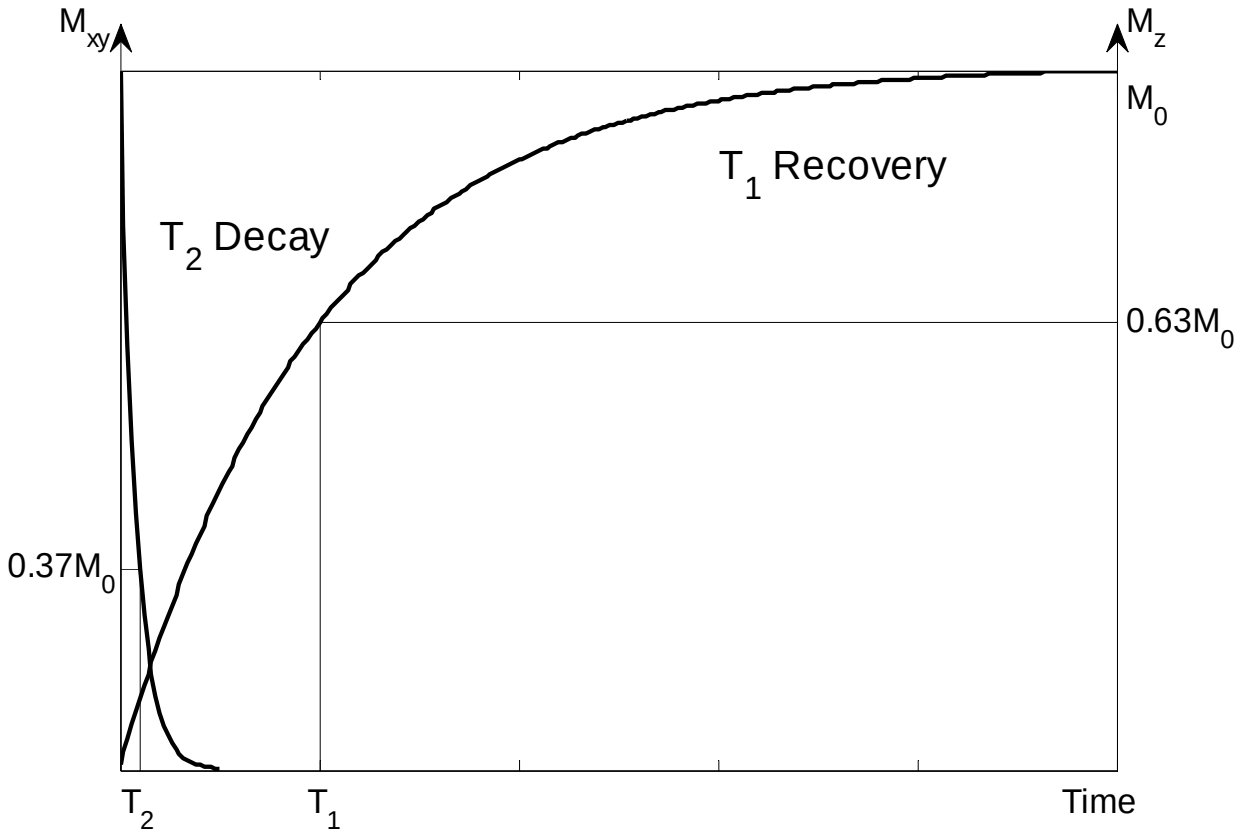

Figure 1 T_1 and T_2 relaxation occur simultaneously, but T_2 is much quicker than T_1.

2.1.3 T_2 under the Effect of a Poor Magnet

The quality of the main magnetic field (also known as inhomogeneity, see next section) will cause differences in the precession rate. A poor magnet may cause a rapid loss in transverse magnetization and, therefore a shortening of the T_2 relaxation process. The combined effect of true T_2 and an imperfect magnetic field is known as T_2^* (Figure 2). The T_2^* quantity is commonly observed in sequences (please refer to pulse sequences, section 2.2) without refocusing gradient, while the true T_2 signal can be only measured with sequences that have a 180° rephasing pulse before data acquisition. In addition, since the net magnetization is affected,

the influence of T_2^* will lead to a different contrast image, and may potentially deteriorate the accuracy of T_1 measurement.

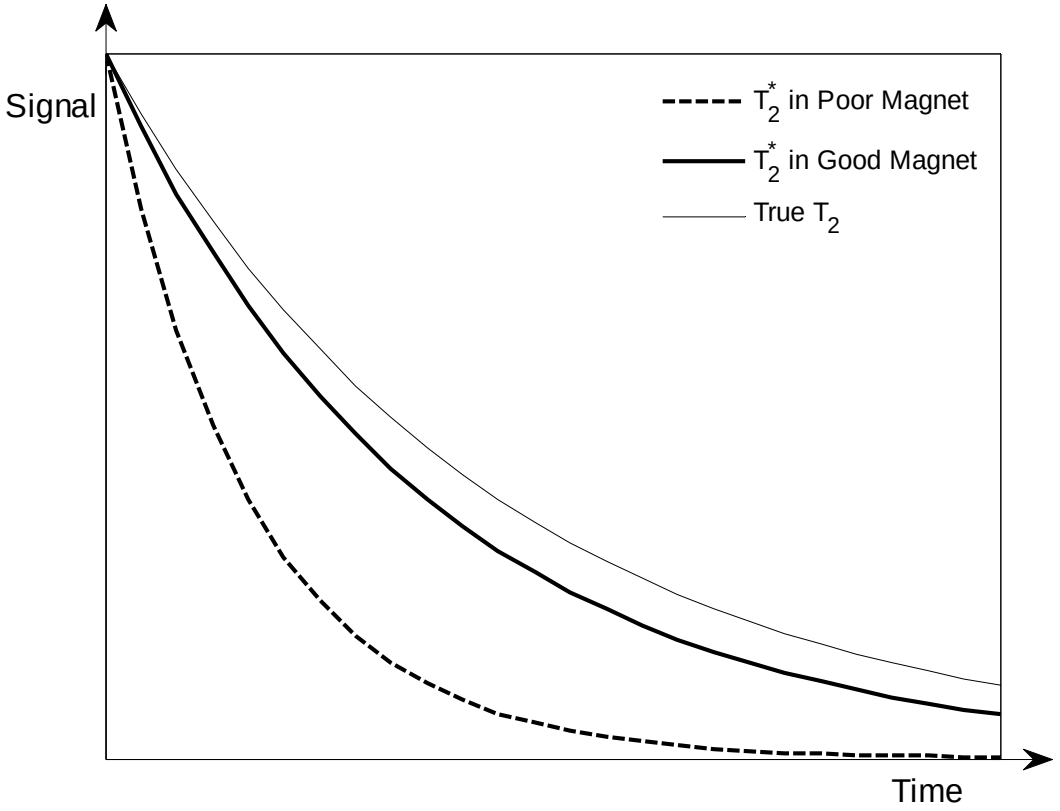

Figure 2 Effect of inhomogeneity on T_2 relaxation

2.1.4 Inhomogeneity

Inhomogeneity in MRI refers to a lack of uniformity in the main magnetic field. Static magnetic field inhomogeneity, usually caused by hardware imperfections, is an unavoidable phenomenon. Field inhomogeneity accelerates transverse relaxation, and its severity is usually expressed using the time constant T_2^* (Figure 2). Although spin echo sequences are not very sensitive to external magnetic field inhomogeneity, in gradient echo sequences, it may cause a significant frequency shift, and therefore change the signal intensity and produce image distortions. The undesired change in the brightness of pixels may cause problems in imaging different tissues. As for the geometrical distortion, resulting in displacement of the pixel locations, it can be problematic in

some cases such as stereotactic brain surgery. Manufacturers try to make the magnetic field as homogeneous as possible; however, even with an ideal magnet, small inhomogeneities remain due to susceptibility effects within the human body.

2.1.5 k-space

In MRI, raw data consists of a matrix of frequency-encoded signals known as k-space. The axes of k-space (2D or 3D) have units of spatial frequency or cm^{-1}. Typically a data buffer temporarily stores the raw data prior to image processing. The complex array of raw data points is treated as a two-dimensional grid with x and y axes corresponding to frequency encoding and phase encoding respectively. In conventional 2D image acquisition, the k-space is filled with raw data one line, every TR milliseconds. The resulting k-space will have the same number of columns and rows as the final image. The final contrast image is obtained by taking the 2D Fourier transform of the k-space data (Figure 3).

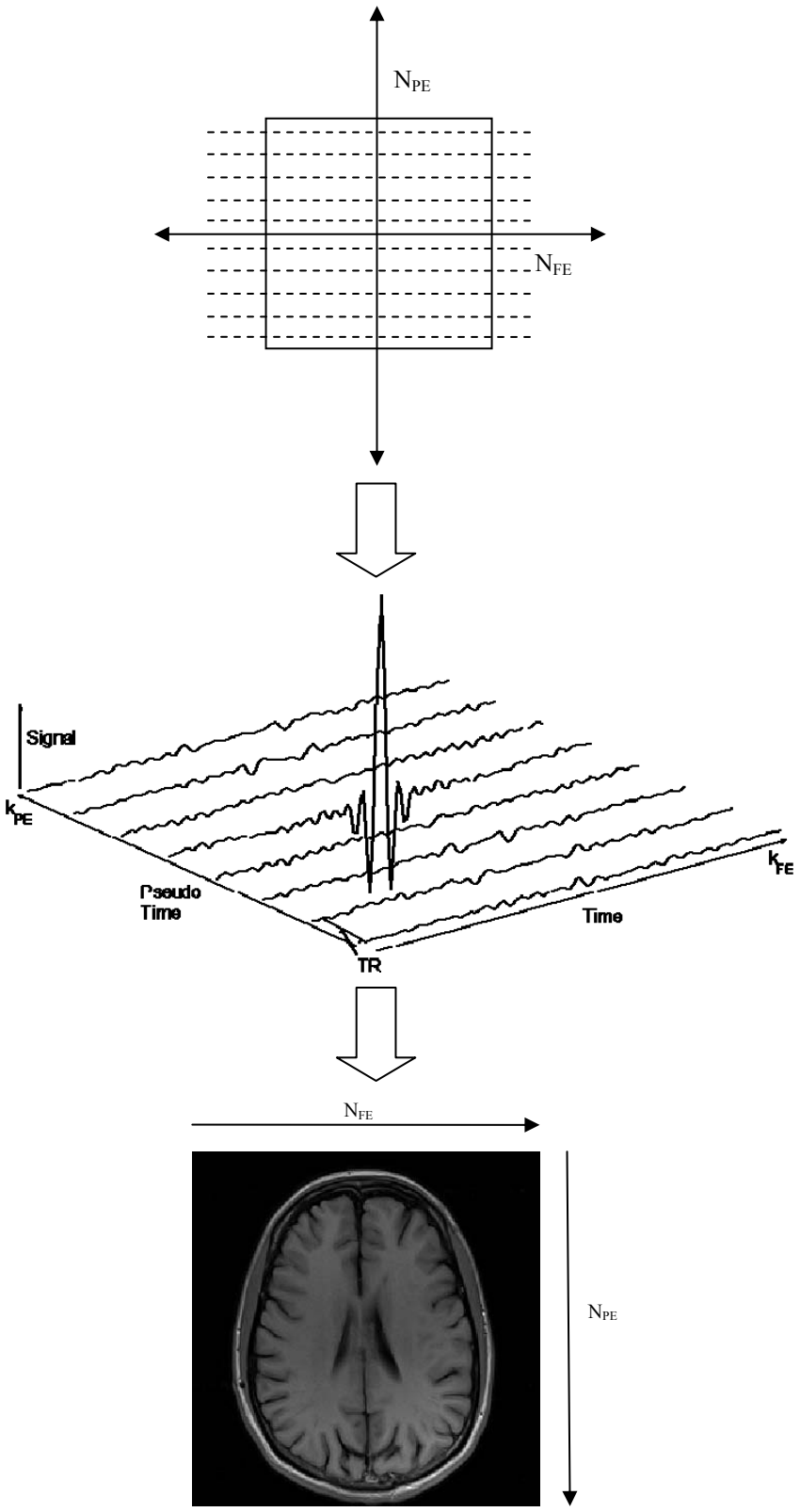

Figure 3 k-space and data acquisition line

2.2 Introduction to Pulse sequences

The engineer's point of view of MR sequences is that they are computer programs that control the MR measurement hardware. More specifically, an MRI pulse sequence is a combination of radio frequency (RF) pulses designed to acquire the image data. These RF pulses, running in specific order with selected time intervals between them, will control the nuclear magnetic resonance (NMR) signal reception and affect the characteristics of MR images. Depending on the clinical application, an MRI sequence may be repeated many times during a scan in order to obtain sufficient data to reconstruct images from NMR signal samples.

Every image sequence must consist of excitation RF pulses and gradients for excitation and localization. The tissue magnetization is first excited using an RF pulse in the presence of a slice select gradient. This gradient ensures that only protons in one slice of tissue are excited. Phase encoding and frequency encoding are additionally used to spatially localize the protons in the other two dimensions. Finally, the process is repeated for a series of phase encoding steps for collecting the entire desired region of interest (ROI). For a particular MR sequence, parameters such as the repetition time (TR), echo time (TE), inversion time (TI), and flip angles can be chosen to best suit the clinical application. These parameters allow the differentiation of tissues within the body and the highlighting of specific pathology.

Gradient Echo (GE) and Spin Echo (SE) are two fundamental pulse sequences. In the GE sequence (Figure 4, right), a negative gradient is applied right after an α° excitation pulse for rapidly dephasing the transverse magnetization. Then a positive gradient is applied to rephase the spins. The positive gradient, however, only compensates for the dephasing caused by the negative gradient lobe. The echo will be formed after all the spins return to the initial position.

Because the GE sequence uses a low flip angle excitation pulse (usually less than 90°), the recovery of longitudinal magnetization is faster and therefore by using shorter TR, the scan time is reduced. However, imaging with a gradient-echo sequence is intrinsically more sensitive to magnetic field inhomogeneities because of the refocusing gradient. Thus the GE sequence produces an image (referred to as of T_2^*, section 2.1.3) which is a combination of T_2 and magnetic field inhomogeneities.[6]

The SE sequence (Figure 4, left) was the first MR sequence ever used. It is based on a repetition of 90° and 180° RF pulses. After applying a 90° excitation pulse, the spins start to dephase naturally. A 180° rephasing RF pulse is applied at TE/2 (half of the echo time) to form an echo at TE (Echo Time). A k-space line is filled at every repetition with different phase encoding. The SE sequence introduces true T_2 dependence to the signal, thus differentiating between tissue with similar T_1 values but different T_2 values.

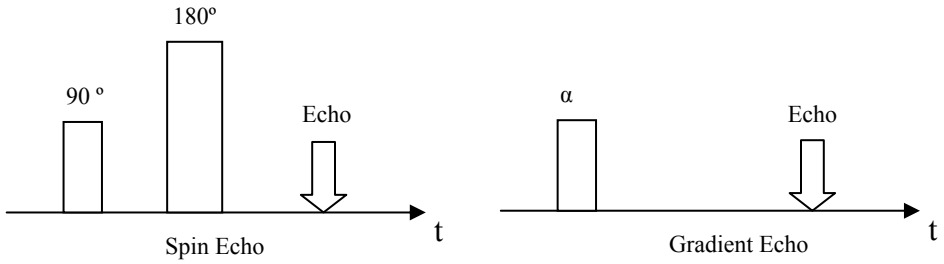

Figure 4 A spin echo sequence (left) and a gradient echo sequence (right).
α is the flip angle and is typically less than 90° for gradient echo pulse sequence

A special variation of the spin echo sequence is worth mentioning because it is very important to T_1 measurement. The inversion recovery sequence (Figure 5) has an extra 180° RF pulse followed by the 90° RF pulse in the spin echo sequence. A sequence parameter, the inversion time (TI) is the duration between the initial 180° RF pulse and the following 90° RF pulse, and it must be selected in the sequence protocol settings. A short TI sequence can be used for fat

suppression to suppress the fat signal.[6] The traditional T_1 measurement makes use of signals with multiple TI values; the details of this approach will be discussed in section 2.3.

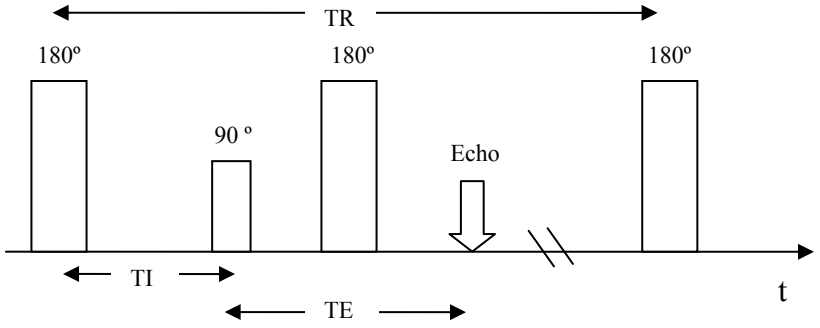

Figure 5 Inversion recovery spin echo sequence

2.3 Introduction to T_1 Measurement Methods

Both T_1 and T_2 can be measured in either spectroscopy or imaging applications. If using an inversion recovery spin-echo pulse sequence (IRSE) with a 90° flip angle, the measured signal will be, in theory

$$S = M_0 \left[1 - e^{-\frac{TI}{T_1}}\right] e^{-\frac{TE}{T_2}} \quad (1)$$

Thus, T_1 can be measured by fitting this formula to multiple measurements with different TI values and long enough TR. T_2 also can be measured by plotting the signal height at each TE. Real measurements of T_1 or T_2, however, are affected by other phenomena, such as the diffusion of protons through an inhomogeneous magnetic field (which adds an irreversible dephasing for the T_2 measurement), or field strength dependency for T_1 measurement. In addition, the fitting equation must be modified to fit different sequences.

Before delving into the various methods for measuring T_1, a brief discussion on assessing the performance of these methods is necessary. The *accuracy* of a particular method is a measure of the discrepancy between the measured and the true T_1 values. It has been shown that to determine water content with an absolute precision of $\Delta w = 0.01$, the T_1 must be computed with a relative precision of $\Delta T_1/T = 0.04$ at the magnetic field strength $B_1 = 1$ T. [19] Previous studies have demonstrated that an accuracy of approximately 2 - 7% can be achieved, which varies depending on the T_1 values of measured subjects.[1,15,17] In our work, we use the normalized root mean square error (RMSE) to quantify accuracy. The RMSE is given by

$$\mathrm{RMSE} = \sqrt{\frac{\sum_{\mathrm{ROI}}\left(\hat{T}_1 - \mathrm{T}_1\right)^2}{N}} \tag{2}$$

where $\hat{T}_1$ is the measured value, T_1 is the true value, and N is the number of voxel in the region of interest (ROI). The summation is taken over all the voxels in the ROI. Another performance metric we may refer to is the *precision*, which measures the statistical deviation of measured T_1 values from the mean in a region where it is supposed to be constant. To quantify precision, we use the conventional standard deviation. A good T_1 measurement should have standard deviation as small as possible, thus indicating high precision of a measurement method. According to the studies with similar multi-echo based T_1 measurement sequences, the statistical standard deviation in the ROI is approximately less than 1- 4% of the estimated values for a phantom study.[15,20] Finally, *reproducibility* is a metric often reported, especially when true T_1 values are not available. It measures the ability to obtain the same T_1 values when the MRI study is repeated and it can be quantified using the RMSE between the studies.

2.3.1 The Conventional Method for T_1 Mapping

The conventional method to measure T_1 is to estimate the longitudinal magnetization recovery curve using the inversion recovery (IR) pulse sequence.[4,6] The IR pulse sequence consists of two parts, a selective inversion pulse and a self-contained sequence such as a RF spin-echo (SE) or gradient echo (GE). The IR/SE combination is most commonly used for T_1 measurement. The spins are first flipped to the 180° position, and then samples of the longitudinal magnetization at different times are taken until all spins are back to the fully relaxed condition. The set of measured amplitudes thus obtained is then used to determine the T_1 values for the tissues.

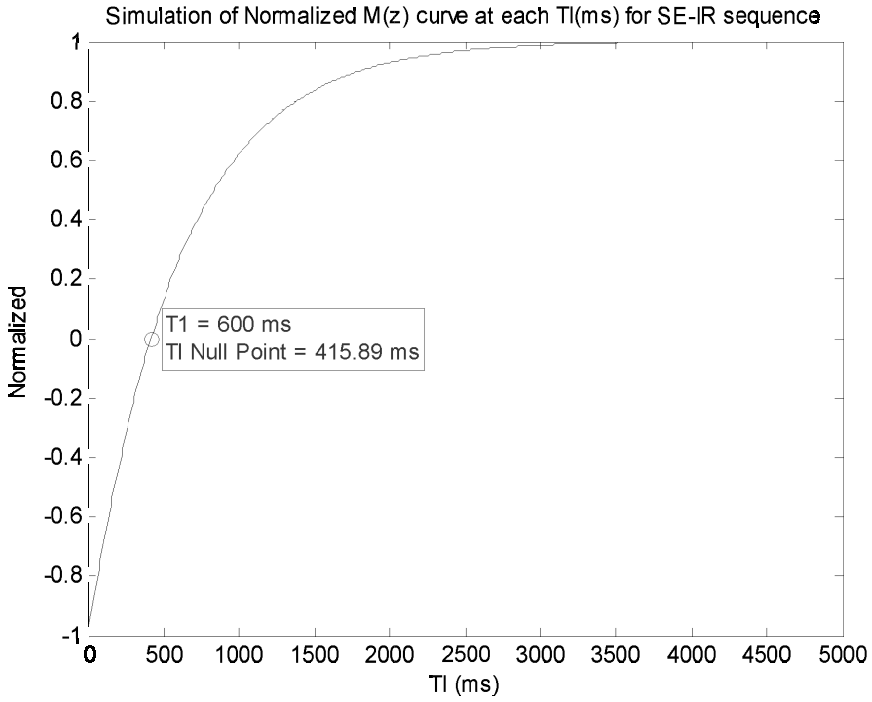

Figure 6 This plot shows the curve of magnetization signal along z axis at each TI for inversion recovery spin echo pulse (IR-SE) sequence. For T_1 = 600 ms, the TI null point (M_z = 0) is at 415.89 ms.

Figure 6 demonstrate the T_1 recovery process. The curve in Figure 6 is sampled repeatedly using the 180° inversion recovery spin echo pulse sequence with various sample time TI. At each TI, the magnetization at the end of the excitation is:[21]

$$M_z(TI) = M_0\left[1 - (1 - \cos\theta_{inv})e^{-\frac{TI}{T_1}}\right] \quad (3)$$

where $M_z(t)$ is the longitudinal magnetization as a function of time, M_0 is the initial magnetization at t = 0, and θ_{inv} is the flip angle of the inversion pulse. However, Equation (3) only holds when TR is infinitely long. If TR is finite, an additional term appears:

$$M_z(TI) = M_0\left[1 - (1 - \cos\theta_{inv})e^{-\frac{TI}{T_1}} + e^{-\frac{TR}{T_1}}\right] \quad (4)$$

If we only consider the optimal condition with a flip angle θ_{inv} = 180° and very long TR, Equation (4) becomes:

$$M_z(TI) = M_0\left[1 - 2e^{-\frac{TI}{T_1}}\right] \quad (5)$$

One particularly useful point on this curve is its zero-crossing. $M_z(TI_{null}) = 0$. The relationship between TI_{null} and T_1 is given by,

$$TI_{null} = \begin{cases} T_1 \ln 2 & TR \to \infty \\ T_1\left[\ln 2 - \ln\left(1 + e^{-\frac{TR}{T_1}}\right)\right], \text{for SE sequence with finite TR} \end{cases} \quad (6)$$

When collecting several samples, one can fit the longitudinal magnetization recovery curve (Figure 6) using the above model to estimate the T_1 value. Five or more points are usually required for T_1 estimation, and the TR should be at least 5 times the tissue's T_1 value in order to obtain accurate results. These requirements imply a long scan time. For example, a 256 × 128 pixel image, calculated from N = 6 points using a repetition time TR = 3.0 s, requires an exam

time equal to 128 × 6 × 3 s, i.e., 39 min. A whole brain study can take up to 7 hours. This makes higher-resolution T_1 mapping impractical.

2.3.2 The Look-Locker Method

The Look-Locker (LL) pulse sequence[22] was originally proposed for spectroscopy. The sequence consists of an initial inversion pulse, followed by a train of acquisition RF pulses. The acquisition RF pulse has a small, constant flip angle and quickly samples the transient phase to obtain a set of build-up recovery curves from the prepared longitudinal magnetization. Finally, T_1 is estimated using the least squares curve fitting procedure. Depending on the required image resolution, the sequence must be repeated numerous times to fill in every line in k-space. In addition, each image can have a unique delay time.

Since a single recovery curve can be inspected with only one preparation pulse, one can avoid the need for long delays between several inversions, thereby consuming less time compared to the conventional method. This method, however, still requires the return to equilibrium of the spin system before the next application of an RF pulse, thus the acquisition time per slice can still be long. Additionally, the LL method suffers from the sensitivity of the T_1 measurements to the flip angle used for the excitation pulse. Low flip angle excitation pulses also result in a reduced signal-to-noise ratio.

More recent studies incorporated Echo-planar imaging (EPI) into the inversion recovery LL-based method[22], by using a nonselective broadband 180° RF pulse followed by interleaving EPI readout for eight different slices. Because EPI acquisition method acquires a complete k-space within only one repetition time, the reduction of scan time can be astonishing. A complete image can be formed from a single preparation pulse. In addition, the LL-EPI sequence uses a special

slice order for every repeated scan to optimize the time efficiency. Although LL-EPI and other its variants [23-25] have proved that the measurement time for T_1 can be significantly reduced, the IR-EPI method sacrifices precision and accuracy to some extent. Images acquired using EPI are extremely prone to image artifacts (such as ghosting), susceptibility distortions and poor spatial resolution. These artifacts cause signal distortion or signal loss, and thus make quantitative measurements unreliable.

The combination of EPI and LL methods does not solve any intrinsic problems caused by either of the methods. The low signal-to-noise ratio resulting from the low flip excitations and the EPI acquisition might not be solved by averaging several repeated scans. The accuracy of the LL-EPI based method, however, remains questionable and could get worse especially for ROIs away from the center of the RF coil. Thus, the LL-EPI method would only be suited to dynamic or single-slice studies unless the above issue can be solved.

2.3.3 The TESO-IRFSE Sequence

The Inversion Recovery Fast Spin Echo with Time-Efficient Slice Ordering (TESO-IRFSE) method has been developed by Zhu and Penn for fast and accurate acquisition of inversion recovery images.[15] The T_1 value for each pixel on every slice is later calculated using curve fitting.

The sequence is basically a combination of Clare and Jezzard's time-efficient slice ordering method[13] and an IR-FSE sequence. Unlike the common IR sequence, the IR-FSE sequence makes use of a 180° nonselective Silver–Hoult adiabatic inversion RF pulse, which inverts spins within the entire sensitive volume, at the beginning of the sequence. The Silver–Hoult adiabatic

inversion RF pulse can provide a uniform inversion of spins even when the pre-existing B_1 field is not uniform. After a selected inversion time (TI) delay, fast spin echo for at least two echo trains would then be utilized for acquiring selected imaging data. While the first segment of data acquisition has finished, the second FSE takes place after the same amount of TI time. The sequence proceeds in the same fashion until all slices have been imaged.

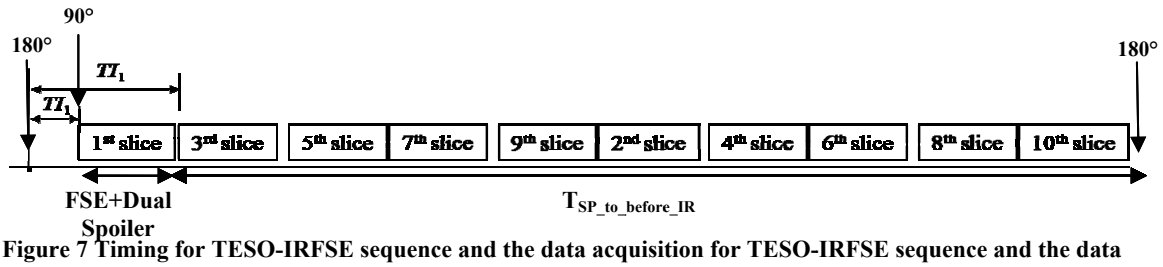

Figure 7 Timing for TESO-IRFSE sequence and the data acquisition for TESO-IRFSE sequence and the data acquisition.

Due to the use of a nonselective inversion RF pulse, the order of data acquisition for slices is neither sequential nor interleaved. Two slices are acquired at each TI increment with a very small gap (about 50 ms), and they are chosen every other slice (Figure 8). The data acquisition for the second slice-ordering scheme starts from the second group of the first slice-ordering scheme. Data are acquired in the same fashion as the first slice-ordering scheme, and all other new slice-ordering schemes also follow the same positioning manner until all different TI for each slice have been obtained. Finally, the T_1 in the region of interest is calculated based on the longitudinal magnetization recovery curve. With the TESO-IRFSE method, the acquisition time is reduced to 1/10 compared to the conventional method.

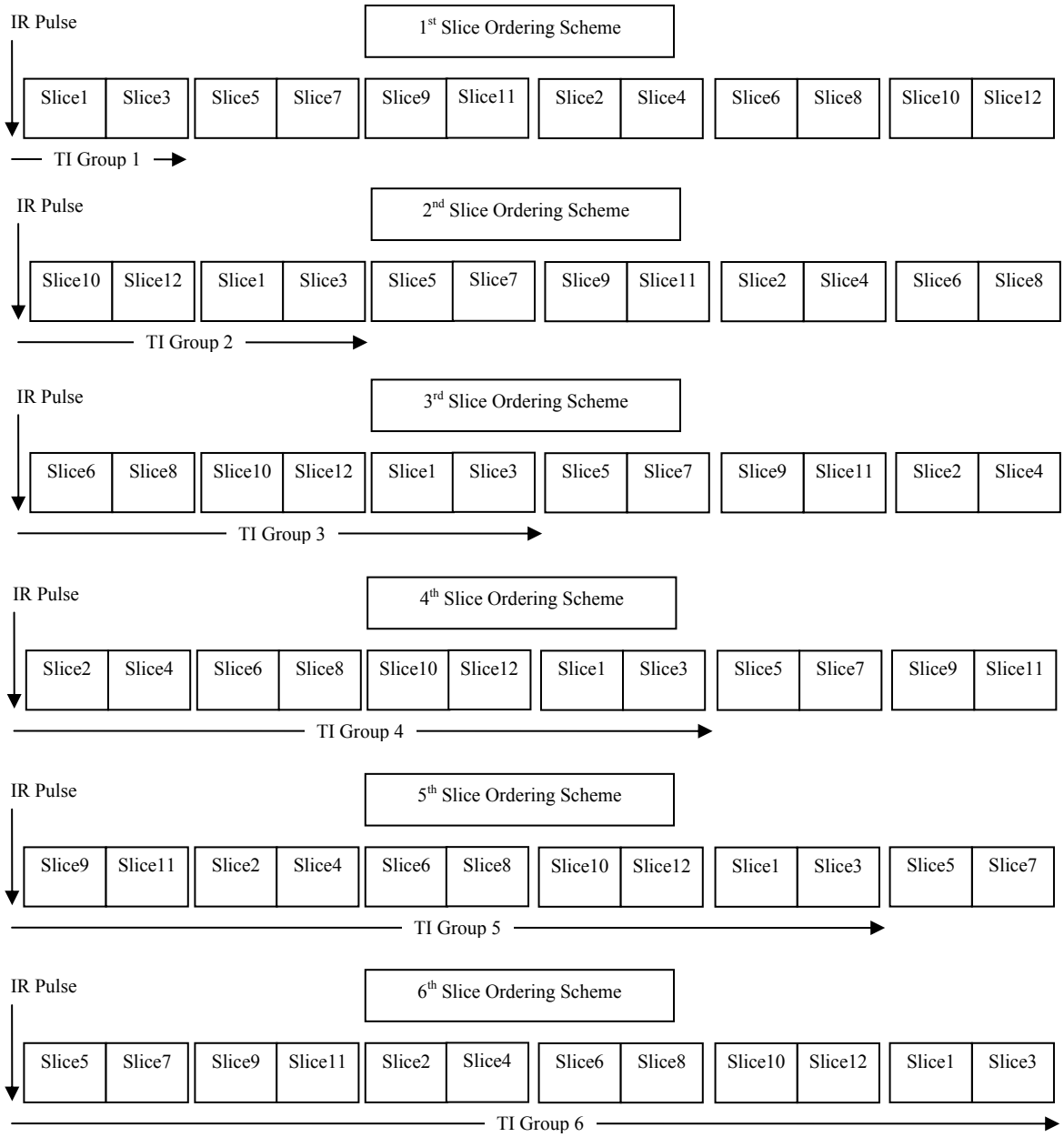

Figure 8 The complete slice ordering schemes for the TESO-IRFSE sequence

Overall, the TESO-IRFSE method has the following advantages.

1. It makes precise higher-resolution scan within reasonably short scan time possible.
2. It has high reproducibility.
3. FSE sequence is now widely used in clinically, and therefore it should be readily implemented on all modern scanners.
4. The reordering pattern is not difficult to configure.

While providing these advantages described above, the TESO-IRFSE sequence is not perfect. The standard procedure will require N = 6 or more points in order to produce an accurate curve fitting. Further research indicated it is possible to use fewer points of TIs with an advanced fitting algorithm while maintaining estimation accuracy.[26-33] If this is true, reducing the scan to only a few minutes for the whole brain could be possible, too. We have also noticed that Zhu's sequence employs the absolute value of the measured signal instead of the real (signed) signal.

The zero-crossing point could be seriously miscalculated and therefore lead to incorrect T_1 estimation. The errors produced by magnetic field inhomogeneity were not adequately examined, either. Although the TESO-IRFSE technique is much less prone to magnetic field inhomogeneity than the gradient-echo images methods, its performance in highly inhomogeneous magnetic field also needs to be further studied.

Chapter 3 Research Design and Methods

3.1 General Equation for the IR-SE and IR-FSE Sequences

In the early research, after data was acquired with the IR-SE sequence, only two parameters were used in the fitting model, the magnetic strength in the steady state and the estimated T_1. [34-37] Some researchers realized that the two-parameter fitting model might lead to inaccurate T_1 estimation due to the underlying assumption of perfect inversion pulses.[4,7] A third parameter, the flip angle, was included in the fitting model in order to ensure that the system imperfections are taken into consideration. Although using a three-parameter fitting model usually requires more acquisition points and increases the reconstruction complexity, several studies have reported an improvement in accuracy for T_1 estimation.[37,38] In contrast to the three-parameter fitting model, the precision of the two-parameter fitting model can be improved as TR is increased with constant TI times, and the amount of improvement found varied with T_1.[11,18] In a nutshell, the traditional two-parameter fitting model may produce more precise results for very long TR, but the three-parameter model may still be more accurate.

Unfortunately, the above conclusion may not be completely satisfactory to the signals measured with the IR-FSE (rather than IR-SE) sequence because these studies usually did not consider the off-resonance effect (crosstalk) during a multi-slice scan[11,33] or the magnetization transfer which

occurs in most biological tissues.[39] The effect of using different fitting models is also not clear while data were measured with the IR-FSE sequence.

The FSE sequence is a commercial version of the generic RARE (Rapid Acquisition with Refocused Echoes) sequence.[6] It commonly uses evenly spaced multiple refocusing pulses for data acquisition. A series of 180° excitation pulses forms an echo train. The extra echoes used by the FSE sequence collect additional data in different regions of k-space within a signal repetition time TR. Therefore, it reduces the number of phase encodings times by a factor equal to the number of echoes. The factor is called the echo train length (ETL) or turbo factor. Larger turbo factors using more refocusing echoes will result in a significant reduction in total scan time. However, edge blurring and loss of signal strength are likely to occur when using a large turbo factor.

The IR-FSE sequence uses an inversion recovery with a 180° flip angle. The T_1 relaxation can be measured by recording signals at different polarization duration. The magnetization strength is described by the equation[15]

$$\mathrm{S(TI)} = k \cdot M_0 \cdot e^{-\frac{\mathrm{TE}}{\mathrm{T_2}}} \cdot \left[\left(1 - e^{-\frac{\mathrm{TI}}{\mathrm{T_1}}}\right) - f_{\mathrm{inv}} \cdot \left(1 - e^{-\frac{\mathrm{T_{sp\_to\_before\_IR}}}{\mathrm{T_1}}}\right) e^{-\frac{\mathrm{TI}}{\mathrm{T_1}}}\right] \qquad (7)$$

where M_0 is the longitudinal magnetization under fully relaxed conditions, $T_{sp\_to\_before\_IR}$ is the time between the last refocusing pulse and the next Inversion time, f_{inv} is the effective spin inversion fraction and k is a scaling constant that is dependent on the hardware, scan settings, and image reconstruction algorithm. The Equation (7) assumes that a spoil gradient was applied after the last echo was collected. The parameter, f_{inv}, is a measure of the quality of the applied 180° inversion pulse.

Assuming that the scaling factor *k* remains constant for all scans, Equation (7) is reduced to

$$\mathrm{S(TI)} = S_0 \cdot \left[\left(1 - e^{-\frac{\mathrm{TI}}{\mathrm{T_1}}}\right) - f_{\mathrm{inv}} \cdot \left(1 - e^{-\frac{\mathrm{T_{sp\_to\_before\_IR}}}{\mathrm{T_1}}}\right) e^{-\frac{\mathrm{TI}}{\mathrm{T_1}}}\right] \tag{8}$$

where $S_0 = kM_0e^{-TE/T2}$ is the equilibrium magnetization signal. One can compare this to a general equation derived by Rydbery[40] for the FSE pulse sequence

$$\mathrm{S(TI)} = S_0 \cdot \left(1 - (1 - cos\,\theta_{inv})e^{-\mathrm{TI/T_1}} + e^{-(\mathrm{TR-TE_{last}})/\mathrm{T_1}}\right) \tag{9}$$

where θ_{inv} is the flip angle of the IR pulse and $\mathrm{TE_{last}}$ is the echo time of the last echo in the echo train. Because ($\mathrm{T_{sp\_to\_before\_IR}}$+TI) in Equation (8) is approximately equal to (TR-TE), Equation (8) and Equation(9) are equivalent. In addition, Equation (9) more clearly shows the effect of a finite repetition time on the signal. It is worth noticing that although the flip angle, θ_{inv} in Equation (9), might be known in the sequence, it is usually treated as an unknown variable in the fitting procedure because one cannot assume that full inversion was achieved.

Ideally, if the relative error can be minimized in an experiment, in the sense that as TE approaches zero and TR becomes much longer than $\mathrm{T_1}$, the spin-lattice relaxation curve become a function of TI only. $\mathrm{T_1}$ can then be calculated by fitting the observed data to the Equation (8) or Equation (9). If the maximum TI value ($\mathrm{TI_m}$) is selected to be as close as possible to TR, then $\mathrm{S(TI_m)}$ is approximately equal to $\mathrm{S_0}$, Equation (8) can then be simplified by dividing the MR signal by $\mathrm{S_0}$:

$$R_{\mathrm{i}} = \frac{\mathrm{S(TI_i)}}{\mathrm{S_0}} = \left(1 - e^{-\frac{\mathrm{TI_i}}{\mathrm{T_1}}}\right) - f_{\mathrm{inv}} \cdot \left(1 - e^{-\frac{\mathrm{T_{sp\_to\_before\_IR}}}{\mathrm{T_1}}}\right) e^{-\frac{\mathrm{TI_i}}{\mathrm{T_1}}} \tag{10}$$

This normalized equation preserves the same characteristic of T_1 relaxation. The unknown parameters are reduced from three to two, and therefore, the efficiency of the fitting procedure is increased. Although a long TR that results in full magnetization recovery is preferred in order to achieve maximum accuracy, it is not practically feasible due to a prohibitively long scan time. In application of finite TR, however, the accuracy of T_1 estimation using Equation (10) will suffer from the inaccurate estimation of S_0 for high T_1 values as well as the measured uncertainty in TI_m even if S_0 is measured separately. A two-parameter fit may still work by taking the $S(TI)/S(TI_m)$ ratio if k is indeed constant for every scan:

$$R_{\mathrm{i}} = \frac{S(\mathrm{TI(i)})}{S(\mathrm{TI_m})} = \frac{\left(1 - e^{-\mathrm{TI(i)}/\mathrm{T_1}}\right) - f_{\mathrm{inv}} \cdot \left(1 - e^{-\mathrm{T_{SP\_tobefore\_IR}}/\mathrm{T_1}}\right) \cdot e^{-\mathrm{TI(i)}/\mathrm{T_1}}}{\left(1 - e^{-\mathrm{TI_m}/\mathrm{T_1}}\right) - f_{\mathrm{inv}} \cdot \left(1 - e^{-\mathrm{T_{SP\_tobefore\_IR}}/\mathrm{T_1}}\right) \cdot e^{-\mathrm{TI_m}/\mathrm{T_1}}} \qquad (11)$$

where i and "m" are indices referring to the i^{th} and the longest TI values, respectively, with i = 1, 2, 3,. . ., max. The normalized Equation (11) has eliminated the dependency on k, M_0, TE and T_2, but the overall accuracy of T_1 estimation may decrease due to increased noise in the estimated T_1. It also worth noticing that although the fitting procedure using Equation (11) has two unknown parameter, it is different from the popular two-parameter fit which assumes a perfect flip angle [34-36].

It is generally believed that multipoint fitting generates the most accurate and consistent results for T_1 estimation.[37] From a statistical perspective, with N (N>3) images corresponding to N points along the relaxation curve, the systematic error randomly generated by the system imperfections is diminished. Therefore, the precision of estimation is assured to be in an acceptable range. The accuracy, however, is always the question.

3.2 Correction with a Linear Regression Function

Zhu and Penn[15] observed that their time-efficient IR-FSE technique consistently underestimate brain T_1 values. In fact, T_1 underestimation is a known issue for IR-FSE sequence and some of the gradient echo based T_1 measuring sequences with rapid multi-echo acquisition.[15,17,37,41,42,43] Our own acquisitions using the IR-FSE method confirms this asymmetry in the T_1 estimation error. This effect has been attributed to interslice interference by Zhu and Penn.[15] They believe that because the excitation and refocusing RF pulses have imperfect slice profiles, spins in slices acquired later in the ordering scheme can be influenced by earlier acquired slices. Other researchers suggested that another cause for T_1 underestimation may be the magnetization transfer (MT) effect.[26,41-44] This effect causes a reduction in the observed T_1 values especially when a greater number of echoes are used in the multislice IR-FSE sequence.[42]

From the results of Zhu and Penn's study, the T_1 estimation error appeared to remain at the same level. Therefore, to compensate for the underestimation, the authors proposed a simple correction formula that proved to be effective for small underestimation errors. The "true" T_1 is related to its "apparent", or measured value, T_{app}, via the formula

$$\frac{1}{T_1} = \frac{A}{T_{app}} + B \tag{12}$$

where A and B are constants to be determined through linear regression for a set of known (T_1, T_{app}) pairs. The estimation error was cut in half when this correction was applied. In Zhu and Penn's work, the known (T_1, T_{app}) values used to determine the parameters A and B were obtained from a separate scan with a smaller turbo factor (ETL=2) that takes twice as long as the actual scan (ETL=4). The former was used as ground truth for the latter. This method was used

just for error analysis and clearly cannot be used for actual scanning, or else the small turbo factor scan would be used for T_1 mapping.

We propose instead a different calibration method that uses several vials filled with standard gel of known T_1 and placed around the head, perhaps fastened on an attachment to the head coil. The steps involved in calibrated T_1 mapping are as follows: The patient's head is scanned with the calibration vials in place using a time-efficient IR sequence. The MR images are reconstructed and the calibration vials are segmented. The set of calibration pixels is extracted and a collection of (T_1, T_{app}) pairs is used to compute the parameters A and B in equation (12) via linear regression.

Equation (12) is applied to the remaining pixels in the reconstructed MR images. Here we assumed that the parameters A and B are constant across the entire scan, an assumption also made by Zhu and Penn. A phantom simulation will be conducted to verify this assumption.

In theory, only two standard gels are reacquired because there are only two parameters to be computed. In reality, a robust estimate is obtained by using more than two gels. The minimum number of gels is a parameter that will be determined experimentally. The T_1 values for the gels should be chosen to cover the range of T_1 values of interest, roughly 500 to 1000 ms. Notice that this technique does not directly affect the scan time, but improves accuracy and therefore potentially allows a more aggressive use of time-saving techniques. Its only disadvantages are the requirement for a customized head coil and a very small overhead in postprocessing time.

3.3 Correction with a Weighted Fitting Model

Although the T_1 underestimation seems to remain at the same level and may be corrected by applying a linear regression process, more issues may be introduced by applying the linear regression function. For example, tissues with low T_1 values may be exaggerated due to a larger volume of tissue having high T_1 values. After thorough analysis of the signal and noise within the IR-FSE sequence, our preliminary study indicates that the underestimated T_1 estimation is possible to be corrected by exploiting the relationship between signal, noise, and SNR.

We have proposed a correction to the fitting model.[45] Our proposed improvements to the existing T_1 mapping method follows from the experimental observation that echo signal measurements for different values of the inversion time TI are affected by noise differently. In other words, the random variables Si consist of the echo signal and different amounts of noise. Therefore, the N measurements are not equally reliable. This observation can be exploited by giving more emphasis to more accurate signals. We achieve this goal by employing different weights in the cost function used in the curve fitting:

$$\{T_1, f_{inv}\} = \arg\min_{T_1, f_{inv}} \sum_{i=1}^{n-1} w_i \left| \left| \frac{S(T_1, M, f_{inv}, TI_i)}{S(T_1, M, f_{inv}, TI_m)} \right| - \left| \frac{S(\mathrm{TI_i})}{S(\mathrm{TI_m})} \right| \right| \quad (13)$$

If the statistical properties of the measurement noise were known, one could attempt to find the optimal weights w_i analytically. Our own analysis indicates that the noise level increases with TI (Chapter 4.2.1). This suggests that, to emphasize the more reliable measurements, which are those with smaller absolute values, a reasonable choice for the weights w_i is

$$w_i = \frac{1}{|S_i|^{\alpha}} \tag{14}$$

where α is a real number to be determined. This approach has been used, for a weighted mean-square cost function with α = 2, by Bakker [46], in the context of sign restoration when only the magnitude of the IR signal is available.

Since no analytical optimization of the weights can be carried out, due to the lack of a model for measurement noise, we choose the weights according to Equation (14) and we optimize the parameter α using experimental data obtained from a phantom study, where the ground truth (true T_1) is available. The optimum value of α is determined by minimizing the T_1 estimation error over the entire image. The resulting value is to be used for subsequent clinical studies. We should point out that the optimum α is not a constant to be used for any IR-FSE sequence; it is very likely to vary when sequence parameters and scanner model are changed.

The optimum α is also likely to be different for tissues with different relaxation time T_1. Using phantom studies with simulated tissues with different T_1 values, this dependency can be tabulated. Therefore, we propose a two-pass adaptive T_1 estimation technique that attempts to exploit this variation. In a first pass, a rough T_1 map is obtained by minimizing a cost function that uses a globally optimal α. Then, for each pixel, based on the rough estimate, we choose the locally optimal α from the table obtained in the phantom studies. Finally, a refined T_1 estimate is obtained by using the locally optimal α in the cost function.

3.4 The Three-point Subtraction Method

Assume that the inversion recovery RF pulse is performed perfectly, with very short TE and very long TR. Equation (9) will then approximate to

$$M_z(TI) = M_0\left(1 - (1 - \cos\alpha)e^{-TI/T_1}\right) \tag{15}$$

Therefore, the equation can be linearized by taking the natural logarithm of $(1\text{-}R_i)$:

$$D(TI) = \ln\left(\frac{M_0 - M_z}{M_0}\right) = \ln(1 - \cos\alpha) - \frac{TI}{T_1} \tag{16}$$

If $\alpha = 180^{\circ}$, Equation (16) becomes

$$\ln\left(\frac{M_0 - M_z}{M_0}\right) = \ln\left(2e^{-TI/T_1}\right) = \ln(2) - \frac{TI}{T_1} \tag{17}$$

From Equation (16), the T_1 value can be easily calculated by evaluating the coefficients of the first order polynomial fit. This method was first proposed by Hahn[10] and later its accuracy was validated by comparison to other fitting methods by Gerhard et al.[47] The method, unfortunately, was found to produce poor results due to the following reasons:

(1) Error from an unknown M_0 could result in a non-linear curve.

(2) Taking the logarithm will lose the signal weight. By taking the logarithm, the linearization transformation may change the influence of signal data as well as the error structure of the model. The inferential result may end up unpredictable.

(3) Simulation has shown large variation in areas with large signal amplitude.

(4) Measurement may be time dependent.

Similar difficulties were identified by George et al.[48] It was concluded that the linear fit method would only be valid for measuring short T_1 values. More issues arise for larger T_1 due to the variance of M_0 even if M_0 is measured separately.

In the literature, the least square fit with a non-linear function or its variation seemed to be the most preferred and the results were the most reliable. Although the accuracy is doubtful using a semi-log T_1 linear function, the method was not completely abandoned. We interestingly found that a number of researchers tried to take advantage of the T_1 linear function and managed to achieve equally good accuracy as a non-linear fit could.[29,49] Furthermore, the T_1 linear function has been taken to its extreme for T_1 estimation with only two measurements using gradient echo (GE)[32] or spin echo (SE)[28] for data acquisition.

When TR is constrained in order to achieve a certain degree of time efficiency, the linearity found in Equation (16) is lost when we apply the same logarithmic transform to Equation (8). The result of $\ln(1-R_i)$ becomes

$$\begin{aligned}\ln(1-R_{\mathrm{i}}) &= \ln\left(e^{-\frac{\mathrm{TI_i}}{\mathrm{T_1}}} - e^{-\frac{\mathrm{TI_m}}{\mathrm{T_1}}}\right) + \ln(1+f_{\mathrm{inv}}) \\ &- \ln\left(\left(1-e^{-\frac{\mathrm{TI_m}}{\mathrm{T_1}}}\right) - f_{\mathrm{inv}}\cdot\left(e^{-\frac{\mathrm{TI_m}}{\mathrm{T_1}}} - e^{-\frac{-(\mathrm{TR}-\mathrm{TE})}{\mathrm{T_1}}}\right)\right)\end{aligned} \tag{18}$$

The linearity can be restored by increasing TR,

$$\ln(1-R_{\mathrm{i}}) \approx \ln(1+f_{\mathrm{inv}}) - \frac{\mathrm{TI(i)}}{\mathrm{T_1}}, \text{for TR} >> 5\mathrm{T_1} \tag{19}$$

Since Equations (8) and (9) are equivalent, Equation (11) would have similar result by taking $\ln(1-R_i)$

$$\ln(1-R_{\mathrm{i}}) = \ln\left(1 + f_{\mathrm{inv}} \cdot \left(1 - e^{-\frac{\mathrm{T_{sp\_to\_before\_IR}}}{\mathrm{T_1}}}\right)\right) + \ln\left(e^{-\frac{\mathrm{TI_i}}{\mathrm{T_1}}} - e^{-\frac{\mathrm{TI_m}}{\mathrm{T_1}}}\right) - \ln\left[\left(1 - e^{-\frac{\mathrm{TI_m}}{\mathrm{T_1}}}\right) - f_{\mathrm{inv}} \cdot \left(1 - e^{-\frac{\mathrm{T_{sp\_to\_before\_IR}}}{\mathrm{T_1}}}\right) e^{-\frac{\mathrm{TI_m}}{\mathrm{T_1}}}\right] \quad (20)$$

Equation (20) is very sensitive to f_{inv}, which typically varies among tissue types and field strengths from 0.84 to 0.99.[15] The effect of TI_m also becomes significant for large T_1. While a constrained TR compromises the linearity property of the logarithmic T_1 relaxation curve, the linearity may be still preserved, as shown below. A computer simulation was performed to further examine the effect of computing $ln(1-R_i)$ subjected to finite repetition time and the result is illustrated in Figure 9. It appears that the linearity is still preserved at the range of lower TIs which can be utilized to estimateT_1 with negligible loss of accuracy.

With proper selection of two TI values, in addition to TI_m, T_1 can be calculated using the difference between the two transformed values from the result of Equation (20) :

$$\ln\left(1 - \frac{\mathrm{S_1}}{\mathrm{S_m}}\right) - \ln\left(1 - \frac{\mathrm{S_2}}{\mathrm{S_m}}\right) = \ln\left(\frac{\mathrm{e}^{-\frac{\mathrm{TI_1}}{\mathrm{T_1}}} - \mathrm{e}^{-\frac{\mathrm{TI_m}}{\mathrm{T_1}}}}{\mathrm{e}^{-\frac{\mathrm{TI_2}}{\mathrm{T_1}}} - \mathrm{e}^{-\frac{\mathrm{TI_m}}{\mathrm{T_1}}}}\right), \mathrm{TI_1} \neq \mathrm{TI_2} \quad (21)$$

Therefore, a fitting model is suggested using the target function:

$$\mathrm{J} = \left[\frac{1 - \frac{\mathrm{S_1}}{\mathrm{S_m}}}{1 - \frac{\mathrm{S_2}}{\mathrm{S_m}}} - \frac{e^{-\frac{\mathrm{TI_1}}{\mathrm{T_1}}} - e^{-\frac{\mathrm{TI_m}}{\mathrm{T_1}}}}{e^{-\frac{\mathrm{TI_2}}{\mathrm{T_1}}} - e^{-\frac{\mathrm{TI_m}}{\mathrm{T_1}}}}\right]^2, \mathrm{TI_1} \neq \mathrm{TI_2} \quad (22)$$

The fitting model has only one parameter, and therefore T_1 is obtained using a one-dimensional search.

A least square non-linear fitting procedure will be carried out for estimating T_1 by searching the minimum absolute difference for both sides of Equation (22).

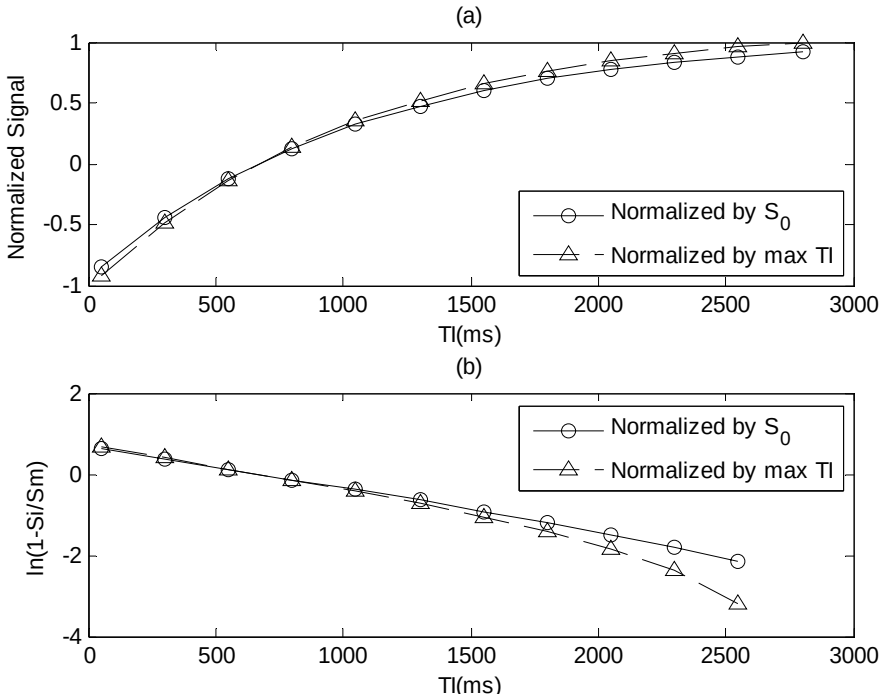

Figure 9 The change of T_1 relaxation curve (computer simulation) due to normalization factor which magnetization is not at fully relaxed state. (a) Original measure curve without transformation. (b) With transformation

3.5 Selection of Points and Polarity Restoration

3.5.1 The selection of TI_m, and the (TI_1, TI_2) Pair

Three measurements, for TI_1, TI_2, and TI_m, are required for the fitting model described by Equation (22). Because fewer measurements are taken, it is anticipated that this method is very sensitive to the selection of inversion times. Since TI_m is only used as a normalization factor and has to be the maximum TI, the remaining sequence parameters to be determined are TI_1 and TI_2.

From Figure 9 and Equation (18), it is rather clear that TI_m should be as close as possible to TR to prevent the curve from being further distorted. Besides, there is good evidence showing that it is very important to choose TI_m as close to TR as possible in order to increase the precision, especially for high T_1 values.[50] The actual options for TI_m may be confined by hardware limitations and the design of a sequence. Once TI_m is determined, theoretically, we can estimate T_1 accurately by using any two measurements in the low TI range (100 to1300 ms) by taking the logarithmic transformation, $\ln(1-R_i)$. However, statistical measurement errors in each scan will seriously affect the precision of the estimated T_1. Without properly choosing TI_1 and TI_2, it is possible to achieve a large error when estimating T_1 and the results may become unpredictable. In order to minimize the estimation error, the standard deviation of the estimated T_1, σ_{T1}, must be minimized by choosing the optimal TI pair. Assuming that TI_m is pre-determined, this minimization can be carried out by the theory for the propagation of errors.[28,30,51] The evaluation of σ_{T1} is in fact identical to the two-point models which have been previously mentioned.[28,32] Therefore, we have obtained the T_1 variance σ_{T1}^2 as:

$$\sigma_{T_1}{}^2 = \frac{S_1{}^2 + S_2{}^2}{S_2 \frac{\partial S_1}{\partial T_1} - S_1 \frac{\partial S_2}{\partial T_1}} \sigma_s{}^2 \tag{23}$$

where σ_s^2 is the variance of the measured signal. To simplify the case, we assume that every acquired signal has the same constant variance although this assumption may not be completely true.[52] The inconstancy for the variance of acquired signals is also observed in our preliminary results for signal analysis. Therefore, we will later perform an independent analysis to validate this assumption and adjust Equation (23) if necessary. A further derivation can be done by introducing the standard equation of T_1 relaxation with the assumption of ideal condition, which is only used here to simplify the case.

$$\frac{\sigma_{T1}}{T_1} = \frac{\sigma_s}{2S_0}\left(\frac{T_1}{TI_2 - TI_1}\right)\frac{\sqrt{e^{-\frac{2TI_1}{T_1}} + e^{-\frac{2TI_2}{T_1}}}}{e^{\frac{-(TI_1+TI_2)}{T_1}}} \tag{24}$$

TI_1 and TI_2 must be different to avoid the singularity from the term $1/(TI_2\text{-}TI_1)$ from equation (24). On the other hand, TI_2 should have a good SNR, which is defined as (S/σ_s), to avoid the potentially increasing of error for measuring T_1 due to the counterbalanced effect between $1/(TI_2\text{-}TI_1)$ and $1/\exp(-(TI_1+TI_2)/TI_1$.

3.6 Polarity Restoration

MR images are generally displayed in magnitude form so that tissues can be readily visualized without considering signal phase and polarity. The lack of the support for real (signed) signal values, however, can seriously deteriorate the accuracy of T_1 estimation. This can be critical in running most of the curve fitting algorithms. Figure 10 shows a typical example where the signal

obtained around TI = 550 ms is vague. The estimated T_1 using LS fitting algorithm can result in more than 3% error if the signal sign at TI = 550 ms is determined improperly. In the TESO-IRFSE method[15], Zhu proposed a fitting discrepancy measure designed to use only the absolute measurement values to calculate T_1.

$$D = \left| \sum_{i=1}^{n-1} \left| \frac{S_i}{S_m} \right| - \left| \frac{\left(1 - e^{-\frac{TI_i}{T_1}}\right) - f_{inv} \cdot \left(e^{-\frac{TI_i}{T_1}} - e^{-\frac{(TR-TE)}{T_1}}\right)}{\left(1 - e^{-\frac{TI_m}{T_1}}\right) - f_{inv} \cdot \left(e^{-\frac{TI_m}{T_1}} - e^{-\frac{(TR-TE)}{T_1}}\right)} \right| \right| \quad (25)$$

Equation (16) seems to be able to avoid the polarity issue but in fact, the error caused by loss of signal polarity persists if a measurement value is too close to zero. While this is a reasonable mean to avoid the limitations of scanner hardware or measurement protocol, the uncertainty of the zero-crossing point will eventually become a critical issue, especially for longer T_1 values.

The issue of uncertainty of the zero-crossing point can be easily solved by obtaining the true signed signal. For clinical MRI applications, unfortunately, the true signed signals may not be always available due to the limitations of scanner hardware or sequence protocol. Although obtaining the true signed signals is the best solution, an alternate, reasonable solution for restoring the polarity of signals can be very helpful.

Several approaches to restore the magnetization polarity have been proposed.[8,46,53-57] Bakker et al [46] proposed a method that searches the zero-crossing point using a weighted second-order polynomial with magnitude data by assuming the one with lowest intensity has a known polarity. Instead of running the numerical search on an exponential model, the quadratic function provides a better efficiency in polarity restoring procedure. Additionally, the zero-crossing searching method does not require a modification of the current sequence or an extra reference scan.[56] A later review[37], however, suggested that with current level of available computer power, it would

be better to fit the magnitude data the correct exponential formula rather than with a quadratic function. Besides, Bakker's approach would fail for very long or very short T_1.

Other approaches[53,54,56,57] try to restore magnetization polarity by using a phase correction technique, which usually require a slight modification of the sequence and an additional scan. An interesting solution proposed by Kim et al[55] to solve the loss of polarity information does not intend to explicitly restore the magnetization polarity. Instead, they add an offset to each image from the one with longest TI to produce a set of signals with only positive intensities. The resulting signal is a monotonic exponential decay and therefore is more suitable to be used in the exponential fitting routine according to the T_1 relaxation equation. The drawback of this method is that additional noise is introduced by the subtraction procedure and a traditional SE data acquisition is preferred to minimize such noise. A more recent publication proposed a new multipoint fitting model that is more robust to solve SE multipoint T_1 mapping problem.[8] Their RD-NLS-PR (reduced dimension nonlinear least square with polarity restoration) method solves the missing signal polarity issue statistically with only magnitude data and does not require searching the zero-crossing time directly.

The methods mentioned above are usually more applicable to multipoint fitting algorithms, and therefore, restoring magnetization polarity may not be easily achievable for a limited number of acquisition data points as is in the case for method we have proposed in previous section. When an additional scan or a modification of the sequence is not realistic, a slight modification to Barral's method[8] seems to be the best solution.

Because the general T_1 relaxation function given by Equations (7) and (9), always assume a monotonically increasing function, we are able to solve the loss of signal polarity issue by

combining the T_1 relaxation function with a polarity restoration function.[8] We first define the sign-shifting function γ as

$$\gamma_{TI_{null}}(TI_i) = \begin{cases} -1, & TI \le TI_{null} \\ 1, & TI > TI_{null} \end{cases} \tag{26}$$

where the zero-crossing point (TI_{null}) is defined such that

$$\left(1 - e^{-\frac{TI_{null}}{T_1}}\right) - f_{inv}\left(1 - e^{-\frac{T_{sp\_to\_before\_IR}}{T_1}}\right)e^{-\frac{TI_{null}}{T_1}} = 0 \tag{27}$$

and f_{inv} is a constant indicating an imperfect inversion recovery RF pulse. Although it is possible to estimate f_{inv} with a two-parameter fitting method described in Equation (25), an adequate, fixed value of f_{inv} is satisfactory to be used in the polarity restoration procedure. A value of 0.85 to 0.95 is suggested with other multipoint fitting methods.[15,20] It would be reasonable to use a smaller value of f_{inv} for real tissues and a larger value for a phantom simulation.

Since the magnetization is zero at TI_{null}, we let $TI_2 = TI_{null}$ in Equation (21)

$$\ln\left(1 - \frac{S_1}{S_m}\right) = \ln\left(\frac{e^{-\frac{TI_1}{T_1}} - e^{-\frac{TI_m}{T_1}}}{e^{-\frac{TI_{null}}{T_1}} - e^{-\frac{TI_m}{T_1}}}\right) \tag{28}$$

Thus, T_1 and TI_{null} can be estimated by minimizing the following fitting model

$$J_{TI_{null}} = \left[\sum_{i=1}^{2}\left[\gamma_{TI_{null}}(TI_i)\left(1 - \frac{S_i}{S_m}\right) - \left(\frac{e^{-\frac{TI_i}{T_1}} - e^{-\frac{TI_m}{T_1}}}{e^{-\frac{TI_{null}}{T_1}} - e^{-\frac{TI_m}{T_1}}}\right)\right]\right]^2 \tag{29}$$

One will need to perform a 3-D search using the optimization criterion in Equation (29). The case, however, can be simplified because the value of TI_{null} is available from Equation (28):

$$\mathrm{TI_{null}} = \mathrm{T_1}\left(\ln\left(1 - \frac{\mathrm{S_1}}{\mathrm{S_m}}\right) - \ln\left(e^{-\frac{\mathrm{TI_1}}{\mathrm{T_1}}} - \frac{\mathrm{S_1}}{\mathrm{S_m}}e^{-\frac{\mathrm{TI_m}}{\mathrm{T_1}}}\right)\right) \tag{30}$$

With the basic assumption that the signal intensity is increasing and $TI_2 > TI_1$, thus, running a 1-D search two times using Equation (22) is adequate. The best solution will be the computed (T_1, TI_{null}) pair which satisfies the following estimate:

$$(\mathrm{T_1}|\mathrm{TI_{null}}) = \arg\min_{\mathrm{T_1}}\left[\left|\left(1 - e^{-\frac{\mathrm{TI_{null}}}{\mathrm{T_1}}}\right) - f_{\mathrm{inv}}\left(1 - e^{-\frac{\mathrm{T_{sp\_to\_before\_IR}}}{\mathrm{T_1}}}\right)e^{-\frac{\mathrm{TI_{null}}}{\mathrm{T_1}}}\right|\right] \tag{31}$$

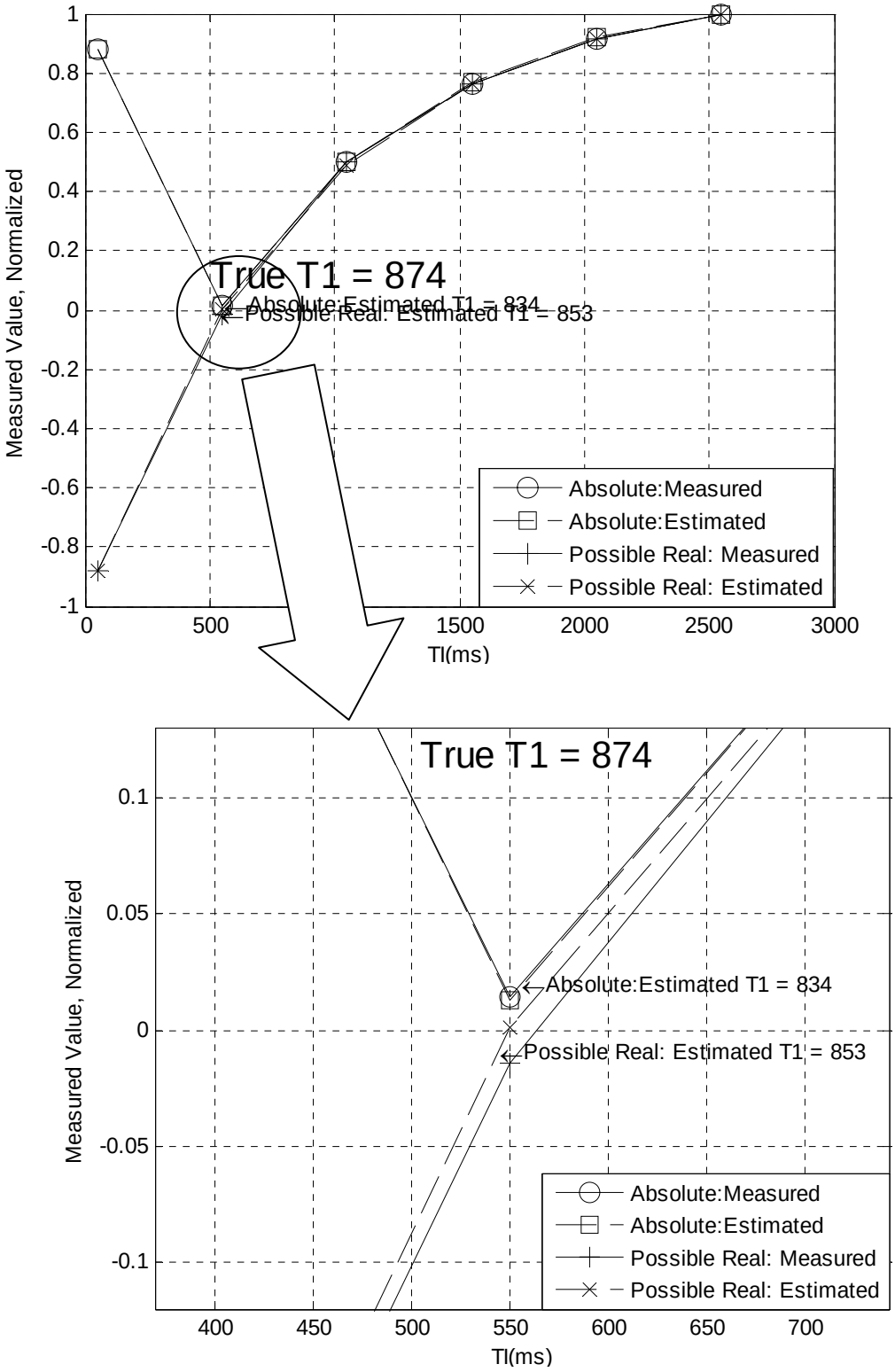

Figure 10
The improvement of T_1 estimation if the sign of the measured value can be restored.

3.7 Experiment Design and Sequence Protocol Settings

3.7.1 Phantom Development and True T_1 measurement

A tissue-mimicking phantom was developed to evaluate the performance and accuracy of the proposed T_1 mapping methods. The material of the phantom is made of nickel-doped agarose gel according to the method developed by Kraft et.al. [58] The proton relaxation time for this type of gel is less sensitive to temperature and magnetic field fluctuations. Therefore, this material is the best choice for use in quantitative relaxometry.

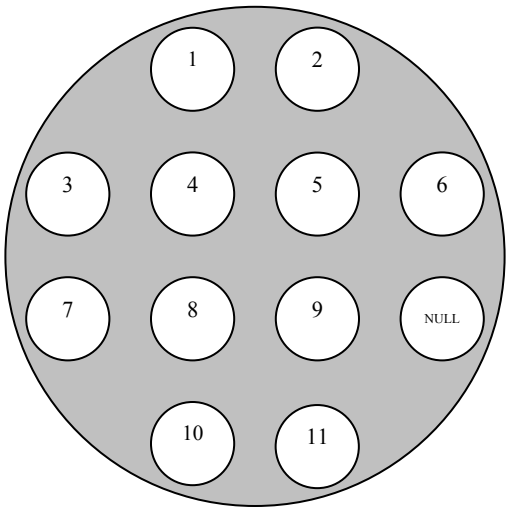

Figure 11 Phantom for evaluation of T_1 mapping method

The phantom designed in our experiment consists of 11 tubes containing the nickel-doped agarose gels with known T_1 and T_2 values. Each tube was carefully filled with 50 ml of gel solution and sealed properly. Ideally, desired T_1 and T_2 values distributed uniformly so each phantom tube holds only one T_1 and T_2 values. Table 1 lists the amount of each component added in the tube to achieve the required relaxation time. The T_1 range from approximately 550 to 1250 ms was selected for creating these tubes. For T_2, range is from approximately 60 to 110

ms. The ranges of T_1 and T_2 are selected according to the normal range of normal brain tissues measured with a 1.5 T MR scanner.[15,41,59] Labels were then marked on each tube for clear visual identification. After preparation, all tubes were inserted into a precut block of polystyrene filled with deionized water. There are 12 holes in the block but only one hole (position for Tube number 10) is left unused for effortless orientation identification (Figure 11).

Table 1 MRI phantom tube configuration and T_1/T_2 values of gels

T_1, ms	T_2, ms	Total Vol, (mL)	X, Ni (mM)	Y, % Agar	Stock Ni add, (mL)	Agarose add, (g)	Water add (mL)	Tissue
600	80	50	1.94	1.2381	0.970	0.627	49.030	WM, brain: 1.5 T
700	80	50	1.59	1.2653	0.793	0.641	49.207	WM, brain: 1.5 T
750	80	50	1.44	1.2762	0.557	0.513	49.278	WM, brain: 3.0 T
850	100	50	1.21	1.0084	0.605	0.513	49.395	GM, brain: 1.5 T
900	100	50	1.11	1.0159	0.557	0.513	49.443	GM, brain: 1.5 T
950	100	50	1.03	1.0226	0.513	0.517	49.487	GM, brain: 3.0 T
1200	100	50	0.7	1.0476	0.350	0.929	49.650	GM, brain: 3.0 T

Before using the tissue mimicking phantom for actual T_1 mapping, we verified if the designed phantom gel tubes meet the specific requirements. This was achieved by using NMR spectroscopy, which achieves very high accuracy at the cost of losing all spatial information. A Bruker Biospec NMR spectrometer 24/40 at 2.4 T was used to measure the T_1 values of these tubes with the gold standard method described in Section 2.3.1. Three different sets of TIs were selected for different ranges of T_1 subjects and were listed in Table 2.

The values measured using NMR spectroscopy are then considered the true T_1 values and used as a reference in later comparisons and analyses.

Table 2 Sets of TI values for NMR T_1 measurement

T_1 up to 750 ms	T_1 up to 1000 ms	T_1 up to 1500 ms
TI (ms)	TI (ms)	TI (ms)
30	30	30
100	150	200
300	400	600
600	700	1200
1000	1300	2200
1800	2500	3500
2800	4000	5000
4000	6000	7500

3.7.2 The Sequence Development Tools Environment

We had obtained the TESO-IRFSE sequence developed by Dr Zhu[15] for preliminary studies on a 3 T medical system scanner (GE Healthcare, Waukesha, WI). Shortly thereafter, the GE scanner has been phased out though in favor of a more recent 1.5 T Siemens Magnetom Avanto (Siemens Medical Systems, Iselin, NJ). Unfortunately, the sequence developed for the GE system using EPIC (Environment for Pulse programming In C) was not compatible with the Siemens sequence programming environment, IDEA (Integrated Development Environment Applications). In order to make the required modifications to the current pulse sequence, it was necessary to study the Siemens sequence programming environment.

The programming software used by Siemens is IDEA, a C++ programming environment working under the Microsoft Windows XP operating system. IDEA allows developers to simulate the measurement and image calculation of the Magnetom scanner. It is an integrated package that consists of several tools: a sequence programming environment including a C++ compiler, (SDE, Figure 12), a pulse sequence test run and simulation tool (Figure 13)), an image reconstruction tool (Image Calculation Environment, or ICE), and a sequence protocol editor

(POET, Figure 19). In addition, the IDEA environment relies on a pre-installed C++ compiler to generate executable sequences.

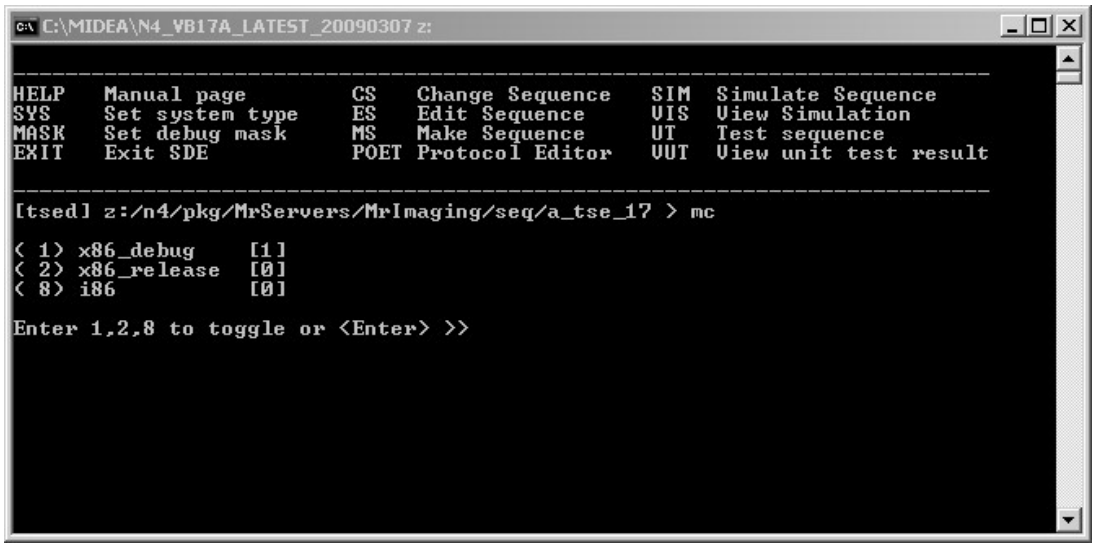

Figure 12 The Siemens IDEA SDE common window

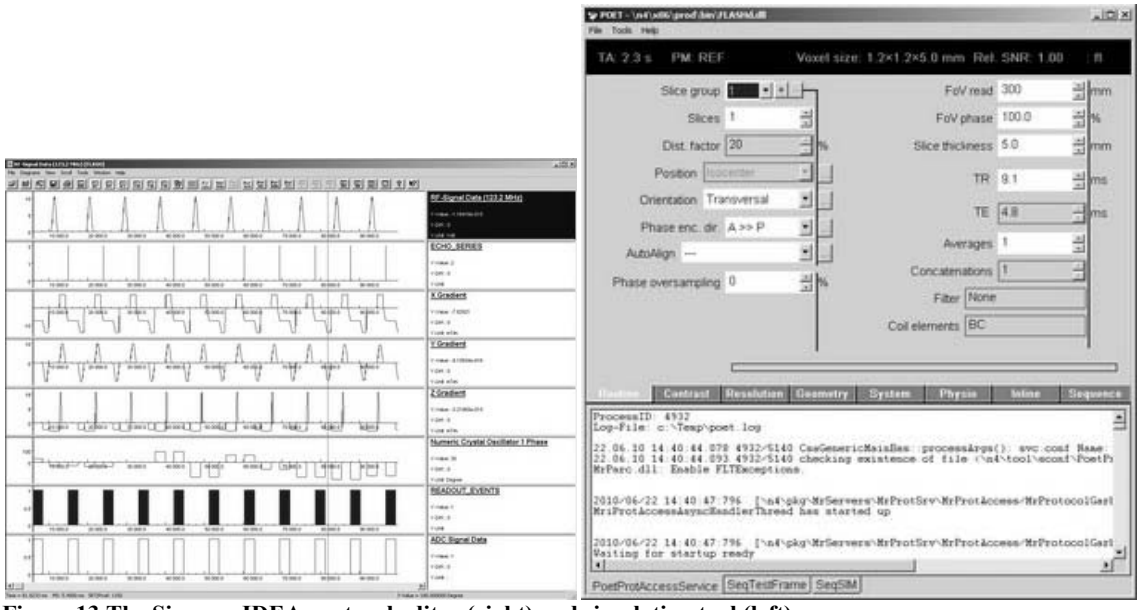

Figure 13 The Siemens IDEA protocol editor (right) and simulation tool (left).

After scanning, the reconstruction process is performed by the ICE (Image Calculation Environment) program specified in sequence. Several built-in ICE programs for standard 2D or

3D reconstruction can be selected in the sequence to satisfy the purpose of examination. Image processing during the scan (in online mode) is also available to reduce the processing time for image reconstruction following scan completion. The ICE program performs reconstruction of the raw data using the Fourier Transform, and outputs the images and related medical information to a file in the DICOM (Digital Imaging and Communications in Medicine) format. [60]

3.7.3 MRI experiments and Image Processing

Experiments were performed with a 1.5 T Siemens Magnetom Avanto (Siemens Medical Systems, Iselin, NJ) scanner using the phantom described in Section 3.7.1. The IR-FSE sequence was used to obtain the T_1 signal from the subjects. A head coil was placed around the phantom. In order to minimize the effect of T_2 recovery, a minimal echo time (usually 12 ms) has been used. Other common parameters are: flip angle $\theta_{inv} = 180^{\circ}$, slice thickness = 5 mm, slice gap = 5 mm, pixel bandwidth = 130 Hz/pixel, field of view = 200 × 200 mm^2, and matrix size = 256 × 256. The obtained signals were stored in real values with proper sign information. Only two slices were obtained for the phantom study in order to avoid possible tissue magnetization transfer effects. For the human brain study, 4 slices were obtained.

To evaluate the effect of using a short repetition time, both TR = 2500 and TR = 3000 ms have been used. To examine the signal loss with larger turbo factors, factors of 4, 8, and 16 have been used. The choice of inversion time varied from one experiment to another and will be discussed in the next chapter.

For performing curve fitting, post-processing, T_1 mapping reconstruction, and simulations, mathematical tool Matlab (The Math Work Inc., Natick, MA. Version 7.5.0.342 (R2007b)) is

utilized to process and analyze measured data. More specifically, the Matlab subroutine "lsqnonlin" is often used for solving the non-linear least square optimization problems. The measured data, DICOM format, were downloaded from the MR scanner to a personal computer running the Microsoft Windows system (Windows XP SP3, Microsoft, Redmond, WA).

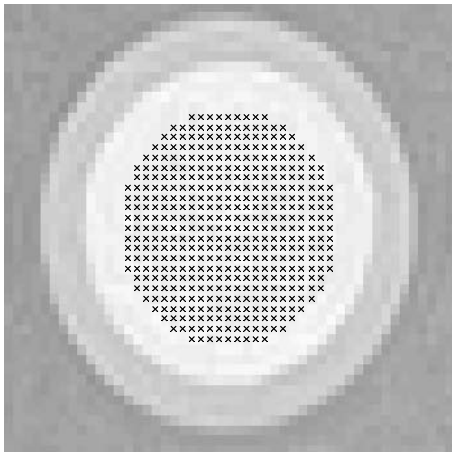

Figure 14
Region of Interest (ROI) in a tube. N = 437. Points with a cross marker indicate the ROI.

Each slice of an MRI study was reordered and reorganized as a matrix for further analysis. A mask with pre-selected regions-of-interest (ROIs) was applied to the images prior to curve fitting, so that only pixels within the gel tubes were processed (Figure 14). In vivo, image processing methods such as region growing or edge detection can be used to select specific ROIs. After the fit, each voxel T_1 value was stored, and the root mean square error (RMSE, equation (2)) as computed with respect to the true T_1 values obtained from either the NMR experiment or the multipoint three-parameter fitting method (see Section 3.7.1). The accuracy was examined by comparing the RMSE for various experimental setting as well as different fitting methods.

Chapter 4 Results

4.1 Phantom Signal Acquisition

Table 3 and Table 4 present the signal values acquired during the phantom study. The signal value is the (signed) intensity value of each voxel obtained after reconstruction from the k-space. These values, as obtained from the scanner, are normalized, dimensionless quantities. Since signal polarity information is available with the FSE sequence, MR signals measured with TR = 3 s were stored as real values with proper sign information, as shown in Table 3. The same gel tubes were also measured with TR = 2.5 s with other settings unchanged. Results are shown in Table 4. Both experiments used a turbo factor ETL = 4.

Table 3(a) shows the mean values from a pre-selected region of interest (ROI) which contains the number of samples N = 437 voxels for each of the two slices (i.e. total N = 2×437 = 874 voxels) for each tube. The true T_1 value is listed together with the mean signal S(TI). Table 3(b) and Table 4(b) list the corresponding standard deviation for the results listed in Table 3(a) and Table 4(a), respectively. The inversion time (TI) in each phantom simulation was selected in a nonlinear manner, with smaller increments around the possible zero-crossing point and with somewhat larger increments when the magnetization approaches equilibrium. For the experiment

using TR = 3 s, the signals were measured at TI = [100, 400, 700, 1000, 1300, 1700, 2000, 2300, 2880] ms; for the experiment using 2.5 s TR, the signals were measured at TI = [23, 300, 600, 900, 1200, 1500, 1800, 2100, 2380] ms. The maximum TI (TI_m) is the largest possible TI allowed by the scanner given the pre-selected repetition time TR. For our two experiments, TI_m is 2880 ms and 2380 ms, respectively. In total, there were 9 TI points obtained in order to achieve the full dynamic range of the longitudinal relaxation curve for further comparison with the multipoint and three-point subtraction methods. The results are listed in the first column of Table 3 and Table 4.

The true T_1 values displayed in Table 3 and Table 4 were measured using the gold standard NMR method spectroscopically described in Section3.7.1. The NMR T_1 values are considered as true T_1 values for accuracy assessment.

Table 3 (a) Mean of Signal Acquired with the Siemens FSE Sequence at 1.5 T with TR = 3 s and ETL = 4

Tube	1	2	3	4	5	6	7	8	9	10
					True T_1					
T_1 (ms)	576	575	682	737	734	834	875	903	907	1258
TI (ms)					Mean of the MR Signal					
100	-949.8	-872.1	-1040.8	-1012.4	-933.1	-1323.5	-1177.1	-1084.32	-1384.9	-1165.8
400	104.3	80.8	-43.07	-95.5	-92.4	-251.3	-261.4	-256.2	-341.3	-464.8
700	658.8	584.6	519.0	432.6	394.2	394.7	301.2	256.0	304.5	4.5
1000	995.3	892.2	889.9	793.6	725.6	861.2	712.1	633.8	788.5	389.1
1300	1192.8	1077.6	1125.2	1029.5	944.8	1182.6	1002.0	903.2	1133.8	687.8
1700	1335.8	1210.9	1310.7	1223.1	1123.7	1458.9	1254.8	1143.2	1441.6	986.0
2000	1392.2	1263.5	1391.6	1311.5	1205.6	1593.0	1380.5	1260.3	1595.9	1152.3
2300	1424.5	1297.5	1444.1	1368.7	1260.5	1685.0	1469.6	1348.1	1707.1	1281.6
2880	1457.8	1324.6	1497.1	1432.1	1316.7	1789.2	1570.7	1446.0	1838.6	1457.1

(b) Standard Deviation for the same study

Tube	1	2	3	4	5	6	7	8	9	10
TI (ms)					Standard Deviation of the MR Signal					
100	31.1	20.5	30.1	25.8	22.3	43.4	35.7	34.6	56.7	36.3
400	11.0	13.8	9.4	10.7	13.5	14.6	12.1	17.9	16.6	16.3
700	21.2	13.4	17.6	14.9	12.1	15.9	13.8	11.9	17.3	10.3
1000	30.6	21.3	26.1	23.8	18.8	29.9	25.0	21.9	36.6	18.1
1300	39.8	26.4	33.1	30.8	23.4	39.7	33.3	30.2	49.9	24.9
1700	44.7	30.78	38.0	35.8	28.1	50.2	40.6	39.5	63.6	32.9
2000	47.6	32.2	40.8	38.8	29.4	53.5	43.6	41.2	68.2	38.3
2300	48.6	34.4	42.2	40.8	31.2	58.3	47.1	46.2	73.	41.7
2880	50.6	34.6	44.5	42.4	33.1	61.0	49.7	49.0	79.3	46.2

Table 4

(a) Mean of Signal Acquired with the Siemens FSE Sequence at 1.5 T with TR = 2.5 s and ETL = 4

Tube	1	2	3	4	5	6	7	8	9	10
					True T_1					
T_1 (ms)	576	575	682	737	734	834	875	903	907	1258
TI (ms)					Mean of the MR Signal					
23	-1284.9	-1171.5	-1331.1	-1263.9	-1163.0	-1595.4	-1405.8	-1284.5	-1629.5	-1279.9
300	-149.2	-149.5	-282.4	-309.7	-290.1	-496.7	-468.9	-440.6	-571.4	-589.8
600	510.9	451.3	372.6	295.0	268.7	236.3	164.7	133.6	152.6	-82.5
900	911.5	816.8	802.1	707.1	648.5	761.9	627.2	557.0	691.3	333.8
1200	1146.9	1034.8	1075.0	978.4	900.1	1125.6	951.1	857.8	1077.9	657.9
1500	1288.90	1167.0	1254.3	1158.8	1066.5	1374.8	1181.9	1072.0	1351.6	912.2
1800	1365.5	1238.2	1356.6	1273.4	1171.3	1543.2	1335.6	1219.3	1542.5	1106.6
2100	1412.5	1284.6	1427.4	1349.9	1243.5	1663.1	1448.9	1326.6	1683.4	1259.3
2380	1437.8	1309.4	1469.1	1397.0	1287.1	1741.8	1522.9	1399.5	1778.5	1371.1

(b) Standard Deviation for the same study

Tube	1	2	3	4	5	6	7	8	9	10
TI (ms)					Standard Deviation of the MR Signal					
23	41.8	25.3	37.3	31.8	25.1	51.2	42.8	40.2	64.7	41.8
300	12.1	18.8	12.4	11.8	17.1	18.9	15.4	21.9	25.0	19.3
600	17.3	10.8	13.9	12.1	10.2	12.0	11.5	11.1	12.5	10.5
900	29.4	19.1	24.7	22.3	16.9	26.9	22.5	20.6	32.1	15.7
1200	39.1	25.4	31.9	29.0	21.7	38.8	31.8	29.8	47.8	24.0
1500	43.8	29.4	38.6	34.5	25.8	46.1	37.6	36.5	57.1	30.9
1800	47.2	32.7	40.7	38.0	29.3	52.4	42.4	42.6	66.7	36.9
2100	48.1	33.2	42.7	40.1	30.0	56.5	46.0	44.4	71.2	40.4
2380	50.6	35.7	43.8	41.6	32.0	59.4	48.4	47.6	76.2	44.0

4.2 Noise Analysis

4.2.1 The Statistical Error of Measurements

The variance of the measured signal indicates the error during the data acquisition. This type of error can represent the noise that caused by the background. Table 3 and Table 4 both clearly show that the standard deviation of the measured signals varied for different TIs. To better point this out, the standard deviation is plotted from low TI to high TI measurements at different T_1 subjects in Figure 15. Figure 15 also compares the measured signal for the two different value of the repetition time.

A dip is clearly seen in the Figure 15. The minimum is located in the lower TI range, but not for the lowest TI. As T_1 increases, the TI corresponding to the minimum error also increases. We find that the minimum position corresponds to the minimal signal strength obtained from Table 3 and Table 4, i.e. the minimal error is found around the zero-crossing time, TI_{null}, where the magnetization strength is zero. It is worth mentioning that although the measurement around TI_{null} has a smallest error, the measurement value could be pure noise due to system imperfections or dielectric effects of surrounding tissue if one of the measurements has set the TI too close to the zero-crossing time.

The standard deviation first decreases until it reaches the global minimum, and then increases with increasing of TI. The overall pattern of the signal error is very similar to the absolute values obtained in each measurement.

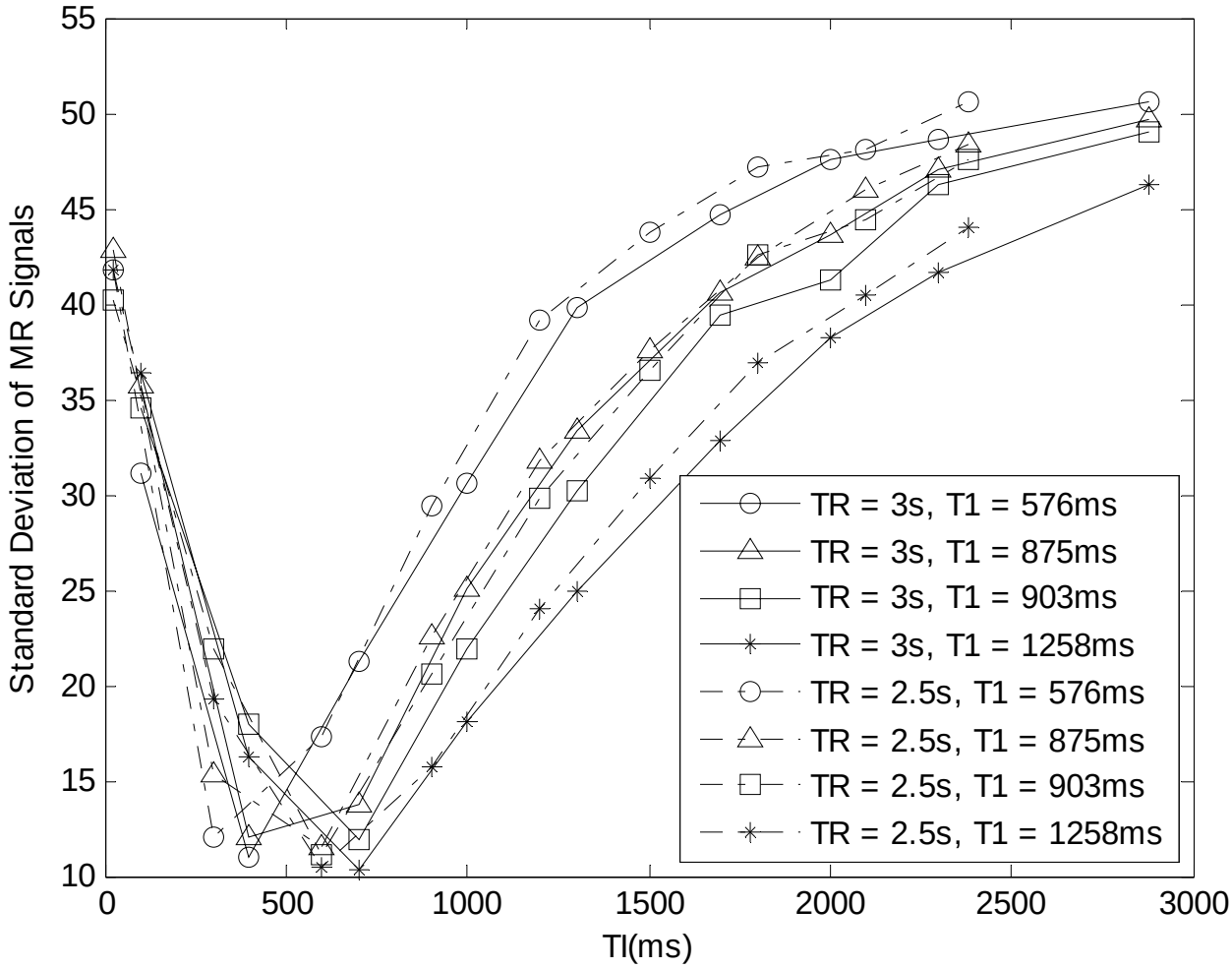

Figure 15 Measurement error vs each TI time for different T_1 subjects with the FSE sequence

The relationship between the measured signal and its noise is plotted in Figure 16. It can be expected that the signal to noise plot show similar pattern as the plot in Figure 15 since the measured signals increase monotonically with TI. From Figure 16, we observe that the noise is small around the signal null (signal strength = 0). In addition, for positive signals, there is a strong correlation between the signal and the error, signals larger than zero show a very strong positive linear correlation for any T_1 subject (correlation coefficient > 0.9, p-value < 0.0001).

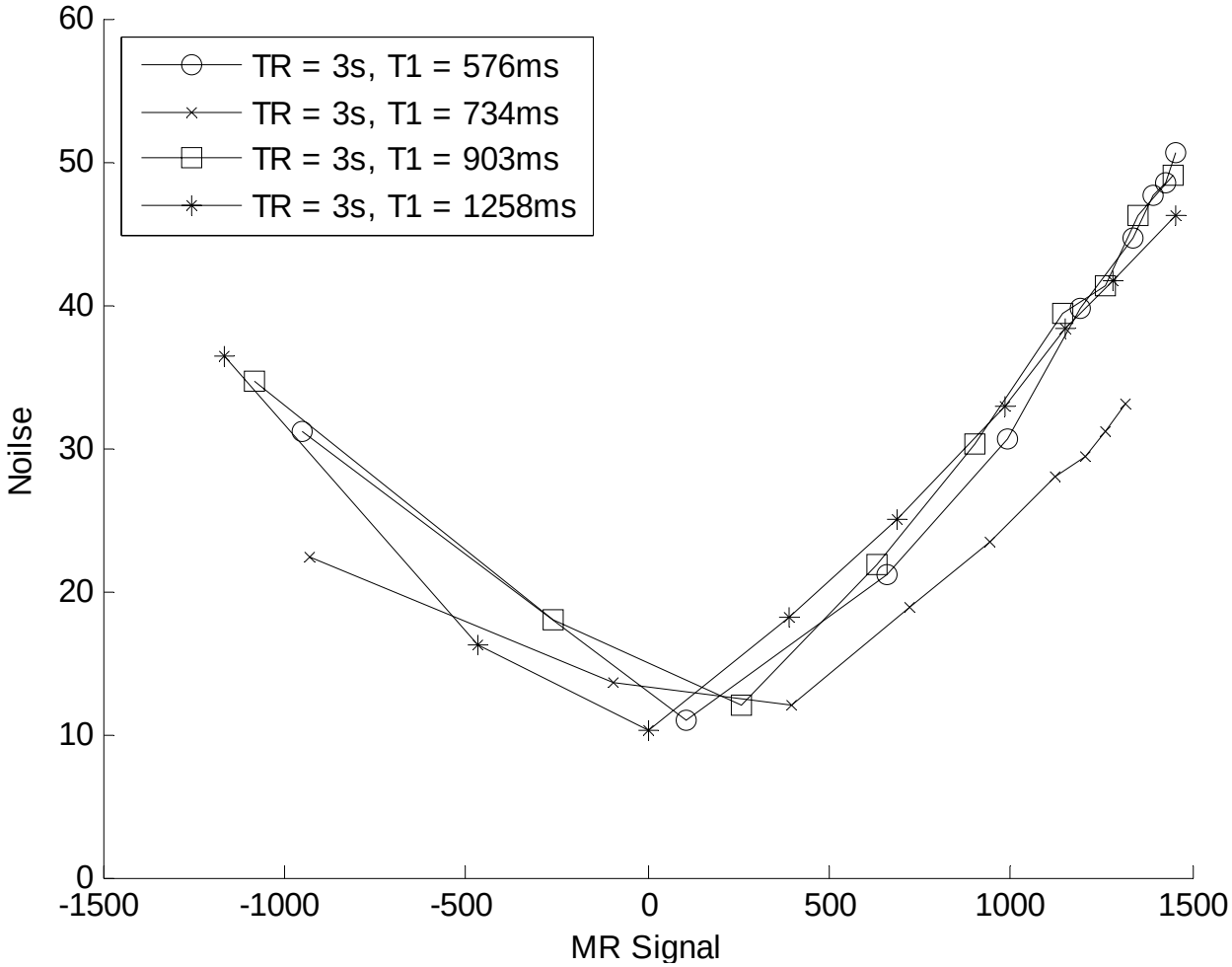

Figure 16 The measurement signals vs Statistical Signal Error

4.2.2 The Signal-to-Noise-Ratio (SNR) of Measurements

Although it is easy to notice from Figure 15 that the noise changed with varying TI values, the signal quality is not revealed by checking the mean and standard deviation alone. It makes more sense to examine the signal quality by computing the signal-to-noise-ratio (SNR) for each TI. The SNR is computed S_i/σ_s and the result is plotted as a function of TI in Figure 17. It is worth mentioning that the definition for SNR here is different from that frequently used in MRI literature, which is defined as S_i/σ_{bg}, where σ_{bg} is the standard deviation of the ghost-free regions of background outside the phantom. However, the results for σ_{bg} are nearly constant for all

measurements (Table 5). High SNR with the traditional definition only indicates good image quality but does not reveal the level of true measurement errors due to the sensitivity of the measuring method. Therefore, the SNR analysis will give more meaningful results by using the presented definition.

Table 5 The standard deviation measured outside the phantom.

TI(ms)	100	400	700	1000	1300	1700	2000	2300	2880
σ_{bg}	10.249	8.999	9.227	9.801	10.551	11.399	12.002	12.592	12.532

A dip is observed in Figure 17 and the global minimum also matches the position found in Figure 15 as well as the approximate zero-crossing time obtained from Table 3 or Table 4. One of the measurement value at 700 ms TI with 3 s TR (marked with a star) has SNR = 0.44, which might indicate that the signal intensity was mostly noise. After reaching the minimum, the SNR increases rapidly and reaches a plateau after TI = 1300 ms for TR = 3.0 s or TI = 1200 ms for TR = 2.5 s. For all measurements, the SNR in the plateau region is approximately equal to 30 with about 10% variation. Some measurements have a minimum SNR larger than 5 and the measured signal at that TI still contains useful information about T_1 , so it can be used in any of the fitting methods that we evaluated. However, the effect of such measurements to the accuracy for multipoint fitting and three-point subtraction fitting method needs to be further examined.

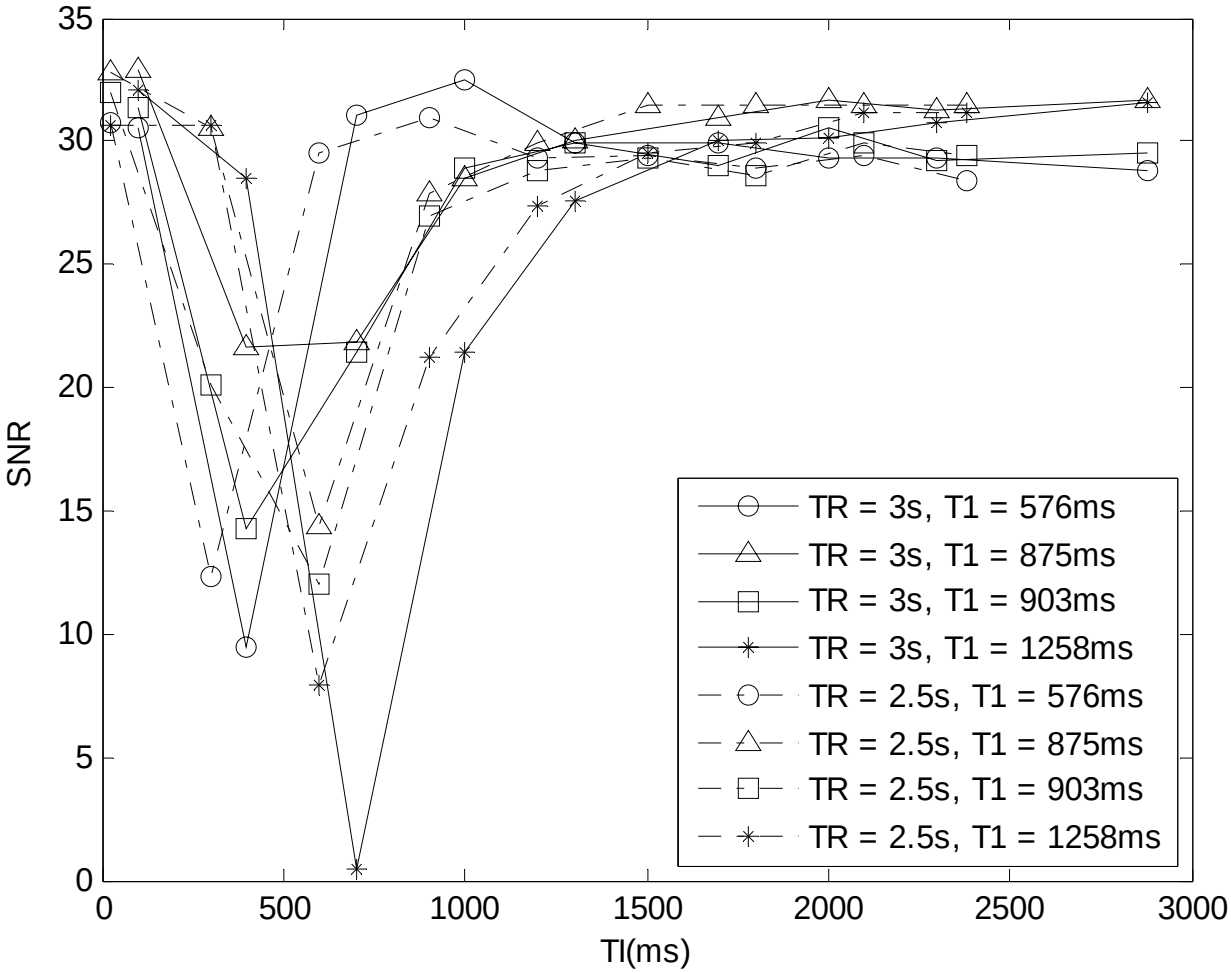

Figure 17 Signal-to-Noise Ratio (SNR) as a function of TI in IR-FSE for different T_1 subjects

4.3 Comparative Analysis of Fitting Algorithms

4.3.1 Two-Parameter fitting vs. Three-Parameter Fitting

The T_1 image reconstruction algorithm has been optimized for computational efficiency, resulting in a reduction of reconstruction time by a factor of three. The processing speed, however, highly depends on computer's processor speed and the size of computer memory. The computational efficiency can be therefore further improved by using a more powerful computation engine.

In the early discussion (Section 3.1), a new two-parameter fitting model was proposed using the normalized general equation given by Equation (11).[15] The new two-parameter fitting model is different from the popular two-parameter fit which assumes a perfect flip angle. [34-36] The normalization process removes the unknown magnetization strength and reduces the number of degrees of freedom to 2. A comparison is performed between the new two-parameter fitting model (Equation (11)) and the traditional three-parameter fitting model. Measured data from Table 3 and Table 4 were utilized with both models, and the results are listed in Table 6. The RMS T_1 estimation error values are also listed in Table 6 in parentheses.

On average, the overall accuracy is better for the two-parameter fitting model (RMS = 50.98) than the three-parameter mode (RMS = 58.73). If we examine the individual tubes, the fitting imprecision (standard deviation) is generally the same for both fitting models and slightly increasing with increasing T_1. The larger RMS error for the three-parameter model results from a higher level of underestimation in the average T_1 values. This underestimation, which has been reported in many articles[15,17,41,42,43], is generally found in both models (Table 7). The

combination effect of relative error and mean error causes the RMS error of the largest T_1 to be almost 4 times higher than for the smallest T_1 subject.

Table 6 Phantom T_1 Comparison Study between Two-Parameter Fitting and Three-Parameter Fitting with IRFSE

TR > 10T_1	TR = 3 s, 4 ETL		TR = 2.5 s, 4 ETL	
True T_1(ms)	T_1(ms) from two-parameter Fitting	T_1(ms) from three-parameter Fitting	T_1(ms) from two-parameter Fitting	T_1(ms) from three-parameter Fitting
576	551±10 (26.72)*	543±8 (33.79)	548±10 (29.55)	542±7 (34.61)
575	558±12 (20.38)	554±12 (24.67)	558±12 (20.60)	552±12 (26.31)
682	646±11 (37.99)	637±8 (45.54)	643±11 (40.53)	636±9 (46.52)
737	694±12 (44.90)	685±11 (53.45)	693±13 (46.04)	685± 12(53.34)
734	696±13 (40.43)	688±12 (47.39)	696±14 (41.03)	689±14 (47.49)
834	784±11 (50.99)	776±10 (58.84)	786±11 (49.52)	777±10 (57.55)
875	822±12 (54.54)	814±12 (61.62)	822±14 (54.94)	814±13 (61.85)
903	846±16 (59.55)	838±16 (66.66)	847±16 (57.92)	839±16 (66.19)
907	861±12 (47.47)	853±12 (55.37)	864±13 (44.93)	855±12 (52.81)
1258	1170±26 (92.09)	1156±21 (103.91)	1167±31 (96.55)	1161±27 (100.79)
Aggregate RMSE	(50.98)	(58.73)	(51.76)	(58.73)

***RMSE compared to true T_1 is indicated inside parentheses after each T_1 value.**

Table 7 Relative Error for Different Fitting Models shows general T_1 underestimation

TR > 10T_1	TR = 3 s, 4 ETL		TR = 2.5 s, 4 ETL	
True T_1(ms)	T_1 relative Error from two-parameter Fitting	T_1 relative Error from three-parameter Fitting	T_1 relative Error from two-parameter Fitting	T_1 relative Error from three-parameter Fitting
576	-0.043	-0.057	-0.048	-0.059
575	-0.029	-0.037	-0.029	-0.041
682	-0.053	-0.066	-0.057	-0.067
737	-0.059	-0.071	-0.060	-0.071
734	-0.052	-0.062	-0.052	-0.062
834	-0.060	-0.069	-0.058	-0.068
875	-0.061	-0.069	-0.061	-0.069
903	-0.064	-0.072	-0.062	-0.071
907	-0.051	-0.060	-0.047	-0.057
1258	-0.070	-0.081	-0.073	-0.077

If the T_1 underestimation error remains at the same level, it is suitable to correct the systematical underestimation with a linear regression function described in section 3.2 and equation (12). A clear linear relationship between the longitudinal relaxation rate ($1/T_1$) with two-parameter or

three-parameter fitting models and the NMR measurement is found based on the same gel phantom tubes. The relationship is plotted in Figure 18.

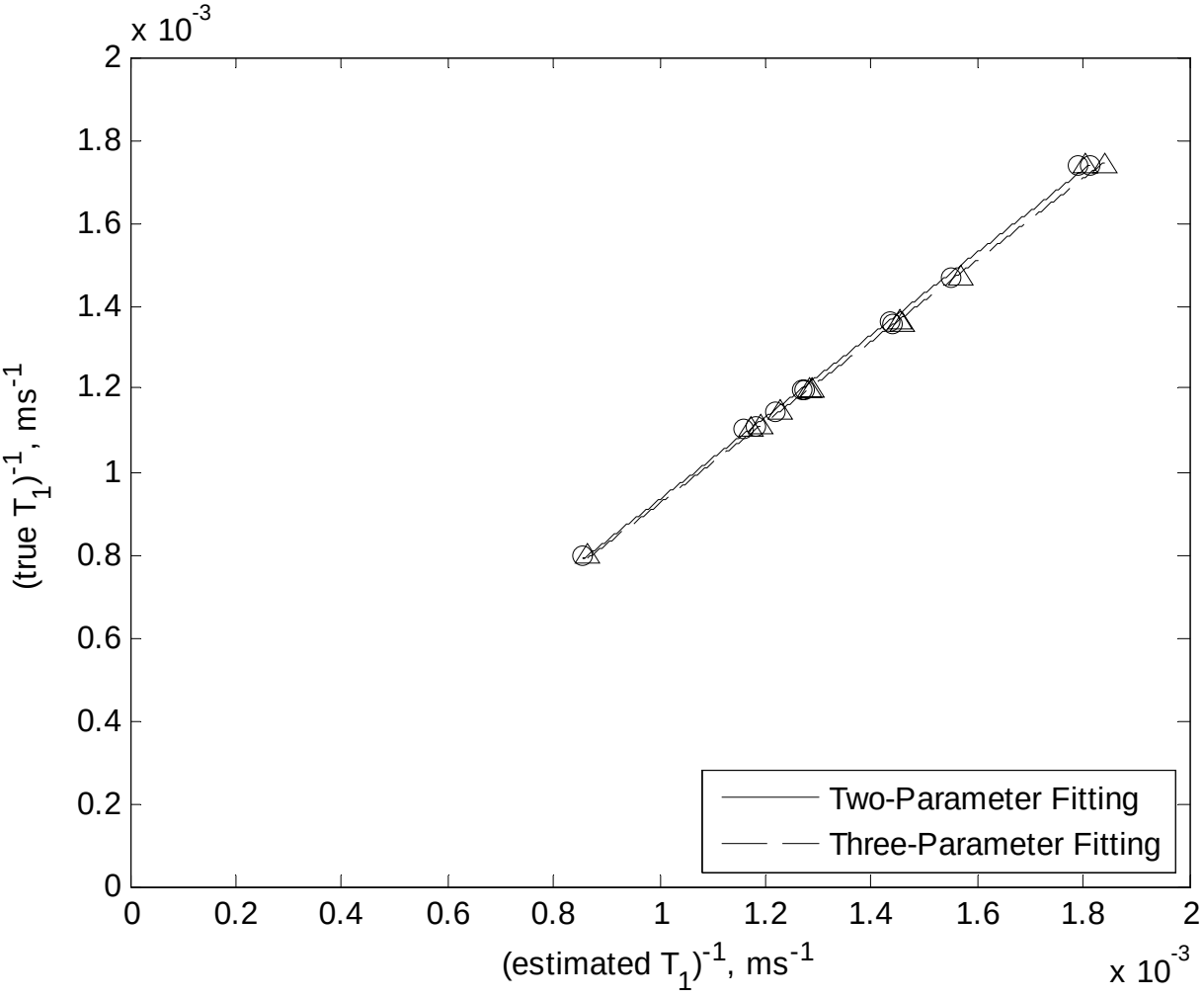

Figure 18 Linear Relationship between Estimated T_1 and True T_1 for 3 s TR experiment

We use the linear relationship to convert the estimated T_1 results from either fitting mode to the equivalent measurement with the NMR measuring method. For the two-parameter fitting, the regression function is

$$\frac{1}{\text{True } T_1} = -6.3524 \times 10^{-5} + \frac{0.9941}{\text{Estimated } T_1} \tag{32}$$

with R square = 0.99934 (1 means perfect fit). For the three-parameter fitting, the regression function is

$$\frac{1}{\text{True } T_1} = -5.8168 \times 10^{-5} + \frac{0.9792}{\text{Estimated } T_1} \tag{33}$$

with R square = 0.99905.

4.3.2 Remaining Parameters

Although these parameters are seldom discussed, it would be beneficial to examine the validation of data by checking the consistency of the remaining parameters used in the fitting model. For the two-parameter fitting model, the remaining fitting parameter is the effective spin inversion fraction (f_{inv}) which indicates the pulse imperfection and all possible effects that may lead to signal distortion; for the three-parameter fitting model, the remaining fitting parameters are the effective spin inversion fraction (f_{inv}) and the S_0 parameter in Equation (7), defined as

$$S_0 = k \cdot M_0 \cdot e^{-\frac{\text{TE}}{T_2}} \tag{34}$$

The results for the estimated f_{inv} are listed in Table 8. They indicate that the inversion pulse had at least 95% effectiveness on the testing subjects. Nevertheless, a strong linear correlation is found between T_1 and f_{inv} with correlation coefficient equal to -0.944, which indicates that the f_{inv} decreases with increased T_1. The p-value for this linear relationship is less than 0.0001 which indicates that the linear correlation has statistical significance.

Although we have observed noticeable differences for the estimated T_1 with different fitting models, we do not see any significant differences for f_{inv} with different fitting models. The estimated error for f_{inv} is usually less than 2% and therefore, is negligible. One should notice that

the f_{inv} assumes that the system imperfection causes the same amount of inversion variations on the every voxel within the ROIs. We can only use f_{inv} to evaluate the average effect of pulse imperfection as well as the possible signal distortion, but it does not represent the pulse effectiveness during each scan.

Table 8 The inversion fraction, f_{inv} obtained using Two-Parameter Fitting and Three-Parameter Fitting with IR-FSE

TR > $10T_1$	TR = 3 s, 4 ETL		TR = 2.5 s, 4 ETL	
True T_1(ms)	f_{inv} from two-parameter Fitting	f_{inv} from three-parameter Fitting	f_{inv} from two-parameter Fitting	f_{inv} from three-parameter Fitting
576	0.9806±0.0178	0.9833±0.0165	0.9717±0.0176	0.9689±0.0166
575	0.9843±0.0185	0.9840±0.0172	0.9711±0.0170	0.9690±0.0156
682	0.9799±0.0171	0.9796±0.0169	0.9701±0.0171	0.9667±0.0165
737	0.9724±0.0180	0.9715±0.0179	0.9624±0.0190	0.9580±0.0193
734	0.9736±0.0190	0.9712±0.0179	0.9610±0.0188	0.9569±0.0171
834	0.9771±0.0170	0.9737±0.0175	0.9696±0.0155	0.9596±0.0157
875	0.9766±0.0169	0.9726±0.0171	0.9678±0.0161	0.9625±0.0159
903	0.9705±0.0178	0.9659±0.0170	0.9598±0.0146	0.9550±0.0129
907	0.9701±0.0180	0.9658±0.0181	0.9567±0.0153	0.9518±0.0154
1258	0.9561±0.0221	0.9561±0.0178	0.9514±0.0207	0.9457±0.0191

Table 9 The Estimated Magnitude at Full relaxation for TR = 3 s and TR = 2.5 s experiments.

TR > $10T_1$	TR = 3 s, 4 ETL	TR = 2.5 s, 4 ETL
True T_1(ms)	Estimated S_0	Estimated S_0
576	1458.28±50.79	1453.34±50.83
575	1328.68±36.21	1324.08±37.82
682	1507.72±44.25	1503.45±45.87
737	1447.57±43.59	1440.48±44.57
734	1332.86±34.47	1328.38±35.70
834	1830.35±63.77	1827.99±63.45
875	1615.25±51.44	1612.10±51.55
903	1492.30±52.96	1488.59±59.30
907	1901.06±82.28	1899.32±82.03
1258	1592.23±51.52	1587.10±52.57

The estimated S_0 values are listed in Table 9. The linear correlation between the estimated S_0 and the estimated T_1 is not statistically significant (p-value = 0.16 > 0.05 with correlation coefficient = 0.4511). Since the TE in Equation (34) is always set to the minimal possible value, the effect of T_2 should be reasonably neglected.

4.3.3 Correction with Weighted Fitting Model

The RMS T_1 estimation error values are listed in Table 10 for the 10 tubes and values of α ranging from -0.2 to +1.0. As anticipated, using different weights for the terms corresponding to different inversion times in Equation (5) leads to a reduction in estimation error for each of the tubes compared to the case with no weights (α = 0). An aggregate estimation error is also computed and reported in the last column of the Table 10. The variation of the aggregate error with α is shown in Figure 3. We observe an overall reduction in estimation error by 36% when α ≈ 0.7 is used. The optimum α is different for phantom tubes with different relaxation time T_1. We exploit this variation using the Table 10 to determine the optimal α for each tube. The aggregate RMS error is reduced to 19.47 with two pass adaptive technique.

Table 10 T_1 estimation error RMS values for the 10 tubes and for different values of α

Tube	1	2	3	4	5	6	7	8	9	10	
						True T_1					
T_1 (ms)	576	575	682	737	734	834	875	903	907	1258	
α						RMS Error					Aggregate
-0.2	25.00	18.66	36.01	42.05	37.54	48.75	52.02	57.09	45.08	92.75	49.25
-0.1	25.57	19.20	36.91	43.95	39.24	50.49	53.55	58.14	45.73	94.02	50.48
0.0	26.72	20.38	37.99	44.90	40.43	50.99	54.54	59.55	47.47	92.09	50.98
0.1	29.47	22.55	38.49	45.47	41.42	50.62	53.41	58.15	46.01	81.99	49.30
0.2	30.39	24.71	27.80	35.72	33.13	45.67	48.72	52.40	40.57	78.35	44.27
0.3	25.39	21.69	24.94	26.67	23.13	37.97	43.04	47.00	36.23	73.72	38.68
0.4	23.80	19.41	22.99	25.55	21.91	24.94	30.76	36.34	28.38	63.29	31.59
0.5	23.01	15.55	21.78	24.01	19.97	21.38	24.69	27.92	18.51	49.11	25.94
0.6	20.01	12.33	18.97	22.74	18.92	19.90	22.58	24.65	16.82	45.07	23.67
0.7	15.77	10.60	14.82	21.93	18.26	18.37	21.31	23.44	17.26	45.37	22.59
0.8	12.24	12.13	10.88	21.53	17.09	19.23	21.23	24.79	18.90	48.33	23.04
0.9	10.48	15.48	11.95	20.65	15.64	19.14	22.48	25.13	20.80	46.24	23.02
1.0	10.22	20.92	14.00	19.85	14.27	18.01	19.25	24.48	25.27	45.55	23.32
1.1	12.92	24.44	17.27	16.08	13.74	2344	23.17	21.69	25.61	46.58	24.70

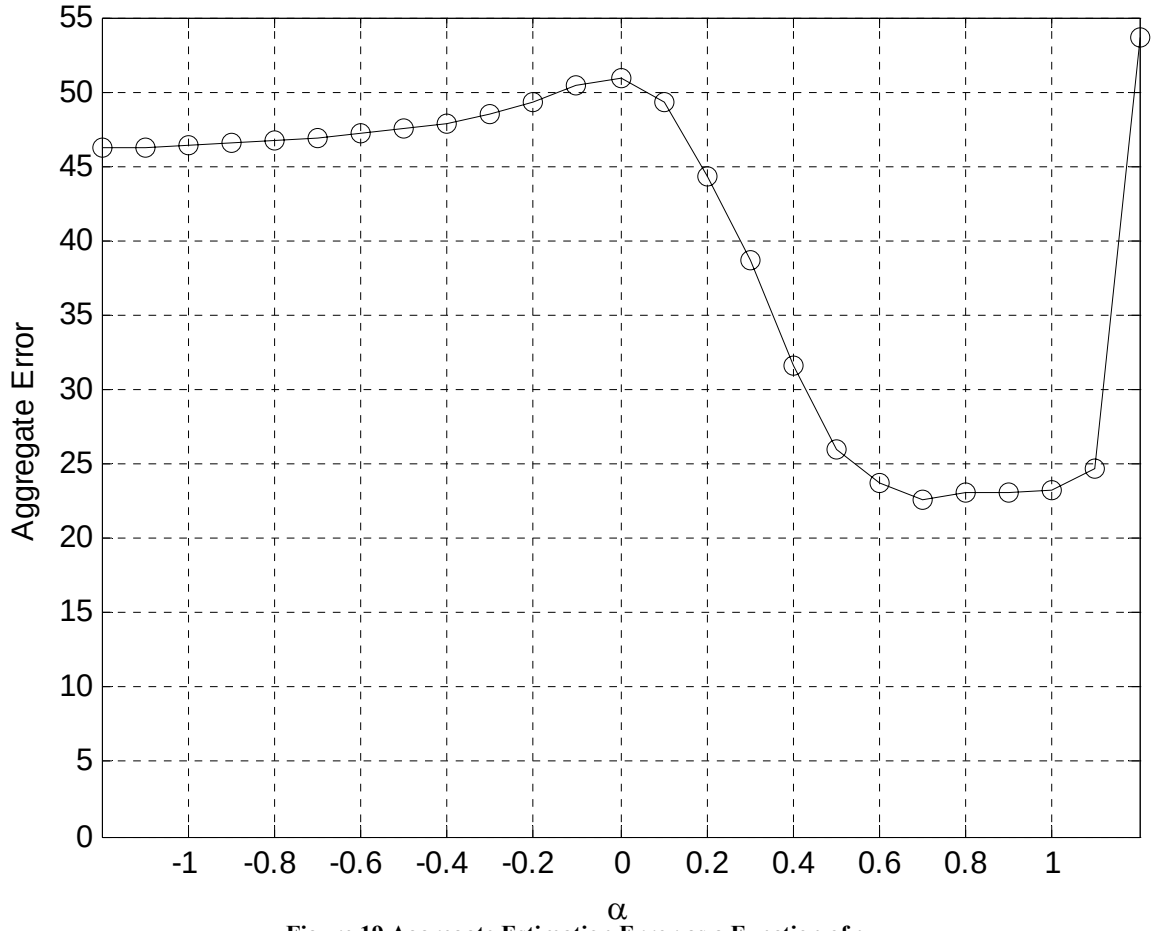

Figure 19 Aggregate Estimation Error as a Function of α

4.3.4 The Effect of Short TR in T_1 Estimation

The estimated T_1 values show very good agreement for different TR experiments using the same fitting method. Reducing the TR from 3 s to 2.5 s has no significant effect on the estimated T_1 accuracy. The overall accuracy for the traditional three-parameter fitting mode is exactly the same (RMS = 58.73) for the two experiments. For the two-parameter fitting model, the overall accuracy RMS = 50.98 for TR = 3 s and RMS = 51.76 for TR = 2.5 s. It is worth noticing that for the longest T_1 phantom tube (T_1 = 1258 ms), the 2.5 s TR used in the protocol is less than twice

its T_1 value, and the T_1 relaxation only returns to approximately 86% of the final value. Yet the precision and accuracy does not seem to be significantly affected by the reduced TR value.

Table 11 Phantom T_1 Comparison Study between Two-Parameter Fitting and Three-Parameter Fitting with IR-FSE

TR > 10T_1	T_1(ms) from two-parameter Fitting		T_1(ms) from three-parameter Fitting	
True T_1(ms)	TR = 3 s, 4 ETL	TR = 2.5 s, 4 ETL	TR = 3 s, 4 ETL	TR = 2.5 s, 4 ETL
576	551±10 (26.72)*	548±10 (29.55)	543±8 (33.79)	542±7 (34.61)
575	558±12 (20.38)	558±12 (20.60)	554±12 (24.67)	552±12 (26.31)
682	646±11 (37.99)	643±11 (40.53)	637±8 (45.54)	636±9 (46.52)
737	694±12 (44.90)	693±13 (46.04)	685±11 (53.45)	685± 12(53.34)
734	696±13 (40.43)	696±14 (41.03)	688±12 (47.39)	689±14 (47.49)
834	784±11 (50.99)	786±11 (49.52)	776±10 (58.84)	777±10 (57.55)
875	822±12 (54.54)	822±14 (54.94)	814±12 (61.62)	814±13 (61.85)
903	846±16 (59.55)	847±16 (57.92)	838±16 (66.66)	839±16 (66.19)
907	861±12 (47.47)	864±13 (44.93)	853±12 (55.37)	855±12 (52.81)
1258	1170±26 (92.09)	1167±31 (96.55)	1156±21 (103.91)	1161±27 (100.79)
Aggregate RMSE	(50.98)	(51.76)	(58.73)	(58.73)

***RMSE compared to true T_1 is indicated inside parentheses after each T_1 value.**

4.3.5 The Effect of a Larger Turbo Factor

With multiple echoes during the acquisition time, the FSE sequence is able to reduce the total scan time. The total scan time can be calculated by the following equation:

$$\text{Scan Time} = \frac{\text{TR} \times \text{N}_{\text{PE}}}{\text{ETL}} \tag{35}$$

Where N_{PE} is the number of line for phase encoding and ETL is the turbo factor. Thus, a FSE sequence with turbo factor 4 will be 4 time faster than the equivalent spin echo sequence. It is reasonable to assume that increasing the turbo factor to 8 or 16 will further increase the efficiency of the overall T_1 measuring process. However, an undesirable accuracy decrease

occurs due to T_2 decay effect along the echo train.[61] Because the spatial resolution will depend on the T_2 of the tissues contributing to the signal, a large echo factor cannot be used without impairing the spatial resolution.

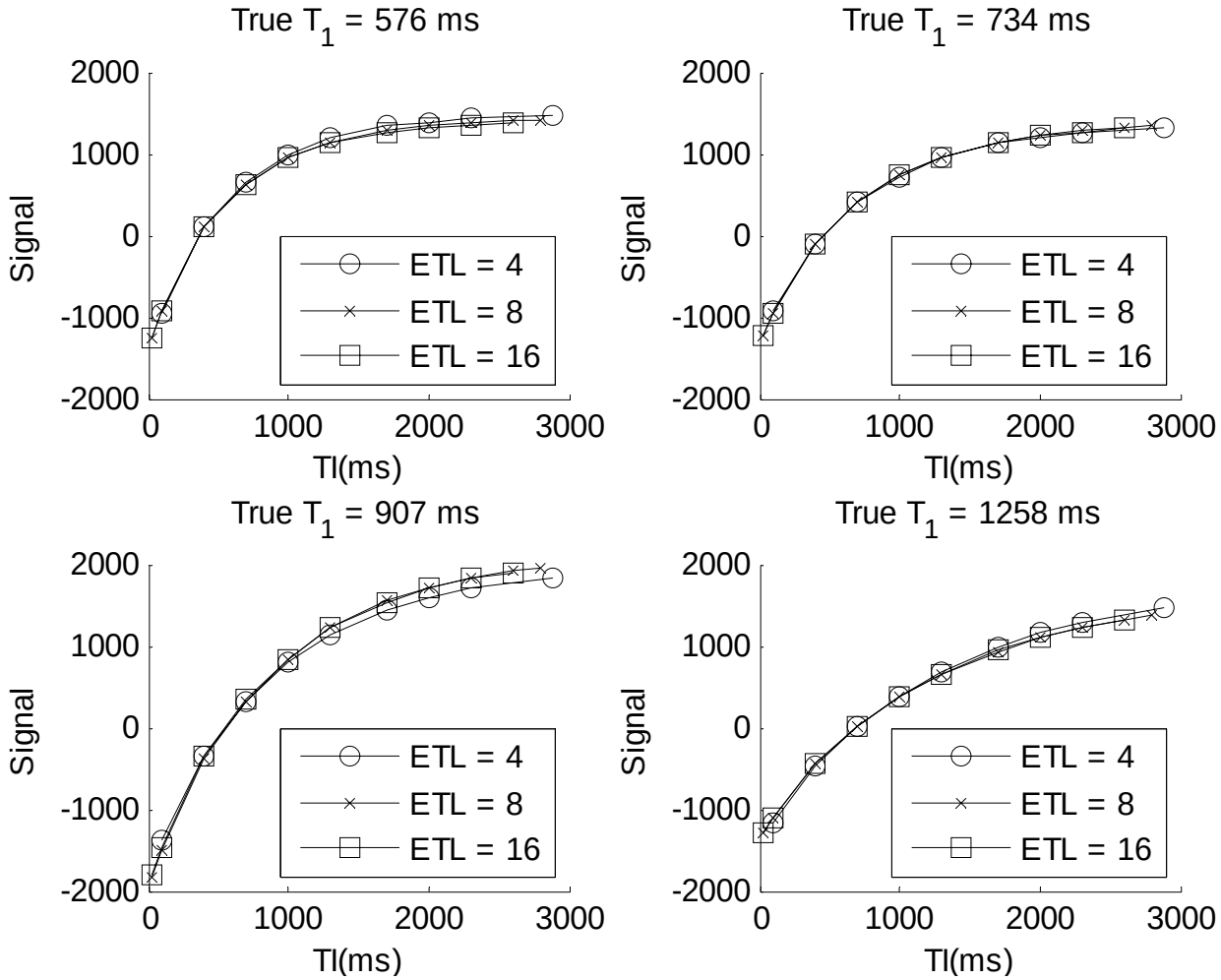

Figure 20 The Inversion Recovery Curve for Different ETL (ETL = 4, 8, 16) in various T_1 subjects

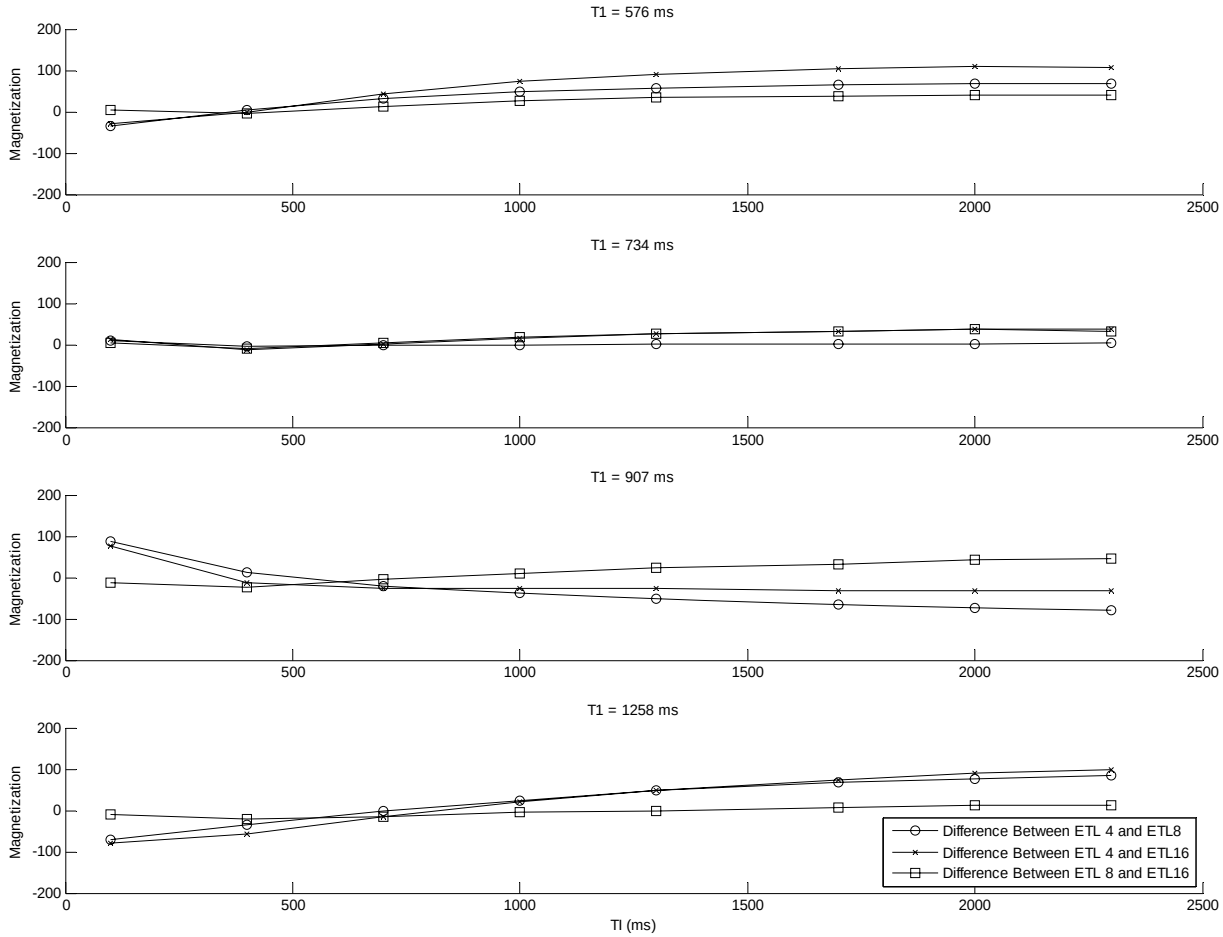

Figure 21 Magnetization values for differences between turbo factors (4, 8, and 16)

If the turbo factor increases from 4 to 8, the scan time decreases from 3 minutes 9 second per slice to 1 minute 35 seconds per slice; if the turbo factor increases to 16, the scan time is further reduced to 47 seconds per slice. The efficiency indeed increases 4 times when we compare a turbo factor of 16 to a turbo factor of 4.

The signal variation caused by increasing the turbo factor is unpredictable. Figure 21 shows the difference between measurements for the different turbo factors for different T_1 subjects in order to better compare the signal variation. Although we can observe the signal differences between different turbo factors, in fact, the signal strength variation is only a few milliseconds and does not have any statistical significance. The estimated T_1 results listed in Table 12 also show a

slight but consistent decrease along with the increase of the turbo factor. However, the accuracy of the estimated T_1 is reduced by approximately 20% when using a turbo factor of 16 due to the deterioration in precision. In addition, the accuracy is not significantly affected when changing the turbo factor from 4 to 8.

Table 12 T_1 Multiple fitting T_1 results for a turbo factor of 4, 8 and 16

TR > 10T_1	TR = 3.0 s, 4 ETL	TR = 3.0 s, 8 ETL	TR = 3.0 s, 16 ETL
True T_1(ms)		T_1(ms) from Multipoint Fitting	
576	551±10 (26.72)*	551±10 (26.24)	547±16 (33.11)
575	558±12 (20.38)	558±13 (20.88)	553±16 (20.60)
682	646±11 (37.99)	645±13 (39.09)	639±19 (47.44)
737	694±12 (44.90)	698±13 (41.01)	691±22 (50.85)
734	696±13 (40.43)	698±16 (39.11)	694±22 (45.91)
834	784±11 (50.99)	786±16 (50.49)	781±23 (57.91)
875	822±12 (54.54)	852±18 (52.93)	818±26 (62.96)
903	846±16 (59.55)	849±20 (56.98)	841±31 (69.96)
907	861±12 (47.47)	861±20 (50.16)	857±29 (57.88)
1258	1170±26 (92.09)	1174±32 (89.57)	1161±48 (108.25)
Aggregate RMSE	(50.98)	(49.75)	(59.70)

***RMSE compared to true T_1 is indicated inside parentheses after each T_1 value.**

The linear relationship between the inverted true T_1 and the inverted estimate T_1 persists even when using a larger turbo factor. In order to verify the performance of the correction function, we first take half of the tubes to compute the linear regression function based on equation (12), and then we use the computed function to test on the remaining tubes.

For a turbo factor of 8, the regression function is

$$\frac{1}{\text{True } T_1} = -3.8512 \times 10^{-5} + \frac{0.9759}{\text{Estimated } T_1} \tag{36}$$

with R square = 0.9996. For a turbo factor of 16, the regression function is

$$\frac{1}{\text{True } T_1} = -2.7214 \times 10^{-5} + \frac{0.9601}{\text{Estimated } T_1} \tag{37}$$

with R square = 0.9994.

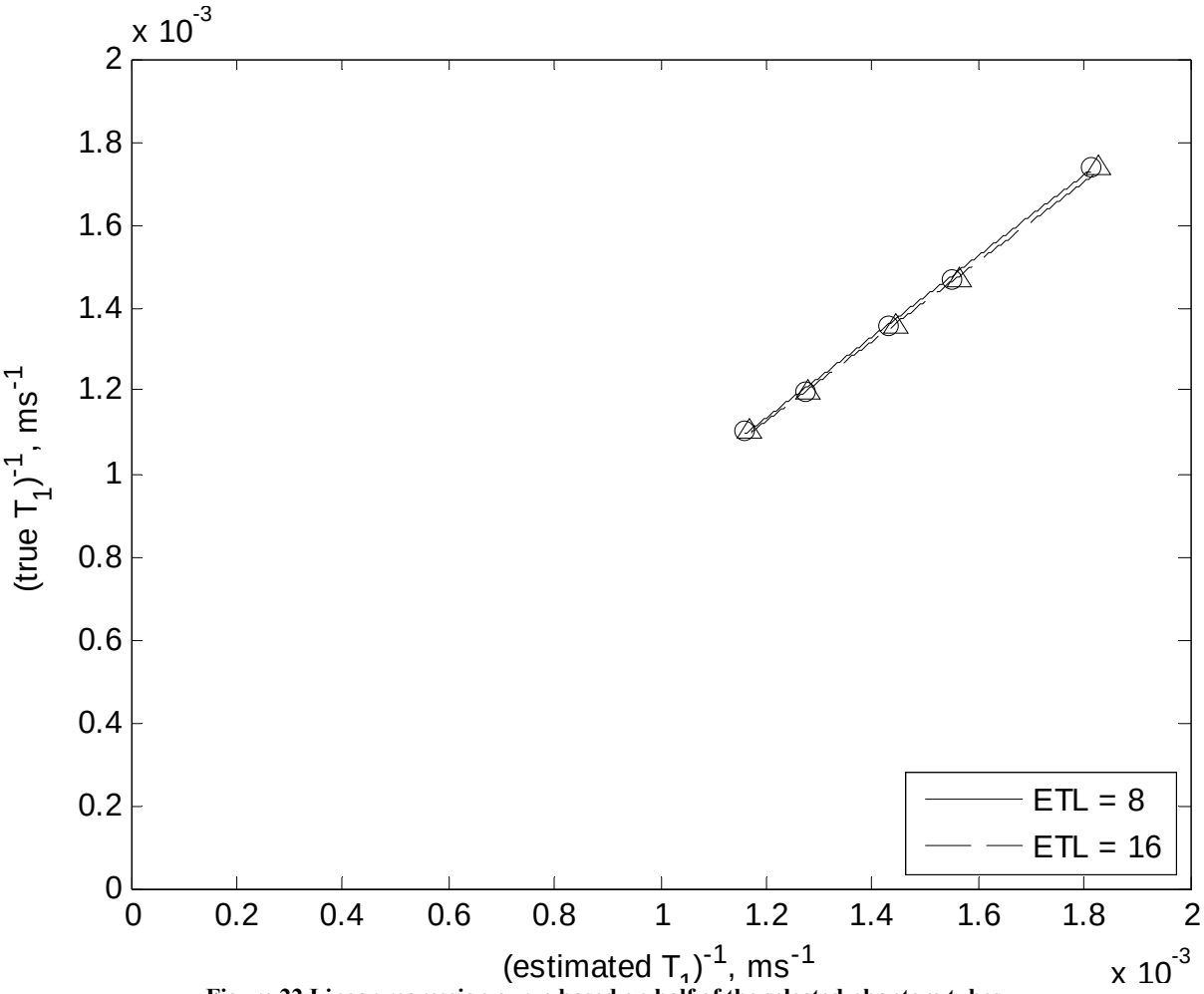

Figure 22 Linear regression curve based on half of the selected phantom tubes

The results after applying the linear correction function are listed in Table 13 (left column). The difference between true T_1 and estimated T_1 is generally reduced to less than 1%. The T_1 results indicate a rather good performance for correcting the T_1 underestimation. However, the RMS error indicates a certain level of inaccuracy due to the statistical standard deviation, which is not affected by this procedure. One of the problems we have observed when using a large turbo factor such as ETL = 16 is that the precision becomes worse especially for high T_1 values. In

addition, the linear correction function is affected by the weight of signal strength, i.e. if the linear correction function produced from the majority of high T_1 tissue, using it on low T_1 tissues can result in unexpected overestimation.

The results for the weighted fitting model correction algorithm are listed in Table 13 (right column) in the same manner as for the linear correction method. The weight, α, is dynamically chosen for different values of T_1. The RMS error for a turbo factor of 8 increases slightly compared to the linear correction method, but the difference is very small (< 7%). For a turbo factor of 16, the RMS error is reduced by approximately 52% compared to the original fitting algorithm while the linear correction can reduce the RMS error by approximately 43%. We have observed the overall improvement from not only the difference between estimated T_1 and true T_1 values, but also the estimated precision by using the correction algorithm with a weighted fitting model.

Table 13 T_1 estimation after applying linear correction (left column) and the weighted model correction (right column)

$TR > 10T_1$	T_1(ms) with linear correction		T_1(ms) with adapted weighted model correction	
True T_1(ms)	ETL = 8	ETL = 16	ETL = 8	ETL = 16
576	N/A*	N/A	N/A	N/A
575	585±13 (16.80**)	585±17 (19.94)	572±12 (12.83)	572±14 (14.16)
682	N/A	N/A	N/A	N/A
737	N/A	N/A	N/A	N/A
734	736±17 (17.43)	737±24 (23.74)	723±14 (17.06)	721±14 (18.97)
834	N/A	N/A	N/A	N/A
875	874±20 (20.03)	872±28 (28.50)	861±18 (22.57)	850±16 (29.65)
903	901±22 (21.98)	898±34 (33.95)	897±21 (22.42)	882±20 (29.00)
907	N/A	N/A	N/A	N/A
1258	1262±36 (36.40)	1251±54 (54.06)	1269±42 (41.97)	1257±44 (43.97)
Aggregate RMSE	(23.64)	(34.20)	(25.41)	(29.03)

*** Tubes used for generating linear regression function are marked as N/A omitted from this comparison.**

****RMSE compared to T_1 is indicated inside parentheses after each T_1 value.**

4.4 Three-point Fitting Method

4.4.1 Multipoint vs. Three-point Fitting Methods

With the noise function described in Equation (24), if TI_1 = 400 ms is chosen, we are able to determine TI_2 = 1050 ms, as a maximum $\frac{T_1}{\sigma_{T_1}}$ was achieved. Therefore, TI = 1000 ms should be entered in the fitting model for the experiment TR = 3 s based on the data we have obtained. Meanwhile, TI_1 = 300 ms and TI_2 = 900 ms are used in the fitting for the experiment with TR = 2.5 s. The estimated T_1 results are listed in Table 14, which also lists the estimated T_1 results from the multipoint fitting method side by side with the three-point subtraction method for comparison. The aggregate RMS T_1 estimation error indicates that the three-point subtraction method is twice as accurate as the multipoint fitting method. The relative error for the normalized two point subtraction fitting method generally decreases from approximately 5% to less than 2% (Table 15), but the standard error increases from 1.5% to 2.3% compared to the two-parameter multipoint fitting method. Nevertheless, the $\frac{T_1}{\sigma_{T_1}}$ of the three-point subtraction method decreases from 50 to 40. The $\frac{T_1}{\sigma_{T_1}}$ indicates a slight increase of the statistical estimation error but the resulting value is still in the acceptable range.

Due to fewer measurements, there is potential for a significant reduction in scan time, as well as in the post-processing time. The total run time for the three-point subtraction method was about 1.8 minutes for the selected ROI and the multipoint fitting method with 9 points took 11.3 minutes which is approximately 6 times slower.

Table 14 also compares the estimated T_1 result for TR = 3 s and TR = 2.5 s. The aggregate RMSE is 24.43 for TR = 3 s and 23.61 for TR = 2.5 s. There is good consistency between the

multipoint and the three-point fitting methods in using shorter TR. The results show that reducing the repetition time from 3 s to 2.5 s does not deteriorate the accuracy of the estimated T_1.

Table 14 Phantom T_1 Comparison Study between Multipoint Fitting and Three-Point Fitting with IR-FSE

$TR > 10T_1$	TR = 3 s, 4 ETL		TR = 2.5 s, 4 ETL	
True T_1(ms)	T_1(ms) from Multipoint Fitting	T_1(ms) from three-point Fitting	T_1(ms) from Multipoint Fitting	T_1(ms) from three-point Fitting
576	551±10 (26.72)	572±15 (15.92)	548±10 (29.55)	570±14 (15.50)
575	558±12 (20.38)	583±16 (17.68)	558±12 (20.60)	581±15 (15.99)
682	646±11 (37.99)	672±16 (18.98)	643±11 (40.53)	671±15 (19.14)
737	694±12 (44.90)	725±19 (22.84)	693±13 (46.04)	728±18 (20.39)
734	696±13 (40.43)	729±19 (19.50)	696±14 (41.03)	730±19 (19.27)
834	784±11 (50.99)	821±17 (21.58)	786±11 (49.52)	824±17 (19.81)
875	822±12 (54.54)	862±20 (23.65)	822±14 (54.94)	864±21 (22.93)
903	846±16 (59.55)	890±22 (25.75)	847±16 (57.92)	893±21 (23.56)
907	861±12 (47.47)	905±19 (19.07)	864±13 (44.93)	911±21 (21.66)
1258	1170±26 (92.09)	1237±41 (45.90)	1167±31 (96.55)	1247±44 (45.40)
Aggregate RMSE	(50.98)	(24.43)	(51.76)	(23.61)

RMSE compared to true T_1 is indicated inside parentheses after each T_1 value.

Table 15 The Relative Error Comparison between Multipoint Fitting and Three-point Fitting Model

$TR > 10T_1$	T_1 relative Error for TR = 3 s, 4 ETL		T_1 relative Error for TR = 2.5 s, 4 ETL	
True T_1(ms)	Multipoint two-parameter Fitting	Three-point Fitting	Multipoint two-parameter Fitting	Three-point Fitting
576	-0.043	-0.007	-0.048	-0.010
575	-0.029	0.013	-0.029	0.011
682	-0.053	-0.015	-0.057	-0.017
737	-0.059	-0.016	-0.060	-0.006
734	-0.052	-0.007	-0.052	-0.012
834	-0.060	-0.016	-0.058	-0.008
875	-0.061	-0.014	-0.061	-0.013
903	-0.064	-0.015	-0.062	-0.011
907	-0.051	-0.002	-0.047	0.004
1258	-0.070	-0.016	-0.073	-0.009

4.4.2 The T_1 Underestimation Issue

The T_1 underestimation issue which is commonly seen in FSE sequence using multipoint fitting model is improved. Figure 23 illustrates the distribution of the estimated T_1 results for the voxels in a particular T_1 phantom gel tube. The upper half figures in Figure 23 reveal clear T_1 underestimation when using the regular two-parameter multipoint fitting method. The phenomenon is prone to be significant for long T_1 subjects. The variation in relative error appears to be systematic, and therefore it is possible to be corrected from the more accurate experimental data, such as the spectroscopy NMR method described in Section 3.7.1. The correction equations (Equation (32) and Equation (33)) were calculated and displayed previously in Section 4.3.1.

By looking at the lower half of Figure 23, we notice that the three-point fitting method also resulted in a well-balanced distribution for every phantom gel tube. However, the distribution is approximately centered at zero so the T_1 underestimation phenomenon is not significant and therefore the correction for estimated T_1 when using the three-point fitting method is no longer necessary.

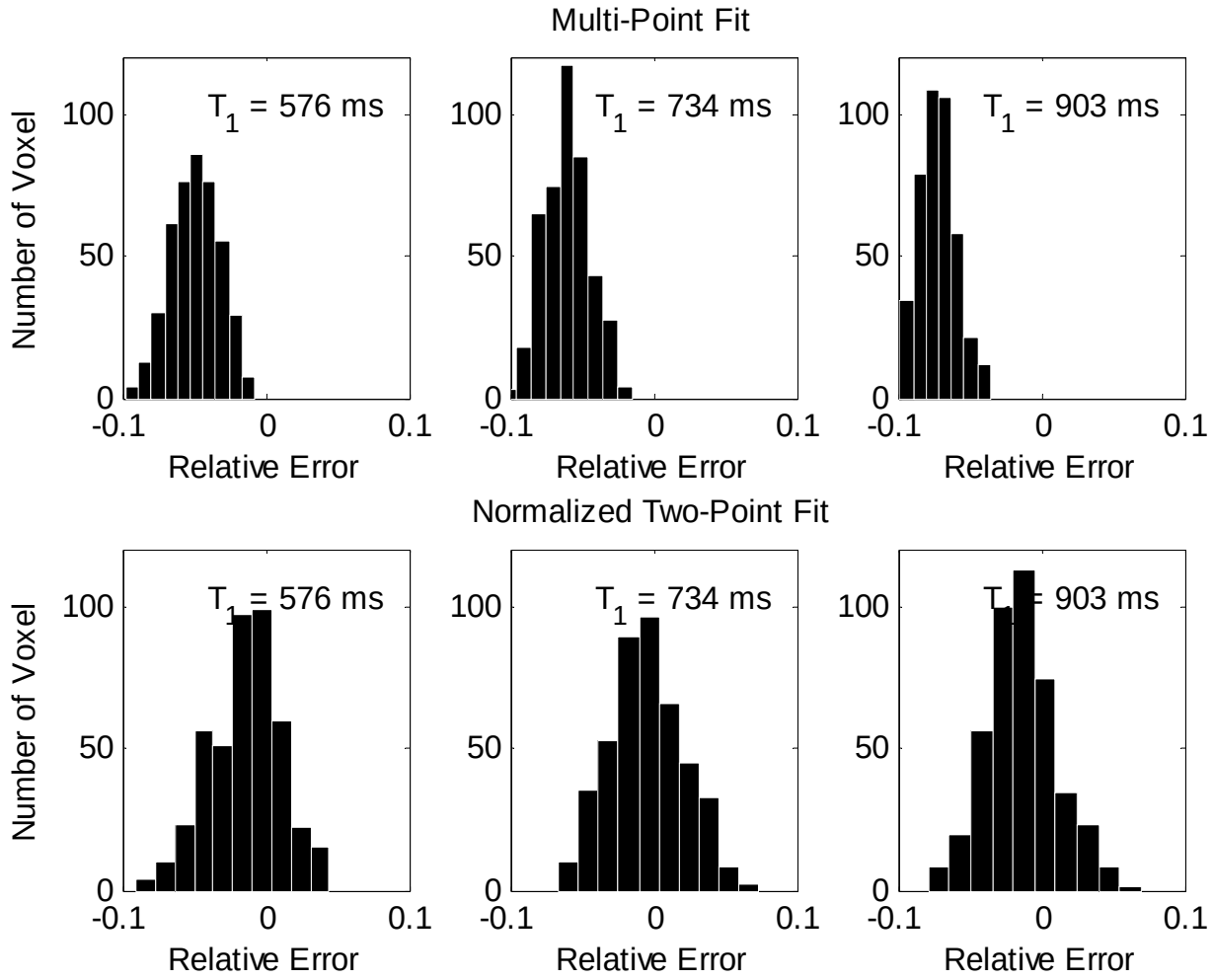

Figure 23 Histogram demonstrates T_1 under-estimation

4.4.3 The Effect of a Large Turbo Factor

In Section 4.3.5, we have examined the effect of increasing the turbo factor for multipoint fitting methods. The same analysis is carried out for the three-point fitting method and the result is shown in Table 16. The aggregate RMSE is 25.31 with a turbo factor of 8 and 29.32 with a turbo factor of 16. The overall decreasing in accuracy is 3.6% from turbo factor 4 to turbo factor 8, 20.02% from turbo factor 4 to turbo factor 16, and 15.84% from turbo factor 8 to turbo factor 16. Although the accuracy decreases in the three-point fitting method by using larger turbo factor, the accuracy is still twice better than using any multipoint fitting method.

Table 16 Three-point Fitting T_1 Result for Turbo Factor 4, 8 and 16

TR > $10T_1$	TR = 3.0 s, 4 ETL	TR = 3.0 s, 8 ETL	TR = 3.0 s, 16 ETL
True T_1(ms)		T_1(ms) from Three-point Fitting	
576	572±15 (15.92)	571±15 (16.19)	570±18 (18.80)
575	583±16 (17.68)	577±16 (16.26)	579±18 (18.82)
682	672±16 (18.98)	668±18 (22.77)	666±19 (24.85)
737	725±19 (22.84)	729±20 (21.89)	725±22 (24.98)
734	729±19 (19.50)	726±19 (21.06)	729±22 (22.82)
834	821±17 (21.58)	821±18 (22.47)	827±20 (26.48)
875	862±20 (23.65)	861±21 (25.26)	856±24 (30.43)
903	890±22 (25.75)	892±23 (25.41)	889±26 (29.83)
907	905±19 (19.07)	905±20 (20.13)	903±23 (22.94)
1258	1237±41 (45.90)	1244±46 (48.51)	1246±56 (56.95)
Aggregate RMSE	(24.43)	(25.31)	(29.32)

***RMSE compared to true T_1 is indicated inside parentheses after each T_1 value.**

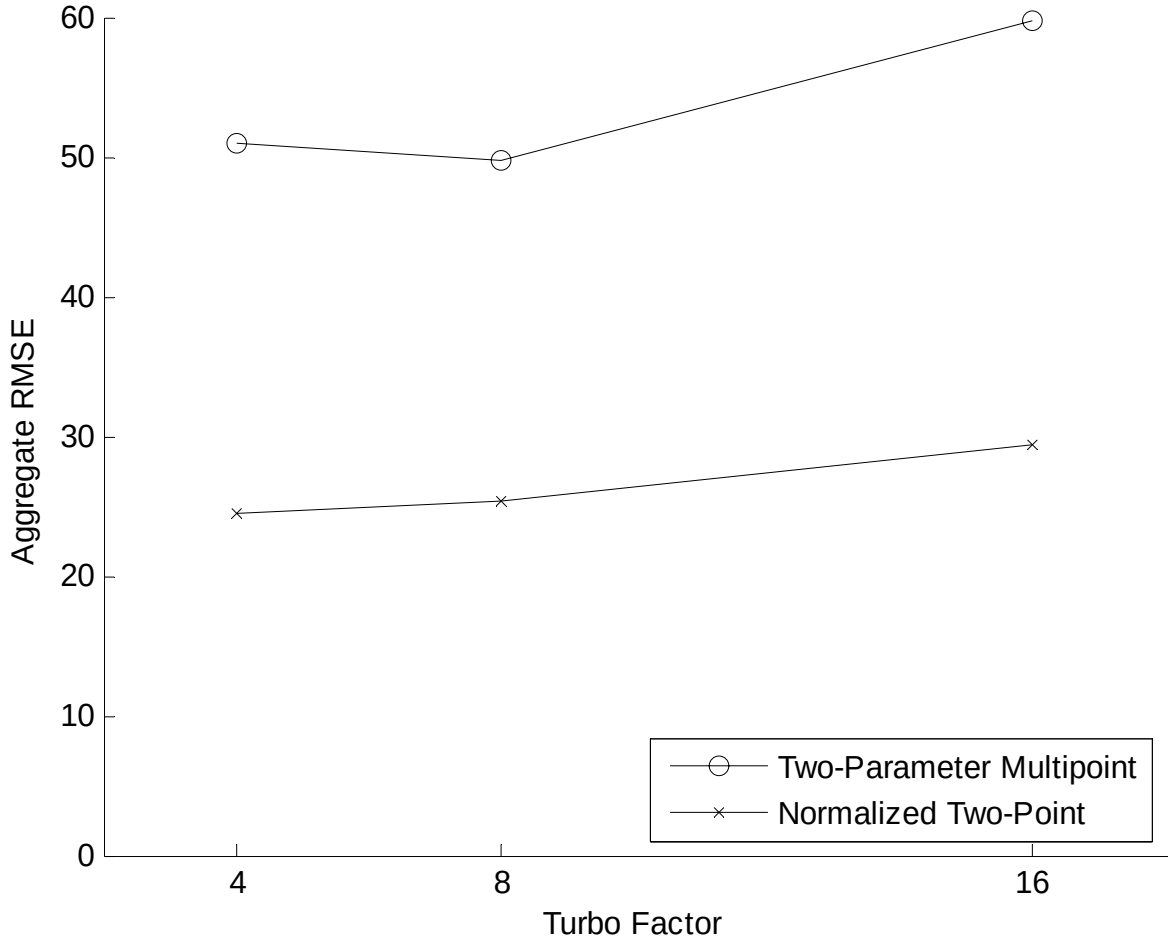

Figure 24 The Comparison for Estimated T_1 Accuracy Between Multipoint and Three-point fitting method in increasing Turbo Factor

4.4.4 Polarity Restoration

Table 17 shows the accuracy of the polarity restoration algorithm with different assumed values of f_{inv}. The RMSE indicates the error of estimated T_1 between true measurement data and magnitude data, which is converted by taking absolute values of real measurements. The total number of estimated voxels is 9414. The result shows that the error is insignificant even for the assumption of a perfect IR pulse (RMSE = 3.807, Error < 0.3%). The error starts to increase when the IR pulse efficiency drops below 85%. The true effectiveness of the IR pulse is around 95% to 98% from Table 8 via the multipoint curve fitting method.

Table 17 The Accuracy of Polarity Restoration

Assumption of IR Effectiveness (%)	Error Count	RMSE
100	28	3.807
95	0	0
90	0	0
85	8	1.204

4.5 T_1 Analysis for Human Brain

Both the multipoint and the three-point methods were applied to brain T_1 mapping of a healthy volunteer at 1.5 T. The experiment was conducted in compliance with the regulations of our university human research protection program. Four slices were acquired using the IR-FSE sequence, and the following parameters were used: TR = 3000 ms, TE = 12 ms, TI = [300, 800, 1300, 2300, 2800] ms, flip angle = 180°, turbo factor = 4, slice thickness = 5 mm, slice gap = 5 mm, pixel bandwidth = 130 Hz/pixel, field of view = 200 × 200 mm^2, and matrix size = 256 × 256. Each scan, with six TI values, took 3 min 09 sec.

Figure 25 shows the T_1 map of the four imaged brain slices for the multipoint (left column) and the three-point (right column) fitting methods, and Figure 26 demonstrates the corresponding aggregated error histogram. Gray matter and white matter were segmented. The estimated T_1 for the multipoint fitting method was 725±92 ms in white matter (N =18965) and 1196±197 ms in gray matter (N = 18150). The estimated T_1 for three-point fitting method was 752±99 ms in white matter (N =18965) and 1192±227 ms in gray matter (N = 18150). The histogram has a sharp cutoff which indicate the lower boundary used in the Levenberg-Marquardt optimization fitting algorithm.

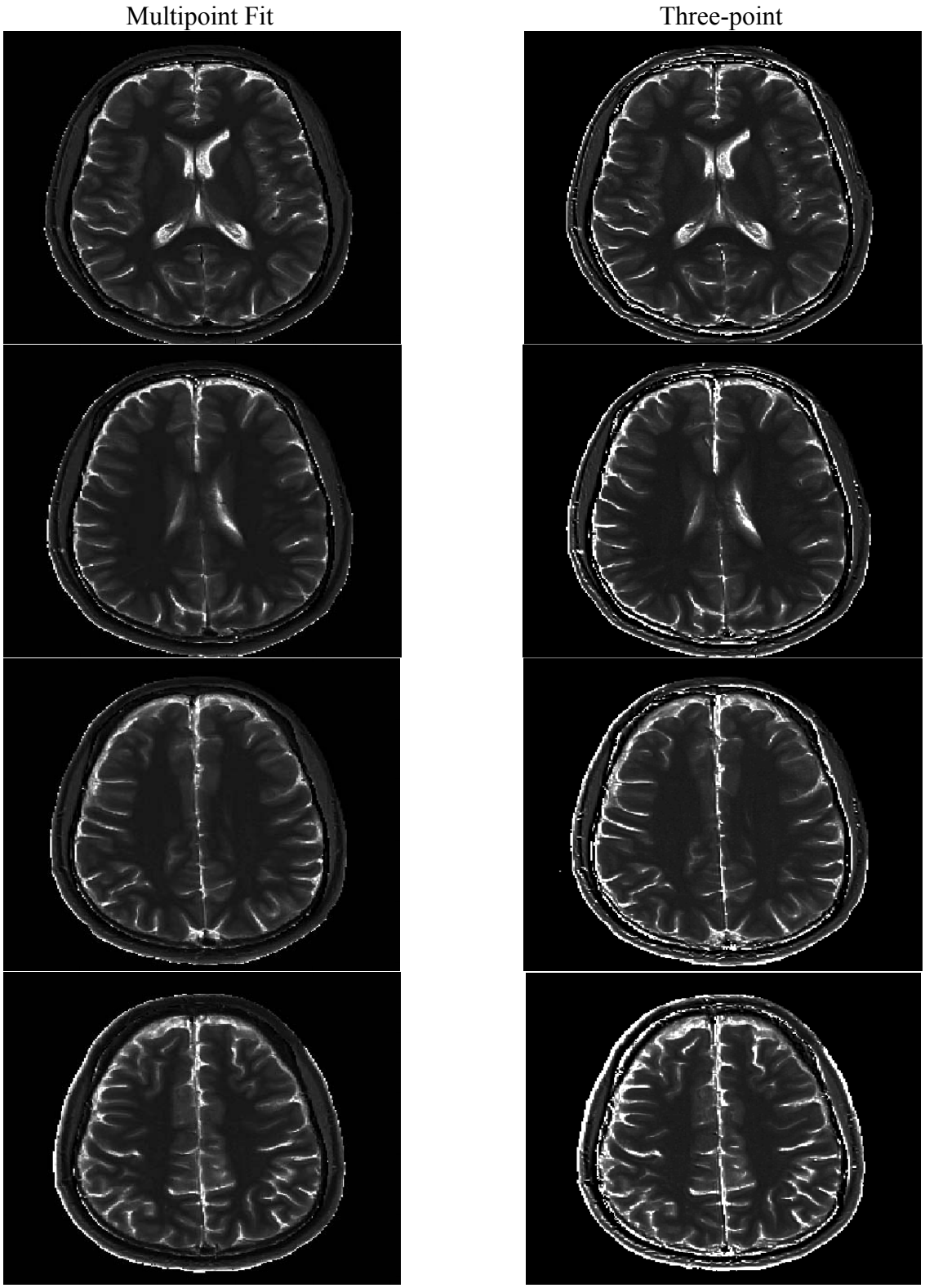

Figure 25 Brain T_1 image at 1.5 T with IR-FSE sequence. Multipoint (left) and three-point (right) fitting method are listed side by side for comparison.

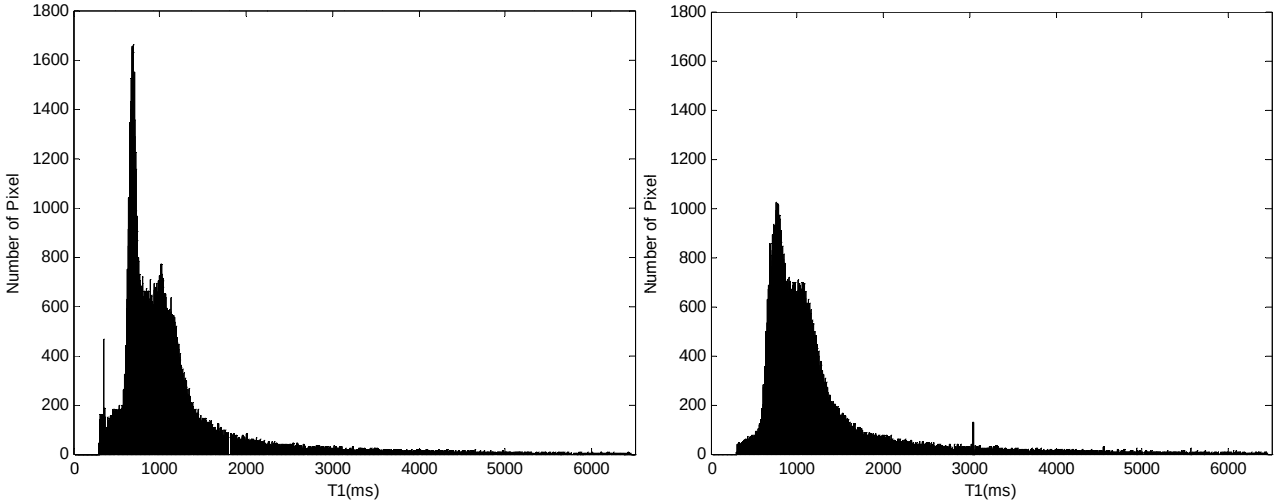

Figure 26 Brain T_1 histogram. The four image slices were aggregated.

The one-way ANOVA test was performed on the T_1 values for the brain white matter and gray matter to examine the variance between two fitting methods (Figure 27). The result for the brain white matter shows a significant difference (F= 395.000, p-value < 0.001) between the multipoint and three-point fitting models. However, for gray matter, the multipoint and three-point fitting model do not appear to be significantly different (F = 1.723, p-value = 0.189).

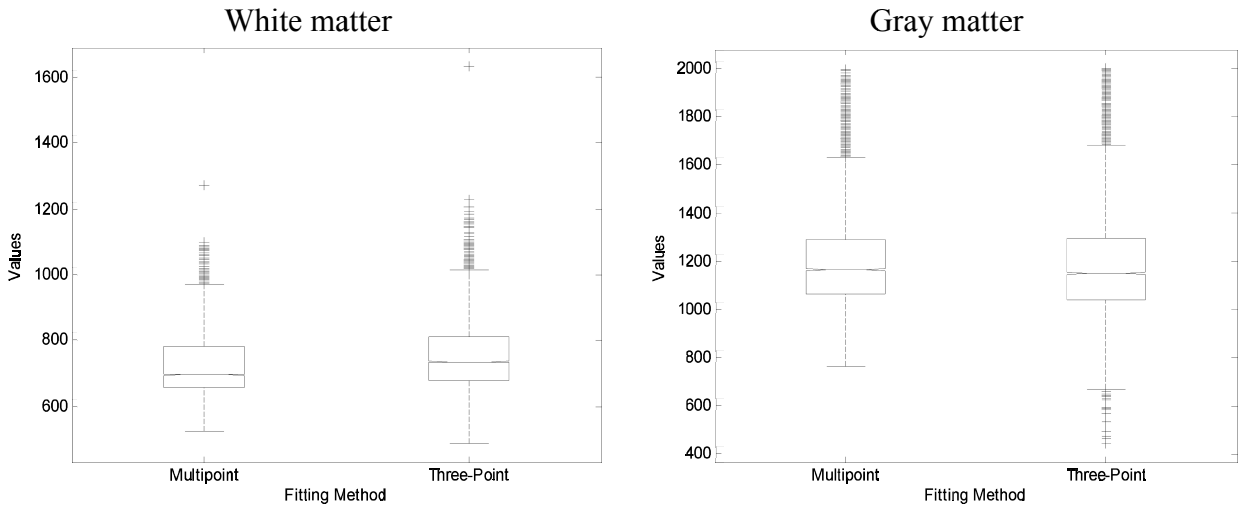

Figure 27 The boxplot for one-way ANOVA test to comparing two fitting models for the brain white matter (left) and gray matter (right)

Chapter 5 Discussion

Signal and Noise Analysis

The performance of T_1 estimation with the IR-FSE sequence was carefully examined with respect to the magnetization strength, signal-to-noise ratio, fitting algorithm, as well as sequence parameters such as the shorter repetition time and larger turbo factor. A custom designed phantom was employed with T_1 values that resemble human brain tissues such as white and gray matter. The true T_1 value of each tube was carefully determined using NMR spectroscopy. The improvement of a measuring sequence or a fitting algorithm for T_1 estimation was then examined by checking the root-mean-square error (RMSE), which provides combined information for the systematic difference and standard error of estimate with respect to the true T_1 values. A smaller aggregated RMSE value indicates a better measuring sequence or fitting algorithm.

The standard error reveals the noise caused by undesirable system interference. The result shows that the noise does not remain constant but increases with the absolute signal magnitude. Most of the noise appears to be similar to the corresponding absolute signal magnitude. The only exception is the signal acquired around the signal null where the noise does not vanish and therefore results in a low signal-to-noise ratio (SNR). Data points with low SNR in the multi-point fitting algorithm may not have significant impact unless the SNR is too small (i.e. SNR < 5), or too many points are acquired around the signal null. The situation can sometimes occur for

tissues with large T_1 values because the magnetization recovery is slower than that of tissues with small T_1. If the majority of signals has relatively low SNR, the estimation will not be as accurate as using solid high SNR signals. In fact, the example in Figure 10 shows that even a single noisy measurement close to the zero-crossing can increase the error by 100%. The same example also indicates that proper determination of the zero-crossing is important because a few accurate measurements obtained near the signal null are essential to improve the accuracy of T_1 estimation.

The Effect on Selection of TIs

From Figure 16, we have observed that the noise increases linearly with the increase of signal strength. A further analysis for signal to noise ratio in Figure 17 shows that the SNR increases from zero-crossing and rapidly reach a plateau. The above results indicate that some measurements around the zero-crossing are more important to improve the T_1 measurement accuracy due to relatively small noise and a good SNR (SNR > 15). The above conclusion is consistent to some researchers' recommendations which the data point at TI = T_1 or 1.3 T_1 needs to be included with a total six or eight data points in a multi-point fitting model for the traditional IR-SE sequence.[37] The signal obtained at TI = T_1 or 1.3 T_1 is always in the range of good SNR and is not too far away from the zero-crossing.

Nevertheless, we have also observed that the noise at the signal null is still noticeable and can result in very low SNR. These data points which are too close to the zero-crossing may deteriorate the T_1 estimation accuracy, and therefore, are suggested to be removed. However, unless the range of T_1 is known, it is difficult to ensure that the data at the specific positions can be acquired or eliminated. A possible solution is to use non-linear spacing TI during the scan and to run the fitting algorithm a second time after a preliminary T_1 data is determined. The zero-

crossing location can be roughly determined from Equation (17) as $TI_{null} = ln(2)T_1 \approx 0.693\ T_1$ in the ideal situation for the IR-SE sequence, or from Equation (19) with f_{inv} = 0.84-0.99 for the IR-FSE sequence. We simply run an additional analysis to evaluate the improvements in term of RMSE for the phantom simulation with low SNR (SNR < 10) data removed from the multipoint fitting algorithm. The results (Table 18) show a slight improvement for almost every phantom gel tube, except for the tube with the highest T_1 value (T_1 = 1258 ms). Nevertheless, we do not see a dramatic improvement. However, the SNR correction can be more effective if more points near the zero-crossing with satisfactory SNR were available for the fitting model. This is usually unlikely unless a specific range of T_1 is known for certain target tissues. Building an indexing chart with phantom simulation prior to the in vivo scan as well as using a special designed non-linear TI spacing will be helpful in improving the reproducibility by avoiding extremely low SNR signals or providing more useful information around the zero-crossing.

Table 18 Performance improvement obtained by removing low SNR data points from the multipoint fitting

NMR, T_1(ms)	Multipoint Fitting, TR = 3 s, 4 ETL, RMS_{T1}	
	9 Points	SNR < 10 Removed
576	26.72	24.07
575	20.38	17.29
682	37.99	35.62
737	44.90	42.41
734	40.43	37.23
834	50.99	48.49
875	54.54	54.54
903	59.55	55.99
907	47.47	45.59
1258	92.09	93.50
Aggregated RMSE	50.98	49.65

Traditional Multipoint Fitting Model and the T_1 Underestimation Issue

The accuracy of several multipoint fitting methods has been evaluated. Results obtained by the traditional three-parameter fitting method tend to be more underestimated than the those obtained by the modified two-parameter fitting method. The standard error of the estimates for both fitting models is not significantly different, and therefore the overall RMS error is smaller for the two-parameter fitting method. Therefore, the modified two-parameter fitting method has better accuracy than the traditional three-parameter fitting method

The remaining parameters in the multipoint fitting models have also been evaluated. In the two-parameter fitting model, S_0 is removed by the normalization process under the assumption that for a specific T_1 subject, the quantity $k \bullet M_0$ in Equation (34) is the same for all TI measurements. The assumption can be validated by comparing the f_{inv} between the two-parameter and the three-parameter fitting models. Because the f_{inv} between two fitting models does not differ significantly ($F = 0.2274 < F_{crit} = 4.414$ and p-value = 0.64) and the difference is usually less than 1%, we conclude that the assumption that every TI measurement has the same S_0 is valid. In addition, an inverse linear relationship is found between T_1 and f_{inv}. This indicates that the effectiveness of inversion pulse in IR-FSE sequence decreases for tissues with high T_1 values. The result of estimated f_{inv} leads to two conclusions: First, the effectiveness of the inversion preparation pulse in IR-FSE sequence is not perfect. Therefore, a traditional two-parameter fitting method, which only has estimators T_1 and M_0, is not suitable to estimate T_1 because it requires that the effectiveness of inversion pulse exceed 97%. Second, the effectiveness of inversion is lower for tissues with large T_1. Therefore, if a T_1 range is known, we should expect some information loss due to the poor performance of the inversion pulse for high T_1 tissues. Finally, the third

parameter S_0, shows a complicated pattern. Its correlation with the T_1 is not clear since S_0 is dominantly determined by the interaction between k and M_0.

The T_1 underestimation with the IR-FSE sequence has been reported[15,17,41,42,43] and the phenomenon is also evident in our experiments with either two-parameter or three-parameter multipoint fitting methods (Table 7). T_1 underestimation is the primary issue that affects the T_1 estimation accuracy. Possible causes for T_1 underestimation have been investigated and it has been suggested that the primary cause is the magnetization transfer effect.[26,41-44] The more number of echoes in the multislice IR-FSE sequence, the stronger the underestimation of the T_1 value.[42] However, our experimental results indicate that for certain T_1 values (roughly in the range 570 ms – 900 ms), the mean value was not significantly affected when the turbo factor was increased with the IR-FSE sequence. Nevertheless, the RMS error indeed got worse when raising the turbo factor due to the decrease of precision. One possible cause for the loss of precision is the impairing spatial resolution due to the T_2 of the subjects contributing to the signal.[6] Our result shows that a turbo factor of 8 may be the most suitable setting in measuring T_1 in consideration of scan efficiency and aggregate RMS error while using a regular multipoint fitting method. For every TI acquisition, the approximate scan time for a slice of 256 by 256 pixels using TR = 3 s and a turbo factor of 8 is 1.6 minutes.

Our results confirm Zhu's finding that T_1 underestimation is consistent for pixels with the same T_1 values and has significant linear relationship with true T_1 values (Figure 18). This linear correlation is also confirmed to persist for large turbo factors, i.e. ETL = 8 or 16 (Figure 22). Therefore, a linear regression function can be applied to adjust for the systematic underestimation even with larger turbo factors. If the correction function equation (12) is applied, the aggregate RMS error for the two-parameter fit with TR = 3 s, turbo factor = 4 can be reduced

to 17.55. Although the linear correlation is able to correct the shifted T_1 values, its limitation is obvious. First, a reference data set with true T_1 value is required. However, obtaining true T_1 values means a repeated, long scan, which is usually not feasible for ill patients. Second, even if the reference data used for T_1 correction is acquired from a well designed phantom with known T_1, its suitability is doubtful because of the complexity of in-vivo environment. Finally, the correction function only affects the estimated T_1 but has no impact on the precision of estimation, which usually leads to serious inaccuracy if some very noisy signals are used in the fitting process.

Correction with a Weighted Cost Function

We have proposed a correction to the fitting model to improve the existing T_1 mapping method without additional data acquisition.[45] By employing a weighted cost function (Equation (13)) that emphasizes more reliable measurement data, our results show significant improvement in T_1 accuracy for sequences with a high turbo factor. The weights, w_i, are applied on each signal measurement during the fitting process according to the magnitude at each TI. An additional parameter, α is critical to determine w_i. Our experimental results indicate that a positive α between 0.4 and 0.6 is optimally reduces the estimation error if a small turbo factor is set in the sequence protocol. For larger turbo factors such as ETL = 8 or 16, the optimum α is approximately 1.0. With a proper weighting factor α selected in the cost function, the aggregated estimation error of T_1 is reduced by to up to 45%. In addition, we notice that the reproducibility is also improved, especially for high turbo factor sequences which usually suffer from poor SNR and signal loss. Thus, the overall performance with a weighted fitting algorithm is better than that of the linear regression correction method. Noting that although the combination of the weighted fitting correction model and the linear regression correction method can be

implemented to work together, there is actually no benefit gained from the combination of two correction methods since the weighted fitting model has been capable to reduced the systemic error to less than 2% with appropriate chosen weighting factor. On the contrary, applying the linear regression correction after using the weighted fitting model may cause significant error on the low T_1 tissues because the low T_1 values can be over-corrected by the linear regression function.

A two-pass adaptive T_1 estimation with weight correction technique was also proposed and evaluated to further exploit the optimum α which varies for different T_1 values. The optimum value of α is determined by minimizing the T_1 estimation error for a single phantom tube. The adaptive method can provides up to 10% further error reduction. Finally, the fine-tuned α can be utilized in the corresponding T_1 range during fitting process for subsequent clinical studies.

A note on the computational complexity of the proposed correction method is necessary. The single-pass, fixed-weights method requires N-1 extra multiplications per evaluation of the cost function (equation (13)). The weights can be pre-computed once for each pixel. The time to perform these additional computations is minor when compared to the other terms in the cost function, in particular $S(T_1, S_0, f_{inv}, TI_i)$. For the two-pass, adaptive-weights method, the reconstruction time can be twice as long.

The Three-Point Technique

While traditional multipoint inversion recovery methods require at least four inputs in the fitting model to achieve desirable precision[34], the three-point fitting method is able to provide a more accurate T_1 map result with carefully selected values of three inversion times. The third TI is always the longest TI available in the sequence protocol setting, and provides a normalization factor. After the normalization process, the other two TIs can be described as a two-point model

(equation (22)). Like other two-point methods[28,30,51], the precision of the estimated T_1 is sensitive to the selection of the (TI_1, TI_2) pair. According to the simplified noise function which has been discussed previously in Equation (24), the first TI (TI_1) should be the shortest possible to minimize the estimation error in T_1. However, after running through all the possible combination for TI_1 and TI_2, we have confirmed that TI_1 must be chosen near the zero-crossing time. Nevertheless, the best TI_2 we found still has good agreement with on the result obtained with equation (23). The three-point technique shows a reduction of up to 50% in aggregated error compared with traditional multipoint IR method.

Compared to other T_1 estimation methods (two-point, multipoint or zero-crossing method), the three-point technique has several advantages: (1) The method uses the full dynamic signal range and therefore has potential to improve accuracy of T_1 estimation. (2) It is more efficient. With fewer data points required and only one parameter to be estimated in the fitting process, the computational complexity is reduced. (3) Unsigned magnitude data is suitable. The polarity restoration technique can determine the appropriate polarity information to selected TIs without actually determining the true zero-crossing point. (4) The estimated T_1 result is less sensitive to shorter TR values (2500 ms) and larger turbo factors (ETL = 8 or 16). This is because the three-point method is more closely related to the zero-crossing time, in particular by careful selection of TI_1. From Figure 20 and Figure 21, it can be observed that the zero-crossing time does not change for different turbo factor.

However, the three-point method has several limitations. First, the precision is slightly worse than traditional multipoint fitting methods. This is due to the fact that according to equation (23), if TI_1 increases, σ_{T1} will increase. In addition, the TI acquired near the zero-crossing sometimes has poor SNR, which may potentially increase the uncertainty for T_1 estimation. Second, because

a relatively shorter TR is exploited in this technique, measuring tissue with higher T_1 such as CSF is not applicable. Therefore, unless longer TR is employed in the setting protocol, the study should mainly focus on brain gray and white matter.

It is worth emphasizing that choosing the first TI around the zero-crossing point is very important. In the case that a target tissue contains a wide range of T_1 values, some very low or very high T_1 values may be estimated inaccurately due to the selection of TI. It will be better to acquire an additional signal between TI_2 and TI_3 to cover all the possible zero-crossing point. The other advantage for acquiring an additional TI is that a two-pass post-processing is able to perform for more accurate estimation in the case of wide T_1 variation.

Modified ordering scheme using the three-point technique

Since the three-point technique uses only three TI values for data fitting, it is feasible to modify the original six-point TESO-IRFSE sequence[15] with a more efficient slice ordering scheme. A proposed complete slice ordering scheme is illustrated in Figure 28. The modified scheme collects data at four different TIs for a total of twelve slices of T_1 mapping images. Each TI group described in Figure 28 has same TI increment between slices. The TI increment between Group1, Group2 and Group3 can be the same. The slices in the last group always have the longest TI available in the sequence protocol setting. The number of slices in the proposed ordering scheme must be 4N, where N = 1, 2 or 3. Compared to the TESO-IRFSE sequence, the new slice ordering scheme can reduce the scan time by approximate 33% and therefore it comes closer to providing T_1 mapping in a timely manner.

An essential limitation for the proposed slice ordering scheme needs to be addressed. Because nonselective inversion pulses are used in the sequence, successive slices will have different TI_1 and TI_2 values. Therefore, some voxels may not have the optimal inversion time for the highest

SNR_{T1}. Slice-dependent errors in estimating T_1 are very likely introduced. However, since signals are acquired at four different TI for every T_1 estimate, it is possible to reduce the slice-dependent errors by using a two-pass post processing. First we can perform T_1 estimation with a three-point technique to receive coarse T_1 mapping images. We then use the results of first-run T_1 mapping images and the corresponding optimum TI_1s and TI_2s for a better result.

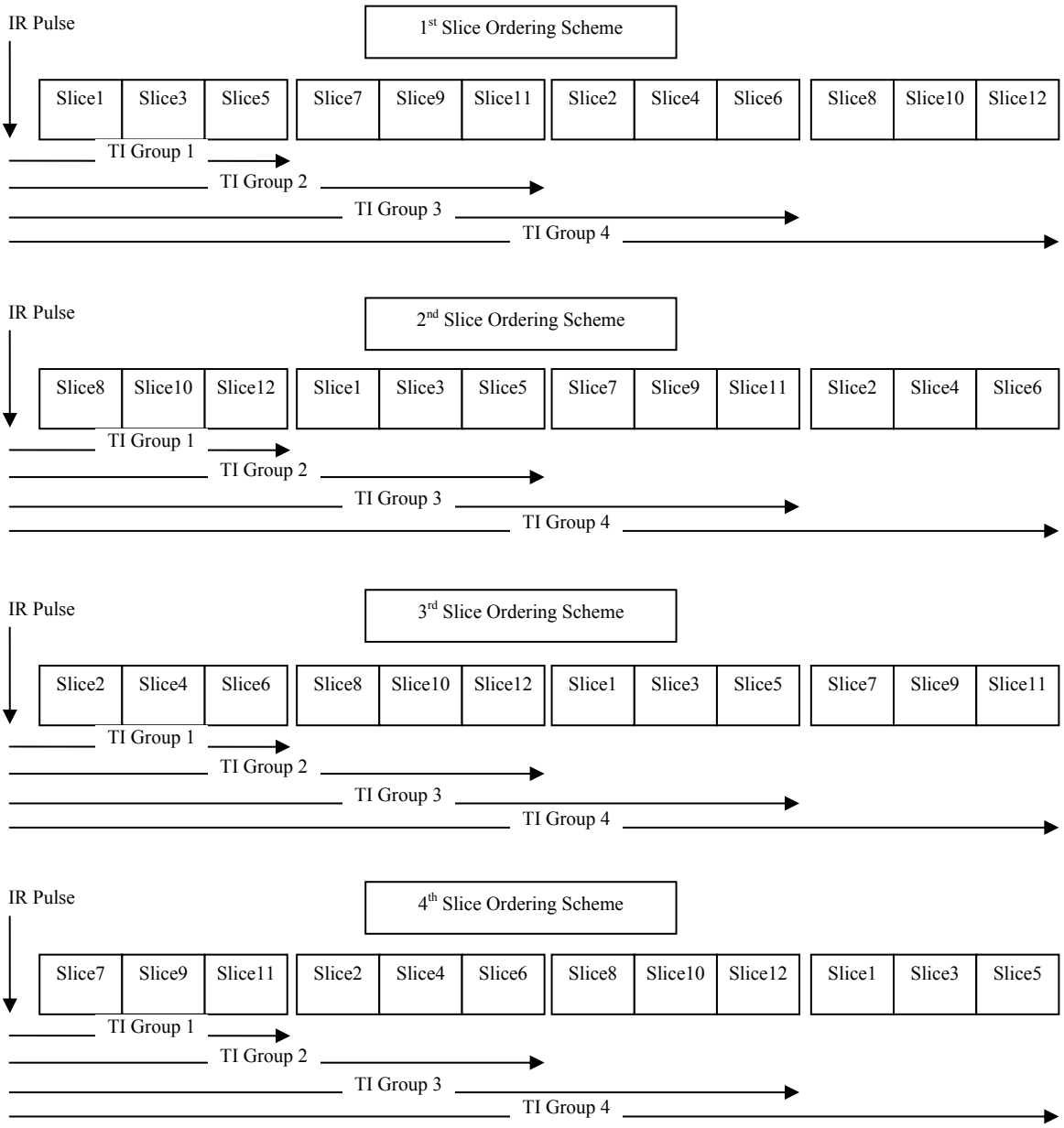

Figure 28 New ordering scheme for the four-point TESO-FSE sequence.

Brain Scan T_1 Mapping

We have performed a brain scan on a normal healthy volunteer. The resulting T_1 map has been segmented into different tissue types, in particular gray matter and white matter. With two-parameter multipoint fitting method (six points in data set), the estimated T_1 value for white matter was 725±92 ms and for gray matter was 1196±197 ms, which are in good agreement with the values reported by Zhu et al (Zhu & Penn, 2005). The estimated T_1 for the three-point fitting method was 752±99 ms in white matter 1192±227 ms in gray matter. The peaks corresponding to white matter (725 ms for the multipoint fit and 752 ms for the three-point fit) and gray matter (1196 ms for the multipoint fit and 1192 ms for the three-point fit) in the whole brain histogram are visible. Nevertheless, a loss of precision resulting from non-optimal TI values chosen in the fitting can be observed from the whole brain histogram for the three-point fitting method.

From the result of the one-way ANOVA test, we conclude that the difference between the two fitting models for the brain white matter is significant (p-value < 0.001). The difference for the brain gray matter, however, is not statistically significant. Taking into account the underestimation error that is commonly seen while using IR-FSE T_1 measuring method, it is reasonable to consider that the T_1 mapping result for the brain white matter is closer to the true T_1 with three-point fitting method than with the multipoint fitting method. On the other hand, due to a lack of true T_1 values for the human brain, we are not able to draw definite conclusions about the actual performance.

Motion Artifacts

Although the patient's head was secured and immobilized, the estimation may still suffer from slight movement due to the long scanning process. It is difficult to ensure the locations of the

selected ROIs are exactly the same for each TI acquisition. In fact, this type of motion artifact can be easily found around the edge of the brain and in regions with large T_1 gradient. The resulting measurements for some pixels in such areas may not show a monotonically exponential recovery curve. Since all fitting methods are based on the assumption of a signal increasing with TI, data that does not satisfy this assumption can produce undesired results.

Since traditional multipoint fitting uses more than four points for data fitting, this built-in redundancy ensures that the fitting result may still comply with the monotonically exponential pattern even though some data points do not have good fit. The three-point method, however, uses only three points in the fitting and therefore would severely suffer from the non-monotonically exponential increasing pattern so the fitting process will fail. The T_1 mapping values around the edges of the brain or the region with large T_1 variation is unreliable.

A solution that is likely to correct image motion artifact is using image registration.[62] The process identifies image features such as points, lines or contours and builds up the correspondence between the images obtained for different TI values. For intensity images such as the ones used in T_1 mapping, the center point on the corresponding sub-images is considered as the feature reference so we can register a set of sub-images to a reference image. Then image processing techniques such as rotation and translation will be performed on the sub-images according to the correlation between the reference image and registered sub-images. The Image registration technique has been studied for MRI T_1 image on various regions of human body, such as knee[63,] breast[64] or heart [65]. As the results of numerous studies, the technique has gained significant improvement on motion correction for T_1 mapping image.

Based on the mutual information registration algorithm, we have carried out a series of analyses to evaluate the feasibility of motion artifact correction for possibly distorted brain T_1 images. Unfortunately, after implementing the image registration, using the corrected images does not demonstrate any improvement in comparison with the original fitting result. One of the possible reasons for this negative outcome could be underestimating the true anatomy complexity. In fact, the movement between slices is presumed very little, the correction process may not detect such tiny movement properly. Besides, the rotation algorithm used for registration can introduce aliasing to the image. The jointing effect resulted from incorrect mutual information registration and image aliasing may bring in more complications.

Chapter 6 Conclusion

The signal resulting from the IR-FSE sequence has been thoroughly analyzed in order to improve the accuracy of quantitative T_1 mapping of the human brain. It was determined that the accuracy of T_1 estimation can be improved by collecting more data points around the zero-crossing time of the relaxation curve with good signal-to-noise ratio. As a result, the TI for each measurement is better to be chosen nonlinearly with emphasis around the zero-crossing. Besides, the measurements near the zero-crossing with poor SNR will result in the increase of errors while estimating T_1, and therefore are suggested to be removed from the input data in the fitting process.

Several optimized post-processing algorithms have been studied and compared in terms of their T_1 mapping accuracy. Several algorithm optimizations have been proposed and their effects on performance have been evaluated. The traditional multipoint three-parameter fitting method does provide a very good precision but seriously underestimates T_1 with the IR-FSE sequence. The modified multipoint two-parameter fitting method, which uses the longest TI measurement as a normalization factor to reduce the fitting complexity, however, produces less underestimation compared to the traditional multipoint three-parameter fitting method. The precision of the modified two-parameter fitting method is as good as that of the three-parameter fitting method, and therefore, results in a smaller T_1 estimation error.

Moreover, the proposed methods for correcting the underestimation error by using a linear regression algorithm and a weighted fitting model have been validated. The linear regression correction reduces underestimation even for a large turbo factor IR-FSE sequence such as ETL = 8 or 16, which usually shows heavier underestimation phenomena and produces unreliable T_1 estimation results due to loss of precision in measured MR signals. Since the average underestimation error is consistent for all T_1 values, the linear regression method is very effective in correcting it. It, however, does not effectively increase the precision for IR-FSE sequences with a large turbo factor. Besides, if the linear correction function is obtained mostly from tissues with high T_1 tissues, using it on low T_1 tissues can result in undesired overestimation. In order to avoid the disadvantages of the linear regression correction method, we have proposed a novel method that uses weighted fitting.45 Our experiments have shown that with properly selected weighting factors, $w_i = \frac{1}{|S_i|^{\alpha}}$, curve fitting generates a more accurate T_1 estimation than the regular multipoint fitting methods. The precision of the T_1 estimation for a large turbo factor sequence can be increased and therefore, the aggregate RMSE for T_1 mapping can be effectively reduced.

Based on the above correction methods, we proposed an intra-scan correction technique that makes use of several vials filled with standard gel of known T_1 and placed around the head. A corresponding linear regression function or an appropriate weighting factor can be computed in advance, and employed in post-processing. This technique does not directly affect the scan time, but improves accuracy and therefore potentially allows a more aggressive use of time-saving techniques, especially while using the IR-FSE sequence with a large turbo factor. Its only disadvantages are the requirement for a customized head coil and a very small overhead in post-processing time.

To further explore the possibility of exploiting the IR-FSE sequence more efficiently, we derived a new fitting model that uses only three different TI measurements from the general equation of the IR-FSE sequence. Our experiments show that with carefully selected values for TI_m and the (TI_1, TI_2) pair, the three-point method achieves very accurate T_1 estimation in a very efficient manner. The only disadvantage for the three-point method is that the precision decreases slightly, but it is still in an acceptable range. A new IR-FSE reordering scheme was proposed as well, based on the three-point fitting method. The new designed scheme utilizes a non-selective inversion recovery pulse and collects data with a maximum of four different TIs within the repetition time of a sequence. Eventually, four reordering schemes will be adequate to collect a maximum of four different TI measurements for 12 slices and therefore reduce the total scan time by 1/3 compared to the TESO-IRFSE sequence originally proposed by Zhu.[15]

To further verify the performance of the three-point fitting method on the human brain, we have performed the T_1 measuring experiment on one health male volunteer with the IR-FSE sequence with a turbo factor of 4. The estimated T_1 result for gray and white matter of the human brain is consistent to the results computed using the multipoint fitting method.

For the real human brain experiment, the issue of motion artifacts was briefly examined. A possible solution to correct the motion artifact is using the image registration technique[62], in particular the mutual information registration algorithm. Unfortunately, the correct to the motion artifact for brain T_1 mapping image with image registration technique was not successful in our preliminary analysis. The true anatomy for the human brain may present more complexity than our initially considered. In addition, more samples from the true anatomy are most likely helpful to the future research on the addressed issues.

Bibliography

1. Fatouros, P.; Marmarou, A. Use of magnetic resonance imaging for in vivo measurements of water content in human brain: method and normal values. J Neurosurg 1999, 90 (1), 109-115.
2. Schwarcz, A.; Berente, Z.; Osz, E.; Dóczi, T. Fast in vivo water quantification in rat brain oedema based on T(1) measurement at high magnetic field. Acta Neurochir (Wien) 2002, 144 (8), 811-816.
3. Vrenken, H.; Geurts, J.; Knol, D.; van Dijk, L.; Dattola, V.; Jasperse, B.; van Schijndel, R.; Polman, C.; Castelijns, J.; Barkhof, F.; Pouwels, P. Whole-Brain T1 Mapping in Multiple Sclerosis: Global Changes of Normal-appearing Gray and White Matter. Radiology 2006, 240 (3), 811-820.
4. Neema, M.; Stankiewicz, J.; Arora, A.; Dandamudi, V. S. R.; Batt, C. E.; Guss, Z. D.; Al-Sabbagh, A.; Bakshi, R. T1- and T2-Based MRI Measures of Diffuse Gray Matter and White Matter Damage in Patients with Multiple Sclerosis. Neuroimaging 2007, 17 (Supplement s1), 16S-21S.
5. Steen, R.; Hunte, M.; Traipe, E.; Hurh, P.; Wu, S.; Bilaniuk, L.; Haselgrove, J. Brain T1 in young children with sickle cell disease: evidence of early abnormalities in brain development. Magn Reson Imaging 2004, 22 (3), 299-306.

6. McRobbie, D. W.; Moore, E. A.; Graves, M. J.; Prince, M. R. MRI from Picture to Proton, 2nd ed.; Cambridge University Press, 2007.
7. Shah, N.; Neeb, H.; Zaitsev, M.; Steinhoff, S.; Kircheis, G.; Amunts, K.; Häussinger, D.; Zilles, K. Quantitative T1 mapping of hepatic encephalopathy using magnetic resonance imaging. Hepatology 2003, 38 (5), 1219-1226.
8. Barral, J. K.; Gudmundson, E.; Stikov, N.; Etezadi-Amoli, M.; Stoica, P.; Nishimura, D. G. A Robust Methodology for In Vivo T1 Mapping. Magn Reson Med 2010, 64 (4), 1057-1067.
9. Drain, L. E. A Direct Method of Measuring Nuclear Spin-Lattice Relaxation Times. Proceedings of the Physical Society, Section A 1949, 62 (5), 301-306.
10. Hahn, E. L. An Accurate Nuclear Magnetic Resonance Method for Measuring Spin-Lattice Relaxation Times. Phys. Rev. 1949, 76, 145-146.
11. Ordidge, R.; Gibbs, P.; Chapman, B.; Stehling, M.; Mansfield, P. High-speed multislice T1 mapping using inversion-recovery echo-planar imaging. Magn Reson Med 1990, 16 (2), 238-245.
12. Tong, C.; Prato, F. A novel fast T1-mapping method. J Magn Reson Imaging 1994, 4 (5), 701-708.
13. Clare, S.; Jezzard, P. Rapid T1 Mapping Using Multislice Echo Planar Imaging. Magn. Reson. Med. 2001, 45, 630-634.
14. Tyler, D. J.; Moore, R. J.; Marciani, L.; Gowland, P. A. Rapid and accurate measurement of

transverse relaxation times using a single shot multi-echo echo-planar imaging sequence. Magn Reson Imaging 2004, 22 (7), 1031-1037.

15. Zhu, D. C.; Penn, R. D. Full-Brain T1 Mapping through Inversion Recovery Fast Spin Echo Imaging with Time-Efficient Slice Ordering. Magn Reson Med 2005, 54 (3), 725-731.
16. Deichmann, R. Fast High-Resolution T1 Mapping of the Human Brain. Magn. Reson. Med. 2005, 54, 20-27.
17. Neeb, H.; Zilles, K.; Shaha, N. J. A new method for fast quantitative mapping of absolute water content in vivo. NeuroImage 2006, 31 (3), 1156-1168.
18. Hsu, J.; Glover, G. Rapid MRI method for mapping the longitudinal relaxation time. J Magn Reson 2006, 181 (1), 98-106.
19. Fatouros, P.; Marmarou, A.; Kraft, K.; Inao, S.; Schwarz, F. In vivo brain water determination by T1 measurements: effect of total water content, hydration fraction, and field strength. Magn Reson Med. 1991, 17 (2), 402-413.
20. Kingsley, P. B.; Monahan, W. G. Effect of increased repetition time TR on precision of inversion-recovery T1 measurements. Magn Reson Imaging 2001, 19 (2), 279-282.
21. Bernstein, M. A.; King, K. F.; Zhou, X. J. Handbook of MRI Pulse Sequences; Academic Press, 2004.
22. Look, D. C.; Locker., D. R. Time Saving in Measurement of NMR and EPR Relaxation Times. Rev. Sci. Instrum. 1970, 41, 250.

23. Stehling, M. J.; Howseman, A. M.; Ordidgem, R. J.; Chapman, B.; Turnerm, R.; Coxonm, R.; Gloverm, P.; Mansfield, P.; Coupland, R. E. Whole-body echo-planar MR imaging at 0.5 T. Radiology 1989, 170 (1 Pt 1), 257-263.

24. Gowland, P.; Mansfield., P. Accurate measurement of T1 in-vivo in less-than 3 seconds using echo-planar imaging. Magn. Reson. Med. 1993, 30 (3), 351-354.

25. Freeman, A. J.; Gowland, P. A.; Mansfield, P. Optimization of the ultrafast Look-Locker echo-planar imaging T-1 mapping sequence. Magn. Reson. Imag. 1998, 16 (7), 765-772.

26. Dowell, N.; Tofts, P. Fast, accurate, and precise mapping of the RF field in vivo using the 180 degrees signal null. Magn Reson Med. 2007, 58 (3), 622-630.

27. Lin, M. S. Interpolative computation of spin-lattice relaxation times from signal ratios. Magn Reson Med 1985, 2 (3), 234-244.

28. Kurland, R. Strategies and tactics in NMR imaging relaxation time measurements. I. Minimizing relaxation time errors due to image noise--the ideal case. Magn Reson Med 1985, 2 (2), 136-158.

29. Canet, D.; Brondeau, J.; Elbayed, K. Superfast T1 determination by inversion-recovery. J Magn Reson 1988, 77 (3), 483-490.

30. Imran, J.; Langevin, F.; Saint-Jalmes, H. Two-Point Method For T1 Estimation With Optimized Gradient-Echo Sequence. Magn Reson Imaging 1999, 17 (9), 1347-1356.

31. Crawley, A. P.; Henkelman, R. M. A Comparison Of One-Shot And Recovery Methods In

T1 Imaging. Magn Reson Med. 1988, 7 (1), 23-34.

32. Jahnga, G.-H.; Stables, L.; Ebel, A.; Matson, G. B.; Meyerhoff, D. J.; Weiner, M. W.; Schuff, N. Sensitive and fast T1 mapping based on two inversion recovery images and a reference image. Med Phys 2005, 32 (6), 1524-1528.
33. Mason, G. F.; Chu, W.-J.; Hetherington, H. P. A General Approach to Error Estimation and Optimized Experiment Design, Applied to Multislice Imaging of T1 in Human Brain at 4.1 T. J Magn Reson 1997, 126 (1), 18-29.
34. Kingsley, P. B. Signal Intensities and T1 Calculations in Multiple-Echo Sequences with Imperfect Pulses. Conc Magn Reson 1999, 11 (1), 29-49.
35. Gupta, R. K.; Ferretti, J. A.; Becker, E. D.; Weiss, G. H. A modified fast inversion-recovery technique for spin-lattice relaxation measurements. J Magn Reson 1980, 38 (3), 447-452.
36. Kingsley, P.; Ogg, R.; Reddick, W.; Steen, R. Correction of errors caused by imperfect inversion pulses in MR imaging measurement of T1 relaxation times. Magn Reson Imaging 1998, 16 (9), 1049-1055.
37. Kingsley, P. B. Methods of Measuring Spin-Lattice (T1) Relaxation Times: An Annotated Bibliography. Conc Magn Reson 1999, 11 (4), 243-276.
38. T. Phil Pitner, J. F. W. Simulation of nuclear magnetic resonance spin lattice relaxation time measurements for examination of systematic and random error effects. Analytical Chemistry, 1979, 2203-2206.

39. Hajnal, J.; Baudouin, C.; Oatridge, A.; Young, I.; Bydder, G. Design and implementation of magnetization transfer pulse sequences for clinical use. J Comput Assist Tomogr 1992, 16 (1), 7-18.

40. Rydberg, J. N.; Riederer, t. J.; Rydberg, C. H.; Jack, C. R. Contrast optimization of fluid-attenuated inversion recovery (FLAIR) imaging. Magn Reson Med 1995, 34 (6), 868-877.

41. Stanisz, G. J.; Odrobina, E. E.; Pun, J.; Escaravage, M.; Graham, S. J.; Bronskill, M. J.; Henkelman, R. M. T1, T2 Relaxation and Magnetization Transfer in Tissue at 3T. Magn Reson Med 2005, 54 (2), 507-512.

42. Meara, S. J. P.; Barker, G. J. Impact of Incidental Magnetization Transfer Effects on Inversion-Recovery Sequences That Use a Fast Spin-Echo Readout. Magn Reson Med 2007, 58 (4), 825-829.

43. Wright, P. J.; Mougin, O. E.; Totman, J. J.; Peters, A. M.; Brookes, M. J.; Coxon, R.; Morris, P. E.; Clemence, M.; Francis, S. T.; Bowtell, R. W.; Gowland, P. A. Water proton T1 measurements in brain tissue at 7, 3, and 1.5 T using IR-EPI, IR-TSE, and MPRAGE: results and optimization. Magn Reson Mater Phy 2008, No. 21, 121-130.

44. Wang, J.; Qiu, M.; Kim, H.; Constable, R. T1 measurements incorporating flip angle calibration and correction in vivo. J Magn Reson. 2006, 182 (2), 283-292.

45. Chang, Y.-Y.; Kraft, K. A.; Docef, A. On Improving The Accuracy of T1 Mapping of The Human Brain. European Signal Processing Conference, Barcelona, Spain, 2011.

46. Bakker, C.; De Graaf, C.; Van Dijk, P. Restoration of signal polarity in a set of inversion

recovery NMR images. IEEE Trans Med Imaging 1984, 3 (4), 197-202.

47. Gerhards, R.; Dietrich, W. The analysis of spin-lattice relaxation time experiments. J Magn Reson 1976, 23 (1), 21-29.

48. George, H. W.; Guptaj, R. K.; Ferretti, J. A.; Becker, E. D. The choice of optimal parameters for measurement of spin-lattice relaxation times. I. Mathematical formulation. J Magn Reson 1980, 37 (3), 369-379.

49. Steen, R. G.; Gronemeyer, S. A.; Kingsley, P. B.; Reddick, W. E.; Langston, J. S.; Taylor, J. S. Precise and accurate measurement of proton T1 in human brain in vivo: validation and preliminary clinical application. Magn Reson Imag 1994, 4 (5), 681-691.

50. Ogg, R. J.; Kingsley, P. B. Optimized Precision of Inversion-Recovery T1 Measurements for Constrained Scan Time. Magn Reson Med 2004, 51 (3), 625-630.

51. Bevington, P. R. Data reduction and error analysis for the physical sciences; New York, 1969; pp 235-236.

52. Constable, T. R.; Smith, R. C.; Gore, J. C. Signal-to-noise and contrast in fast spin echo (FSE) and inversion recovery FSE imaging. J Comput Assist Tomogr 1992, 16 (1), 41-47.

53. Gowland, P. A.; Leach, M. O. A simple method for the restoration of signal polarity in multi-image inversion recovery sequences for measuring T1. Magn Reson Med 1991, 18 (1), 224-231.

54. Gowland, P. A.; Leach, M. O. Fast and accurate measurements of T1 using a multi-readout

single inversion-recovery sequence. Magn Reson Med 1992, 26 (1), 79-88.

55. Kim, S.; Hu, X.; Uğurbil, K. Accurate T1 determination from inversion recovery images: application to human brain at 4 Tesla. Magn Reson Med 1994, 31 (4), 445-449.

56. Park, H.; Cho, M.; Cho, Z. Real-value representation in inversion-recovery NMR imaging by use of a phase-correction method. Magn Reson Med 1986, 3 (1), 15-23.

57. Ahn, C. B.; Cho, Z. H. A new phase correction method in NMR imaging based on autocorrelation and histogram analysis. IEEE Trans Med Imaging 1987, 6 (1), 32-36.

58. Kraft, K. A.; Fatouros, P. P.; Clarke, D.; Kishore, P. R. An MRI Phantom Material for Quantitative Relaxometry. Magn Reson Med 1987, 5 (6), 555-562.

59. Sled, J. G.; Pike, G. B. Quantitative Imaging of Magnetization Transfer Exchange and Relaxation Properties In Vivo Using MRI. Magn Reson Med 2001, 46 (5), 923-931.

60. NEMA. DICOM. http://medical.nema.org/ (accessed Jan 01, 2011).

61. Deoni, S. C. L.; Rutt, B. K.; Peters, T. M. Rapid combined T1 and T2 mapping using gradient recalled acquisition in the steady state. Magn Reson Med 2003, 49 (3), 515-526.

62. Brown, L. G. A survey of image registration techniques. 1992, 24 (4), 325-376.

63. Studler, U.; White, L. M.; Andreisek, G.; Luu, S.; Cheng, H.-L. M.; Sussman, M. S. Impact of motion on T1 mapping acquired with inversion recovery fast spin echo and rapid spoiled gradient recalled-echo pulse sequences for delayed gadolinium-enhanced MRI of cartilage (dGEMRIC) in volunteers. J Magn Reson Imaging 2010, 32 (2), 394-398.

64. Lo, J. L.-C.; Brady, M.; Moore, N. Simultaneous multiple image registration method for T1 estimation in breast MRI images. Med Image Comput Comput Assist Interv 2006, 9 ((Pt 1)), 865-872.

65. Xue, H.; Shah, S.; Greiser, A.; Guetter, C.; Littmann, A.; Jolly, M.-P.; Arai, A. E.; Zuehlsdorff, S.; Guehring, J.; Kellman, P. Motion correction for myocardial T1 mapping using image registration with synthetic image estimation. Magn Reson Med 2011.

66. Shah, N. J.; Zaitsev, M.; Steinhoff, S.; Zilles, K. A New Method for Fast Multislice T1 Mapping. NeuroImage 2001, 14 (5), 1175-1185.

67. Ordidge, R.; Gibbs, P.; Chapman, B.; Stehling, M.; Mansfield, P. High-speed Multislice T1 Mapping Using Inversion-Recovery Echo-Planar Imaging. Mage. Reson. Med. 1990, 16 (2), 238-245.

68. Wansapura, J. P.; Holland, S. K.; Dunn, R. S.; Ball, W. S. J. NMR relaxation times in the human brain at 3.0 tesla. Magn Reson Imaging 1999, 9 (4), 531-538.